UNIVERSITÉ DE MONTRÉAL

BIOMECHANICAL MODELING OF VERTEBRAL MECHANOBIOLOGICAL

GROWTH AND OF THE DEFORMATION PROCESS IN ADOLESCENT

IDIOPATHIC SCOLIOSIS

HUI LIN

DÉPARTEMENT DE GÉNIE MÉCANIQUE

ÉCOLE POLYTECHNIQUE DE MONTRÉAL

UNIVERSITÉ DE MONTRÉAL

ÉCOLE POLYTECHNIQUE DE MONTRÉAL

Cette thèse intitulée:

BIOMECHANICAL MODELING OF VERTEBRAL MECHANOBIOLOGICAL GROWTH
AND OF THE DEFORMATION PROCESS IN ADOLESCENT IDIOPATHIC SCOLIOSIS

présentée par: LIN Hui

en vue de l'obtention du diplôme de: Philosophiae Doctor

a été dûment acceptée par le jury d'examen constitué de:

M. YAHIA L'Hocine, Ph.D., président

M. AUBIN Carl-Éric, Ph.D., membre et directeur de recherche

Mme. VILLEMURE Isabelle, Ph.D., membre et codirectrice de recherche

M. PARENT Stefan, MD. Ph.D., membre et codirecteur de recherche

M. PETIT Yvan, Ph.D., membre

M. RAUCH Frank, MD., membre

ACKNOWLEDGEMENTS

RÉSUMÉ

La scoliose idiopathique chez l'adolescent est une déformation tridimensionnelle du rachis se développant durant la croissance. Plusieurs études rapportent que la progression de la déformation scoliotique est influencée par des facteurs biomécaniques. La déformation scoliotique, l'asymétrie de la balance du rachis et l'activité musculaire sont responsables du chargement asymétrique sur les plaques de croissances. Ces facteurs modifient la répartition entre le côté concave-convexe du taux de croissance et, par conséquent, conduit à un cercle vicieux de progression de la déformation scoliotique. Le processus biomécanique de la progression de la scoliose a été étudié dans la littérature en considérant principalement une composante de chargement axiale pour la représentation de la croissance.

L'objectif général de ce projet est d'étudier la biomécanique multiaxiale de la progression scoliotique. Le but spécifique du projet est de vérifier que le processus de déformation, impliquant la croissance et sa modulation mécanobiologique par des charges multi-axiales, est stimulable numériquement par la méthode des éléments finis, et que ces charges multi-axiales exercées sur les plaques de croissance épiphysaires sont responsables des déformations caractéristiques des vertèbres et rachis scoliotiques. Le chargement utilisé pour simuler la pathologie consiste en des forces primaires axiales asymétriques combinées à des forces secondaires de cisaillement et de torsion. Afin d'atteindre ce but, le projet a été divisé en trois parties. La première partie a consisté à faire une étude comparative de deux techniques de modélisation afin de simuler les concepts de croissance mécanobiologique. La seconde partie a consisté à développer un nouveau modèle de croissance mécanobiologique, basé sur l'énergie de stimulation, afin de représenter les déformations vertébrales résultant du chargement multiaxial. La troisième partie a consisté à soumettre le nouveau modèle numérique à différents cas de chargements et à analyser leurs influences sur la croissance et sur la progression de la scoliose.

Dans la première partie, les formulations analytiques de la croissance mécanobiologique développées par Stokes et coll. (1990) et Carter et coll. (1988) ont été comparées entre elles à l'aide d'un modèle par éléments finis d'une vertèbre thoracique. La vertèbre et la plaque de croissance adjacente supérieure ont été modélisées par des éléments solides 3D linéaires. Le

modèle de Stokes tient compte seulement du chargement axial, tandis que le modèle de Carter inclut des charges multiaxiales. Les plaques de croissances épiphysaires ont été représentées par trois couches distinctes : une couche sensible aux chargements, une couche de croissance et une couche minéralisée. Les modèles mécanobiologiques de croissance de Stokes et coll. (1990) et Carter et coll. (1998) ont été numériquement intégrés au modèle de la plaque de croissance. Différentes conditions de chargements physiologiques ont été appliquées sur la vertèbre (tension, compression, cisaillement, tension/cisaillement et compression/cisaillement) afin d'étudier la modulation de croissance. Une procédure progressive incrémentale discrète a été utilisée afin de représenter la croissance longitudinale géométrique de la vertèbre. Les résultats de simulations du modèle de Stokes et coll. (1990) ont été comparés aux résultats de simulation du modèle de Carter et coll. (1998) et des différences significatives ont été observées entre les deux modèles. Le modèle de Carter a présenté une faible capacité à retarder la croissance sous l'effet des forces de compression et les forces de cisaillement contribuent significativement à stimuler la croissance. Par contre, le modèle de Stokes retarde significativement la croissance sous l'effet de forces de compression et les forces de cisaillement n'ont pas d'effet sur la croissance. Le ratio des taux de modulation de croissance entre les modèles de Carter et Stokes est supérieur à 10 lorsque le modèle par élément finis est soumis à une combinaison de forces de compression et de cisaillement. Les résultats de simulation ont indiqué que les modèles de Stokes et Carter sont incapables de simuler complètement la croissance selon des conditions de chargement multiaxial.

Afin de pouvoir correctement simuler les conditions de croissance selon les chargements multiaxiaux, un nouveau modèle de croissance, basé sur l'énergie, a été développé. L'énergie est un stimulus transportant la réponse biomécanique responsable de la croissance. Le processus de modélisation de croissance a été représenté par des formulations analytiques et a été divisé en deux composantes : la composante mécano-sensible basée sur le sondage d'énergie ainsi que la composante de mécano-régulation basée sur l'énergie. La composante mécano-sensible est responsable de la transformation du chargement mécanique en réponse biologique à l'aide de l'énergie. La composante de mécano-régulation suit la composante mécano-sensible et induit les modifications biologiques. Le modèle de croissance mécano-biologique basé sur l'énergie a été développé selon ces deux composantes et a été implanté numériquement au modèle par éléments finis de la plaque de croissance développé dans la première partie du projet décrite

précédemment. Ce nouveau modèle de croissance intégré au modèle par éléments finis a été testé selon différents cas de chargement (tension, compression, cisaillement, tension/cisaillement et compression/cisaillement) et l'évaluation a été faite par comparaison avec des études expérimentales et numériques publiées dans la littérature. Les résultats de simulation pour les cas de chargements axiaux sont en accord avec le principe de Hueter-Volkmann, le modèle de Stokes et les expérimentations faites sur les animaux. Les contraintes de cisaillement augmentent la croissance mécano-biologique de 20 à 40% dans les cas de chargements axiaux/cisaillement, ce qui est en accord avec les résultats de Carter.

Le nouveau modèle de croissance développé permet de représenter les chargements multiaxiaux et les modifications de la morphologie vertébrale des adolescents atteints de scoliose idiopathique. Le processus de modification morphologique a été simulé avec un modèle par éléments finis. Le nouveau modèle de croissance a été intégré dans un modèle numérique pédiatrique d'un segment fonctionnel T7-T8 personnalisé à un patient mâle non pathologique âgé de 11 ans. Des cas de chargement axiaux, de cisaillement, de torsion et des effets combinés axial/cisaillement et axial/torsion ont été simulés. Les mesures prises sur les modèles numériques incluent les angles d'inclinaisons des plateaux de T7 (cunéiformisation), qui sont des mesures essentielles de la déformation vertébrale chez les patients scoliotiques, et la rotation axiale entre T7 et T8. Les résultats de simulations ont indiqué que les chargements axiaux et non axiaux modifient l'inclinaison des plateaux vertébraux dans le plan coronal (1.4^o~4.8^o) et la rotation intervertébrale (0.7^o~3.7^o). L'angle d'inclinaison des plateaux dans le plan sagittal n'est pas beaucoup affecté (0.1^o~1.0^o). Le chargement asymétrique axial induit une modification de l'inclinaison des plateaux vertébraux du modèle numérique de 4.8^o, ce qui se rapproche des résultats publiés dans la littérature (5.2^o) de Parent et coll. (2003).

L'étude comparative de la première partie du projet a déterminé les forces et limites des modèles de croissance de Stokes et Carter. En effet, le modèle de Stokes est en accord avec des études expérimentales et s'ajuste correctement dans le cas des chargements axiaux. Cependant, le modèle de Stokes n'est pas capable de représenter la croissance selon des chargements multiaxiaux, ce qui limite son application afin de prendre en compte les environnements mécaniques complexes du rachis tels que ceux observés chez les patients

scoliotiques. Le modèle de Carter tient compte des effets mécano-biologiques des charges multiaxiales et dérive théoriquement des modèles de formation de l'os. Toutefois, ce dernier modèle ne tient pas compte de l'orientation de croissance résultant des stimuli de contraintes de chargement 3D. Le nouveau modèle de croissance développé dans ce projet utilise le concept de stimulus énergétique, intégrant physiquement des contraintes mécaniques multiaxiales. Les résultats de simulations pour le nouveau modèle de croissance développé est en accord avec la plupart des études expérimentales et les études théoriques et mécano-biologiques de Carter. Ce projet confirme l'implication des charges axiales et non axiales dans le développement de la scoliose. Aussi, cette étude conclut que l'inclinaison des plateaux vertébraux chez les patients scoliotiques est présente uniquement dans le plan coronal. Cette étude confirme le rôle primaire du chargement axial et le couplage secondaire des efforts de cisaillement et de torsion dans le développement de la scoliose. Le concept d'énergie peut également expliquer les mécanismes de couplage existants dans les charges multiaxiales. Les charges multiaxiales induisent des composantes de contraintes axiales et non axiales, ce qui est physiquement intégré de manière non linéaire dans le modèle énergétique. Cette non linéarité mène au couplage mécano-biologique généré par les charges multiaxiales.

Cette étude propose une approche biomécanique permettant de trouver des risques de progression de la déformation scoliotique du rachis. Cette étude permet également le design et l'optimisation d'un schéma de correction pour la scoliose à partir de résultats de simulation. La méthodologie innovatrice de la croissance mécanobiologique développée dans le modèle par éléments finis offre une aide pertinente dans la compréhension biomécanique de la scoliose et dans le design de traitements minimalement invasifs.

ABSTRACT

Adolescent idiopathic scoliosis is a three dimensional deformity of spine that mostly occurs during the growth spurt. It is generally accepted that the progression of scoliotic deformities is influenced by biomechanical factors. Asymmetrical loading of vertebral growth plates resulting from an initial scoliotic curve or asymmetric balance or muscle recruitment are modifying the concave-convex side growth rate, thus leading to a vicious circle of scoliosis progression. The mechanobiological process of scoliosis was previously investigated, but mainly considering the axial loading component for growth.

The general objective of this project was to study the multi-axial biomechanics of scoliosis progression. The specific objective was to model the deformation process, including the spinal growth and mechanobiological growth modulation due to multi-axial loads, and analyze how these loads are involved in the resulting characteristic scoliotic deformities. This tested pathomechanism presents the primary loading characteristics of asymmetric axial forces combined with secondary shear and torsion. In order to address the proposed research objectives, this project was divided into three parts. The first one was a comparative study and analysis of two modeling techniques to simulate existing concepts of mechanobiological growth. The second part was the development of a novel model of mechanobiological growth based on energy stimulus that enabled to represent the vertebral changes due to multi-axial loading. In the last part, this model was exploited to simulate the effect of different loads and analyze how they influence the growth process and how they relate to the scoliotic pathomechanism.

In the first part, the analytical formulation of mechanobiological growth developed by Stokes et al. (1990) and Carter et al. (1988) was compared using a finite element model representing a thoracic vertebra as solid elements. Stokes's model only concerned axial stress, while Carter's model involved multi-axial stresses. The epiphyseal growth plates were represented using three layers similar to those found in the vertebral bodies: a loading sensitive area, a growth area, and a mineralized area. The two mechanobiological growth models were numerically integrated into the growth plate model. The two models were further used to simulate vertebral growth modulation resulting from different physiological loading conditions applied on

the vertebra (tension, compression, shear, as well as combined tension/shear and combined compression/shear). The growth simulation used a stepwise incremental procedure to represent the longitudinal growing geometry of the vertebra. Significantly different growth patterns were triggered in both models by the loading cases. Carter's model presented a weak capability of retarding the growth under compression forces but shear forces had a more important contribution in stimulating growth. In contrast, Stokes's model significantly retarded the growth under compression but shear forces had no effect. The combined compression/shear further highlighted the differences with much over ten times of the ratio of growth modulation rates between the two models. Simulation results indicated that neither models were fully able to simulate growth under multi-axial loading conditions.

In order overcoming the limitations of the two tested mechanobiological models, an innovative model was proposed. The energy was proposed as a stimulus for carrying out the mechanobiological response. The modeling process was divided into two components and represented as analytical formulations: energy-triggered mechanosensing and energy-based mechanoregulation. Mechanosensing carried out the transformation of mechanical loading into biological response by energy. Mechanoregulation followed the mechanosensing and induced the biological modification. The energy-based mechanobiological growth model was finally developed from those two analytical procedures. It was implemented in the growth plates of the previously developed vertebra finite element model. The model was tested with different loading conditions (tension, compression, shear, combined tension/shear, and combined compression/shear), and the validation was based on comparisons with published experimental studies on growth response to axial and shear loading in animals, and numerical simulation of growth modulation in humans. Simulation results under axial loading conditions agreed with the Hueter-Volkmann law, the Stokes' model and animal experiments. The shear stress increased the mechanobiological growth (20%-40%) in the combined axial /shear loading condition, which agreed with the Carter's mechanobiological theory.

The energy-based growth model involved multi-axial stresses and made it possible to reproduce the modification of vertebral morphology similarly as what is seen in adolescent idiopathic scoliosis. The morphological modification process was simulated by using finite

element modeling technique. Energy-based model was integrated into a pediatric FEM model of a thoracic functional unit T7-T8 personalized to an eleven-year-old healthy male child. The spinal loads were designed as axial loading, shear, torsion, and combined axial/shear or torsion. The measurement included the wedging angle of T7, which was an essential characteristic to measure a vertebral deformity, and intervetebral axial rotation between T7 and T8. Simulation results indicated that both axial and non-axial loading (shear) were able to induce the wedging of the vertebrae in the coronal plane (1.4^{o}~4.8^{o}) and the intervertebral rotation (0.7^{o}~3.7^{o}). The wedging angle in the sagittal plane was little modified (0.1^{o}~1.0^{o}). The asymmetric axial loading induced a 4.8^{o} wedging angle that approached published measurements (5.2^{o}) of Parent et al (2003).

The comparative study found the strengths and limits of two modeling techniques. The Stokes's model was supported by experimental studies and recognized in the axial loading conditions. However, the exclusion of non-axial stresses would limit its application on a complex mechanical environment of spine such as those seen in scoliosis. Carter's model considered the mechanobiological effects of multi-axial stresses and was theoretically derived from model of bone formation. Carter's model did not intrinsically incorporate growth orientation resulting from the 3D stress stimuli. Energy stimulus physically involved multi-axial stresses in terms of mechanics. The innovative model using energy stimulus thus naturally integrated multi-axial stresses.   The simulation study indicated that this model agreed with most experimental studies and Carter's theoretical studies in mechanobiology. This study confirmed the mechanobiological contribution of both axial and non-axial loading to the development of scoliotic vertebrae. This study found that scoliotic wedging occurs only in the coronal plane. This study confirmed the primary role of axial loading on inducing scoliotic vertebrae and coupling secondary role of shear and torsion. The energy concept can also explain coupling mechanisms existing in multi-axial loads. Multi-axial loads resulted in axial and non-axial stresses, which non-linearly physically integrated into energy. This non-linearity led to coupling mechanobiological impact generated from those loads.

This study provides a biomechanical approach to find potential risk of spine deformation progression in adolescent idiopathic scoliosis. Designing and optimizing a correction scheme for scoliosis also benefit from this study by means of biomechanical simulation to find the potential

outcome of a correction. The innovative methodology on mechanobiological growth developed with the finite element model offers a biomechanical assistance for the understanding of scoliosis biomechanics and the design of minimal invasive treatments.

CONDENSÉ EN FRANÇAIS

La scoliose idiopathique des adolescents (AIS) est une déformation tridimensionnelle de la colonne vertébrale qui se développe durant la poussée de croissance. Les causes de progression de cette pathologie sont inconnues. On croit que les facteurs mécaniques jouent un rôle important dans la déformation scoliotique. Le chargement mécanique a été rapporté comme une stimulation épi-génétique, modifiant la croissance, la modélisation et le remodelage osseux changeant la morphologie de l'os, son histologie et ses propriétés mécaniques, comme observé dans la scoliose.

La réponse biologique des tissus squelettiques aux stimuli mécaniques (mécanobiologie) se traduit par la modification du développement du squelette. La loi de Wolff et le principe de Hueter-Volkmann sont considérés respectivement comme des concepts de base du remodelage osseux et de la modulation de croissance. Fondamentalement, le processus mécanobiologique comprend : le mécano-sondage, la mécano-transduction et la mécano-régulation. Ces procédures conduisent à la transformation des stimuli physiques en réactions biochimiques ainsi qu'en réponses biologiques finales. Les réponses existent au niveau de la croissance, la modélisation et le remodelage osseux.

Deux modèles d'analyse de la croissance mécano-biologique ont été développés selon deux méthodes différentes: le modèle de Stokes et le modèle de Carter. Le modèle de Carter décrit initialement un modèle d'ossification d'un os long et associe la contrainte de compression hydrostatique et la contrainte de cisaillement octahédrale avec l'ossification du cartilage. La théorie de Carter a été appliquée au niveau de l'incorporation de la croissance et de l'ossification endochondrale, permettant ainsi le développement d'un modèle de croissance mécanobiologique. Ce nouveau modèle fut plus tard intégré dans les modèles d'éléments finis (FEM) du fémur proximal et distal pour prédire la dysplasie développementale de la hanche et l'angle bicondylien du fémur résultant de la croissance longitudinale du fémur. Le modèle de croissance de modulation de Stokes était initialement issu de la relation hypothétique linéaire entre le taux de croissance et de la contrainte axiale. Ce modèle a été créé pour les côtes et pour simuler la déformation thoracique liée à scoliose. Des travaux expérimentaux complémentaires supportent

le modèle de Stokes et permettent l'évaluation des paramètres du modèle. Ce modèle a ensuite été appliqué au modèle biomécanique de la colonne vertébrale pour étudier l'effet de la croissance sur le développement de la scoliose. Le modèle a été intégré dans un modèle par éléments finis de la colonne vertébrale pour simuler la croissance du corps vertébral et pour trouver les mécanismes mécano-biologiques de la scoliose. En outre, le modèle de croissance des jonctions neurocentrales utilise ce modèle pour l'étude du rôle des jonctions dans le développement de l'AIS.

À ce jour, seul le modèle de Stokes est appliqué à l'étude biomécanique de la scoliose. Toutefois, seulement une contrainte axiale est impliquée dans ce modèle. Puisque la colonne vertébrale, saine ou pathologique, est soumise à des charges dynamiques complexes (multi-axiales), le modèle de Stoke comporte plusieurs limites. En outre, il n'existe aucune étude sur des techniques de modélisation afin d'identifier leur rationalité physiologiques. Les effets mécanobiologiques sur le chargement multiaxial de la croissance vertébrale favorisant le développement de vertèbres scoliotiques devrait être étudiés. Les vertèbres et structures intervertébrales complexes affichent des caractéristiques géométriques pouvant entraîner des environnements mécaniques complexes.

Par conséquent, le processus de croissance mécanobiologique et ses impacts sur le développement des vertèbres scoliotiques seraient pertinents dans l'évaluation des pathomécanisme de la AIS. L'objectif général de ce projet est d'étudier les impacts mécanobiologiques de charges multiaxiales sur le développement des vertèbres scoliotiques. Le but spécifique du projet est de vérifier que le processus de déformation, impliquant la croissance et sa modulation mécanobiologique par des charges multi-axiales, est simulable numériquement par la méthode des éléments finis, et que ces charges multi-axiales exercées sur les plaques de croissance épiphysaires sont responsables des déformations caractéristiques des vertèbres et rachis scoliotiques.

Les objectifs suivants ont été proposés dans cette thèse:

Objectif 1   Faire une étude comparative des techniques de modélisation existantes. Cet objectif inclut les sous-objectifs suivants:

Objectif 1.1   Élaborer un modèle conceptuel d'une plaque de croissance et créer un modèle par éléments finis.

Objectif 1.2   Évaluer les modèles actuels de croissance mécanobiologique.

Objectif 2   Développer un modèle de croissance physiologique mécanobiologique des vertèbres.

Objectif 2.1   Élaborer un modèle de croissance plus physiologique et mécanobiologique que les modèles existants.

Objectif 2.2   Simuler la croissance longitudinale vertébrale par l'intégration avec le modèle de croissance développé.

Objectif 2.3   Évaluer le nouveau modèle de croissance mécanobiologique.

Objectif 3   Identifier les pathomécanismes possibles du développement des vertèbres scoliotiques par simulation de la croissance:

Objectif 3.1   Exploiter le modèle mis au point pour analyser les effets de chargement axial et non axial sur le développement morphologique des vertèbres.

Objectif 3.2   Identifier l'effet de couplage mécanobiologique des charges multiaxiales sur la génération des vertèbres scoliotiques.

Pour le premier objectif, les modèles de Stokes et de Carter ont été analysés et comparés en utilisant une approche par éléments finis d'une vertèbre. Les modèles intégraient un modèle conceptuel de la plaque de croissance. Ce modèle a été utilisé pour simuler la modulation de croissance vertébrale résultant de différentes conditions de chargements physiologiques appliquées sur la vertèbre (tension, compression, cisaillement, tension/cisaillement et compression/cisaillement).

Cette étude a permis de développer un modèle permettant de simuler la croissance et sa modulation mécanobiologique. Ce modèle est basé sur l'énergie provenant de forces multi-axiales appliquées sur les plaques de

croissance. Ces procédures ont permis la mise au point d'un modèle de croissance mécano-biologique. Le modèle a été testé sur le modèle par élément finis d'une vertèbre. Les tests étaient basés sur les aspects suivants: les études théoriques de Carter sur la mécanobiologie, les études expérimentales sous un chargement axial et de cisaillement et la comparaison avec le modèle de simulation numérique de Stokes à des conditions de chargement axial. Les conditions de chargement testées comprenaient le chargement axial, le chargement non-axial et les cas de chargement combiné, et ont été utilisés par les études publiées. Ces conditions de chargement étaient physiquement présentées comme: tension, compression, forces de cisaillement, forces de tension-cisaillement et forces de compression-cisaillement.

Le modèle de croissance fondé sur l'énergie a été utilisé pour étudier le développement mécano-biologique lié à des vertèbres scoliotiques. Ce modèle a été intégré dans un modèle par éléments finis d'une unité fonctionnelle thoracique T7-T8 qui a été personnalisée sur un enfant de onze ans de sexe masculin en bonne santé. L'évaluation d'une vertèbre scoliotique a été basée sur des mesures de la géométrie vertébrale. Les mesures comprenaient l'angle d'inclinaison de T7 (cunéiformisation) et la rotation axiale intervertébrale entre T7 et T8. Le chargement axial, le cisaillement, la torsion et les chargements axiaux combinés au cisaillement et à la torsion ont été rapportés dans les études expérimentales et ont été utilisés pour simuler l'évolution des morphologies vertébrales.

Dans la simulation pour l'étude de comparaison, des taux de croissance différents ont été déclenchés par la compression et par du chargement combiné tension-cisaillement. Les ratios des taux de modulation de la croissance (Carter/Stokes) étaient de 0,6 et 1,5 respectivement pour ces cas. Des résultats significativement différents entre les modèles ont été trouvés pour les cas de chargement de cisaillement et de cisaillement-compression : le rapport entre les taux de modulation pour le modèle de Carter et le modèle de Stoke était supérieur à 10.

Pour le modèle basé sur l'énergie, des conditions de chargement similaires à celles appliquées sur le modèle de Stokes ont été appliquées. Un taux de croissance mécano-biologique négligeable (51 μm) a été mesuré sous les charges de cisaillement pures. L'expérience de Moreland a affiché des résultats similaires (1980). La contribution positive mécano-biologique du

cisaillement, responsable de l'augmentation du taux de modulation de croissance de 20%-40%, a été trouvé dans le cas du chargement combiné.

Les simulations sur le modèle d'unité fonctionnelle T7-T8 montre que le chargement axial induit une inclinaison de 4.80° du plateau de la vertèbre T7, ce qui concorde avec les mesures de Parent (2003). En outre, une rotation intervertébrale de 3,40° a également été produite. Des charges de cisaillement ont également déclenché des changements d'inclinaison de T7 de 2.50°-3.00° dans le plan frontal et des rotations de 1.70°-1.90°. Les charges multiaxiales ont induites des inclinaisons vertébrales de 2.30°-4.40° et des rotations vertébrales de 1,90°-3,10°. Des inclinaisons vertébrales de 0.10°-1.00° dans le plan sagittal ont été également produites.

Les résultats de simulation pour l'étude de comparaison ont montré que le modèle de Stokes était supporté par les études expérimentales sur les conditions de chargement axial. Le modèle de Stokes a été reconnu comme une représentation rationnelle dans des environnements mécaniques à charge axiale. Toutefois, le modèle de Stokes ne tient pas compte de la contribution de la pression non-axiale de la croissance mécano-biologique qui peut se produire dans un environnement mécanique complexe. En comparaison, le modèle de Carter a considéré la contribution mécano-biologique de charges multiaxiales. Cependant, ce modèle n'a pas intrinsèquement incorporé une orientation de la croissance résultant des stimuli de pression en 3D, ce qui a abouti à des résultats contradictoires sur la simulation de compression par rapport aux études expérimentales.

Le nouveau modèle, le modèle à base d'énergie, considère les impacts mécano-biologiques axiales et non-axiales. Les tests biomécaniques simulés ont indiqué que ce modèle est en accord avec les études expérimentales sur des animaux dans des conditions de chargement axial et respecte la loi de Hueter-Volkmann. Le modèle à base d'énergie est également en accord avec le modèle de Stokes pour cette condition de chargement. Le modèle à base d'énergie souligne également l'effet mécano-biologique positif du cisaillement et donc, est en accord avec la théorie mécano-biologique de Carter. Ce modèle a permis de simuler la croissance vertébrale sous des charges multidirectionnelles.

Cette étude applique le modèle à base d'énergie afin d'étudier le développement de la vertèbre scoliotique due à la croissance mécano-biologique. Il a été constaté que le chargement axial était capable d'induire des morphologies de vertèbres avec des charactéristiques d'inclinaison similaires à celles mesurées sur des échantillons scoliotiques. Cette étude a montré que les charges axiales et non axiales modifient mécano-biologiquement l'évolution morphologique des vertèbres et peuvent mener à la formation de vertèbres scoliotiques. En outre, un mécanisme de couplage favorisant la progression de la scoliose et existant dans ces charges multiaxiales a également été trouvé. Le mécanisme de couplage est créé à partir d'énergie qui intègre, de manière non linéaire, les effets mécano-biologiques des charges axiales et non-axiales. Il a été observé que la distribution d'énergie sur une plaque de croissance régit les caractéristiques de l'inclinaison vertébrale. Ce résultat est en accord avec la conclusion de Robling (2009) qui affirme que la formation mécano-biologique de l'os était compatible avec la distribution de l'énergie mécanique en vue d'un changement adaptatif avec le stimulus mécanique.

L'objectif général d'étudier la génération des vertèbres scoliotiques fournit une approche biomécanique permettant d'évaluer le risque potentiel de développement de la AIS. La méthodologie novatrice sur la croissance mécano-biologique développée avec le modèle par éléments finis peut contribuer à la conception et l'optimisation d'un schéma de correction de la scoliose.

TABLE OF CONTENTS

LIST OF TABLES

LIST OF FIGURES

LIST OF APPENDIX

NOMENCLATURE

a_e, b_e = loading sensitive factors

$\vec{Df}$ = morphological expression of growth plate tissues

$d\delta$ = displacement along the mechanical loading orientation

dv = volume of a micro element

E = elastic modulus

E_g = energy contribution index

$F_u(\ )$ = function based on the variable of energy

$F_{sI}(\ )$ = function based on the variables of integrated stresses

$F_{sS}(\ )$ = function based on the variables of stresses $\quad G$ = shear modulus

f = mechanical force

Gm = longitudinal baseline growth for vertebrae

h_g = initial height of the growth area

$\vec{i}$, $\vec{j}$, $\vec{k}$ = the direction vector of axes for a local coordinate system

$\vec{i}_p, \vec{j}_p, \vec{k}_p$ = principal direction

$\vec{Me}_\varepsilon$ = mechanosensing stimulus

Me_t = tensor for mechanosensing stimulus

M_I = mechanoregulation index

$\vec{n}_p$ = principal vector

$n_{pi_j(i=1,2,3;j=x,y,z)}$ = the component (x, y, z) of the direction vector for each principal vector i .

St_g = stimulus contribution index

V = overall volume

U = strain energy

U_d = strain energy density

U_{dd} = distortional strain energy density

U_{dv} = dilatation strain energy density

W = mechanical work

x, y, z = axes of a local coordinate system

β_l = loading sensitivity factor

$\beta_{le} =$ loading sensitivity factor for axial stress

$\gamma_{xy}, \gamma_{xz}, \gamma_{yz} =$ shear strain

$\varepsilon_{be} =$ baseline growth

$\varepsilon_{me} =$ mechanobiological growth

$\varepsilon_{ml} =$ mechanobiological growth for axial stress only

$\varepsilon_{Tot} =$ overall deformity index

$\varepsilon_{we} =$ overall growth

$\varepsilon_{x}, \varepsilon_{y}, \varepsilon_{z} =$ normal strains

$\varepsilon_{1}, \varepsilon_{2}, \varepsilon_{3} =$ principal strains

$\upsilon =$ Poisson's ratio

$\sigma_{l} =$ axial (longitudinal) stress

$\sigma_{x}, \sigma_{y}, \sigma_{z} =$ normal stresses

$\sigma_{zz} =$ axial (longitudinal) stress

$\sigma_{1}, \sigma_{2}, \sigma_{3} =$ principal stresses

$\sigma_{oct} =$ hydrostatic stress

$\tau_{oct} =$ octahedral shear stress

$\tau_{xy}, \tau_{xz}, \tau_{yz} =$ shear stresses

$\Omega =$ overall displacement caused by mechanical loading

$\Delta \varepsilon_{l} =$ overall growth strain increment

$\Delta G_{l} =$ baseline (normal) longitudinal growth strain increment

INTRODUCTION

Adolescent idiopathic scoliosis (AIS) is a three-dimensional deformity of the spine that develops during growth spurt with unknown cause (Lonstein J.E. 1994). Scoliotic vertebrae display geometric deformities including wedging and torsion due to abnormal growth. Mechanical loading was reported as stimulation to alter skeletal growth, modeling, and remodeling, and thus change bone morphology, histology, and material properties (Carter D.R. et al. 1996; Stokes I.A.F. 2002), as observed in scoliosis (Guo X. et al. 2003; Goldberg C.J. et al. 2008; Kotwicki T. and Napiontek M. 2008).

Bone growth in length is an endochondral ossification process via cartilage growth and ossification through proliferation and hypertrophy as well as extracellular matrix ossification (Villemure I. and Stokes I.A.F. 2009). It should be noted that bone growth in length takes place at the growth plate located at the epiphysis of long bones and vertebral endplates, which present high biological activity during adolescence and become thin and ossified in the adulthood. Bone growth is sensitive to the surrounding mechanical environment. Mechanical loads alter the proliferation and hypertrophy as well as the ossification of chondrocytes existing in the cartilaginous growth plate and thus modulate the growth rate (Alberty A. et al. 1993; Stokes I.A.F. et al. 2007).

Biological response of skeletal tissues to mechanical stimuli is termed as mechanobiology (Van Der Meulen M.C.H. and Huiskes R. 2002). The Wolff's law and the Hueter-Volkmann principle are considered as basic concepts of bone remodeling and growth modulation respectively. Basically, the mechanobiological process includes: mechanosensing, mechanotransduction, and mechanoregulation (Silver F.H. and Bradica G. 2002; Huselstein C. et al. 2008). Those processes carry out the transformation from physical stimuli into biochemical reactions as well as final biological responses. Those responses exist in bone growth, modeling and remodeling. Although mechanical force is considered as general stimuli to trigger the generation and modification of skeleton tissues, the real mechanobiological process still is not clear, as well as the real nature of the growth modulation stimuli (stress, strain, energy, etc.).

Two analytical models of mechanobiological growth were developed based on two different methodologies: the model of Stokes (Stokes I.A.F. and Laible J.P. 1990; Stokes I.A.F. et al. 2006) and the one of Carter (Carter D.R. and Wong M. 1988; Stevens S.S. et al. 1999; Shefelbine S.J. and Carter D.R. 2004). Carter's model initially described bone ossification pattern of a long bone and associated the hydrostatic compression stress and octahedral shear stress with the cartilage ossification (Carter D.R. and Wong M. 1988; Carter D.R. and Wong M. 1988). The octahedral shear stress is also termed as distortional energy stresses with promotion role on endochondral ossification, and the hydrostatic stress is defined as dilatational energy stress with inhibition function on ossification process. Carter's theory was further applied on incorporation of endochodral growth and ossification and thus developed a mechanobiological growth model (Stevens S.S., Beaupre G.S. et al. 1999). This evolved model was later also integrated in finite element models of the proximal and distal femur to predict developmental hip dysplasia and femoral bicondylar angle due to the longitudinal growth of femur (Shefelbine S.J. et al. 2002; Shefelbine S.J. and Carter D.R. 2004; Shefelbine S.J. and Carter D.R. 2004). Stokes's growth modulation model was initially derived from the hypothetical linear relationship between growth rate and the axial stress. This model was first established for ribs and for simulating scoliosis-related thorax deformity (Stokes I.A.F. and Laible J.P. 1990). Experimental works further supported this model and determined the model parameters (Stokes I.A.F., Aronsson D.D. et al. 2006). This model was later applied on the biomechanical model of the whole spine for investigating AIS caused by growth (Aubin C. E. 2002). This model has been integrated into a finite element model of the spine for simulating the vertebral body growth course and finding the mechanism of mechanobioloigy-triggered scoliosis (Villemure I. et al. 2002; Carrier J. et al. 2004; Villemure I. et al. 2004; Huynh et al. 2007). In addition, the neurocentral junction growth also used this model for studying the role of development of this anatomical part on AIS (Huynh, Aubin C. E. et al. 2007). The deformity of thorax also was studied using this model (Carrier J., Aubin C. E. et al. 2004). There is no study to investigate the differences and similarities of those two modeling techniques. The mechanobiological influences on the development of scoliosis triggered by non-axial and multi-axial stresses have not been investigated in published studies.

The spine, normal or pathologic, is subjected to complex dynamic loads, mainly in the axial direction, but also in the transverse plane. The non-axial loads were not accounted in Stokes's model. This model and subsequent derived models (Villemure I., Aubin C. E. et al. 2002; Carrier J., Aubin C. E. et al. 2004; Huynh et al. 2007) so far was the only model applied on the biomechanical study of scoliosis. It is expected that mechanobiological effects on multi-axial loading on vertebral growth and generation of scoliotic vertebrae should be investigated. Both vertebral and intervertebral structures display complex geometric characteristics and thus result in complicated mechanical environments. Therefore, mechanobiological growth process and its impacts on scoliotic vertebrae development would allow identifying the pathomechanism of this disease.

This study targets on the investigation of mechanobiological contribution of multi-axial loading to development of scoliotic vertebrae. Finite element modeling technique is used to biomechanically reproduce the outcome of the development of growth-related scoliotic vertebrae. The growth-related technique combined with finite element model allowed to better understand potential mechanobiological risk of scoliosis.

This thesis is composed of seven chapters. The first chapter presents a review of relevant literature. The second chapter indicates the main objectives and hypotheses of this project. Chapter 3 presents study methodologies for this project. Chapter 4 shows simulation results. In Chapter 5, discussions for simulation results are present in response to proposed objectives and hypotheses. Finally, conclusions and recommendations for future studies are presented in Chapter 6.

CHAPTER 1.   LITERATURE REVIEW

1.1 Anatomy of spine

1.1.1 Spine structure

The spine, or vertebral column, is composed of five main segments: the cervical, thoracic and lumbar curvatures, as well as the sacrum and the coccyx. All of these curvatures of segments provide the structural support and protection for the spinal cord. The spine is composes of bony elements that are termed as vertebrae. Those elements are joined by interverbral discs, ligaments, and articular joins. There are twenty four vertebrae in the spine. The cervical curvature includes seven vertebrae, twelve in the thoracic curvature, and five in the lumbar curvature. In addition, the sacrum consists of five fused vertebrae and the coccyx is composed of three to five fused vertebrae (Maried N.E. 2003). Each segment composes of individual vertebrae, and the anatomy structure of vertebrae in each segment is different because of the structural variety in the different parts of the skeleton system.

- vertebrae

A vertebra basically includes two anatomical components: the vertebral body on the anterior site, and the neural arch, a posterior part. The endplates are located at the superior and inferior sides of the vertebral body and composed of hyaline cartilage. The neural arch consists of a pair of pedicles and laminae, and seven processes including two transverse, one spinous, and a two articular both in superior and inferior sides of the vertebra. The joint which connect one vertebra to another vertebra above or below is called facet joint. The articular facets are located at the end of the articular processes and joined by the pars interarticularis. The facet joints control the spinal movement.

A thoracic vertebra has heart-shape body and the long spinous process that points down (Figure 1-1). The lumbar vertebrae have the largest bean-shape bodies and short spinous processes that point straight back (Figure 1-2).
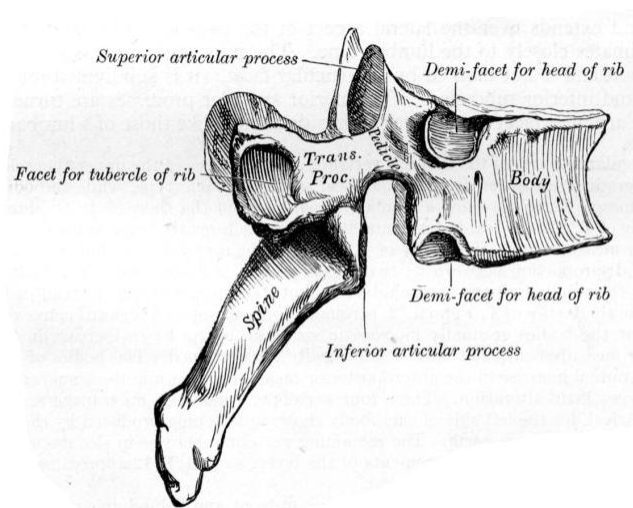
Figure 1-1 thoracic vertebra(Henry Gray F.R.S 1918)
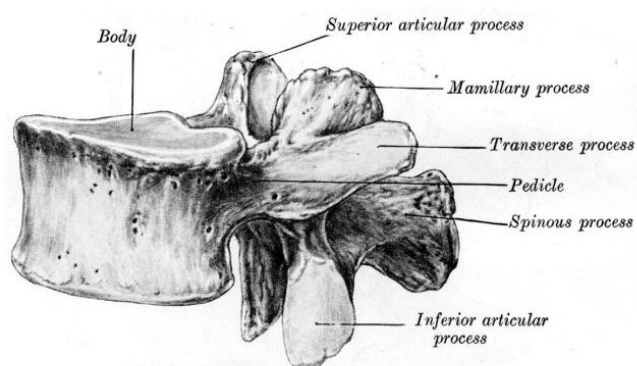
Figure 1-2 lumbar vertebra(Henry Gray F.R.S 1918)

1.1.2 Intervertebral structure

The vertebral bodies are connected by the intervertebral discs. The disc consists of the annulus fibrosus, tough rings of tissue, and the nucleus pulposus, a jellylike substance. The disc is firmly attached to the endplates of the vertebra. The discs allow for flexibility in the spine and absorb shock. In a young person, the discs have a high percentage of water (about 90%), and the disc is spongy and compressible. As the age increases, the disc becomes harder and less compressible.
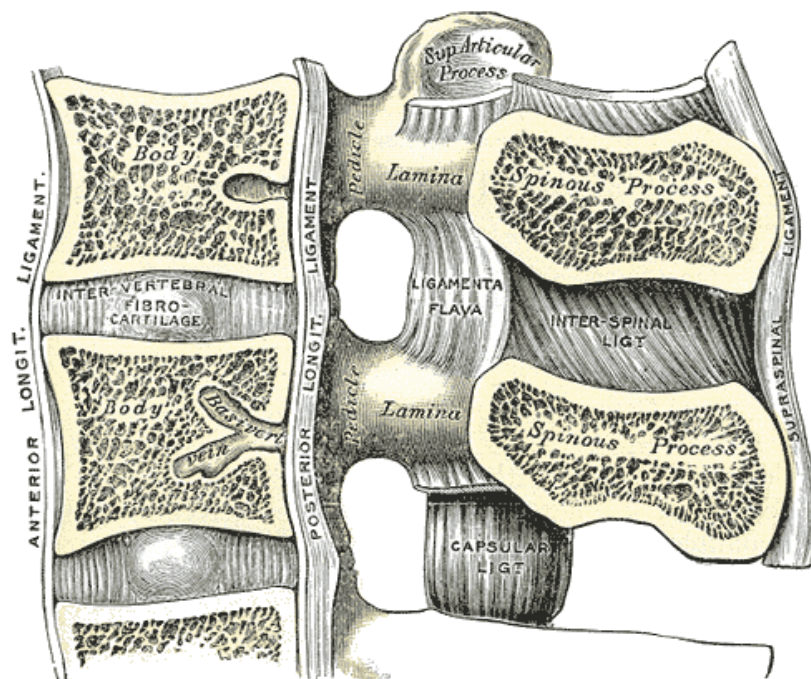
Figure 1-3 Intervetebral ligaments(Henry Gray F.R.S 1918)

Ligaments and tendons are soft collagenous tissues. Ligaments connect bone to bone and tendons connect muscles to bone. Ligament contains collagen fibrils, proteoglycan matix, and fibroblasts (biological cells) that are arranged in parallel rows. The biomechanical function of ligaments is to carry the tensile force from one bone to another bone. A tendon has a similar hierarchical structure to the ligament, but it has slightly higher volume fraction and organization than the ligament. A tendon is able to transfer forces from a muscle to a bone and carry compressive forces. The vertebral ligaments are tough, non-elastic bands (**Figure 1-3**). They hold the vertebrae together and control the amount of movement of a joint. The ligaments are able to absorb energy coming from the body motion and to protect the neural and skeletal system from injury. There are 9 spinal ligaments connected to the vertebrae. The anterior longitudinal ligament (ALL) attached on the anterior side of each vertebra and the intervertebral disc goes through the entire length of the spine. The posterior longitudinal ligament (PLL) also goes through the entire length of the spine and sticks to the posterior side of each vertebral body and intervertebral disc. The ligamentum flavum (LF) links the laminae between adjacent vertebrae. The intertransverse ligaments (ITL) join transverse processes on adjacent vertebrae both in left

and right sides. The interspinous ligaments (Huselstein C., Netter P. et al.) connect the spinous processes of adjacent vertebrae. The supraspinous ligament (SSL) extends through the entire spine and attaches to the tip of spinous processes. The capsular ligaments (CL) link each pair of facet joints and attach the peripheral sides of the facet joint.

1.2   Vertebral bone and cartilage

The spinal skeletal tissues consist of vertebral bony, cartilaginous, and soft collagenous tissues. Vertebral bony tissues include the cortical bone, which exists in the outer shell of the vertebral body, and compacted cancellous (or trabecular) bone, which fills the vertebral internal body. The cartilaginous tissue exists in the endplate and intervertebral discs. The intervertebral ligaments are composed of collagenous tissues.

- Cortical and trabecular bones

Cortical, or compact bone, has high mineral content (approximately 70%) and high occupancy in total bone mass (about 80%). The principle function of the cortical bone is mechanical support. Trabecular (cancellous) bone consists of plates and bars of bone adjacent to small, irregular cavities containing marrows. Trabecular bone serves to reduce the skeletal weight but keep effective strength. The multiple surfaces of the trabeculae play an important role on bone remodeling (Netter F.H. 1987).

Vertebral cortical shell varies at each level of the spine, and the material property of vertebral cortex is also non-uniform in different sites at one vertebra (Figure 1-4)(Thomas Edwards W. et al. 2001; Schmidt H. et al. 2007). The thickness range from 0.25mm to 1.43mm as reported in (Thomas Edwards W., Zheng Y. et al. 2001). In addition, the different regions of a vertebral body have different thicknesses. Bone tissues at the vertebral body present high strength, while the posterior bony tissues are comparatively weak material(Schmidt H., Heuer F. et al. 2007). In general, the morphology of vertebral bone presents high non-linearity and depends on spinal level, anatomic site, age, gender, etc.
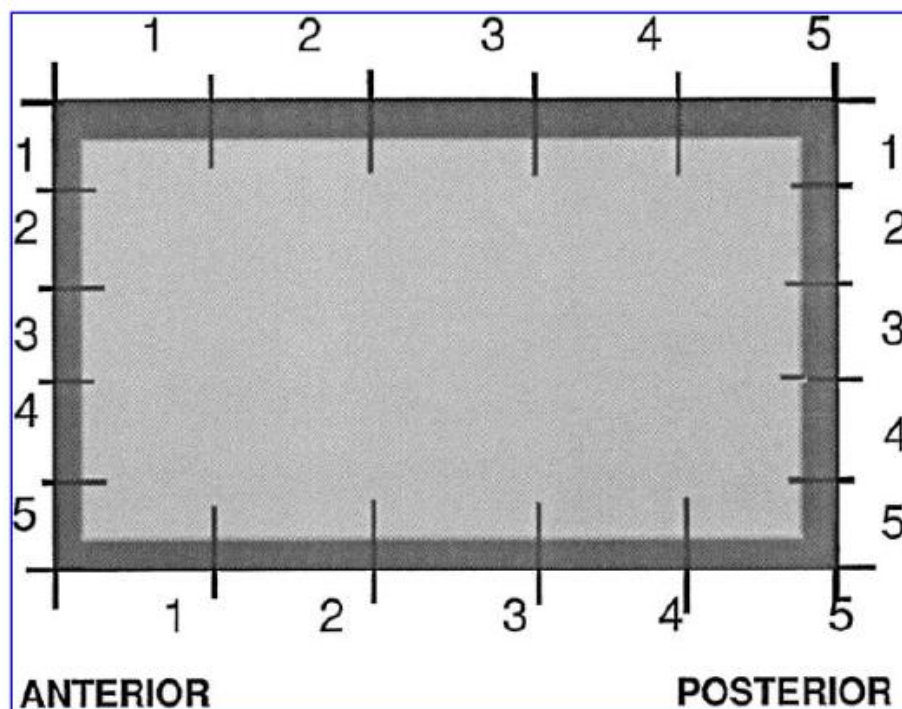
Figure 1-4 vertebral cortical shell present different thicknesses in different regions(Thomas Edwards W., Zheng Y. et al. 2001) (permission was approved)

- Bone cells

Bone tissues present complex, living, constantly changing properties, and bone development and maintenance is carried out by the cellular component (Buckwalter J.A. and Cooper R.R. 1987; Andreassen T.T. and Oxlund H. 2001). There are three kinds of cells involved in the bone development: osteoblasts, osteocytes and osteoclasts. Osteoblasts are bone-forming cells, and osteoclasts break down and reabsorb bone. Osteocytes are mature bone cells, which account for 90% of the human skeleton system (Sommerfeldt D.W. and Rubin C.T. 2001) .

❖ Osteoblasts

Ostroblasts are the cells with cuboidal shape and about 8 weeks of lifespan in human and located at the bone surface. These cells have functions for forming the extracellular matrix and regulate its mineralization, during which time it lays down 0.5-1.5 μm^3/day osteoids (Buckwalter J.A. and Cooper R.R. 1987; Price J.S. et al. 1994). The activities of osteoblasts are close related

to extensive cell-matrix and cell-cell contacts by some special proteins and receptors (growth factors) for maintaining the cellular function and responding to metabolic and mechanical stimuli. There is accumulating evidence that these cells are sensitive to the requirement of bone formation and direct the site of new bone apposition functionally(Buckwalter J.A. and Cooper R.R. 1987).

❖ Osteoclasts

Osterclast cells derived from hematopoietic stem cells with high migratory, multinucleated, and polarized properties. The main characteristic of these cells is to resorb fully mineralized bone. An activated osteclast is able to resorb 200,000μm³/day mineralized bone(Sommerfeldt D.W. and Rubin C.T. 2001; Zvi B.S. 2007).

❖ Osteocytes

Osteocytes derived from osteoblast but are distinctly different in morphology and function, and they are the most abundant cells in bone. As principal cells in adult bone, osteocytes are smaller in size than osteoblasts and have an increased nucleus to cytoplasm ratio (Buckwalter J.A. and Cooper R.R. 1987; Zvi B.S. 2007).

• Cartilaginous tissues

Cartilaginous tissue is a firm and elastic skeletal tissue. It consists of matrix and cells. The matrix contains chondroitin sulfate, a kind of ground substance, and fibers that bind with water. The cellular elements of cartilage are termed as chondrocytes which lie in spaces called lacunae and surrounded by the perichondrium fibrous. There are two basic forms of cartilage existing in the spine:

➢ Hyaline cartilage. A kind of cartilage with translucent matrix. It exists in the endplate and tips of the spinal processes. An important role of hyaline cartilage is to permit the growth.

➢ Fibrous cartilage: cartilage containing collagen fibers. It exists in the intervertebral disks.

1.3   Vertebra development

The vertebrae begin to develop in humans at 4 weeks after conception. The most important biological process during the development of the vertebral column is to create a flexible enclosure to allow continuous growth of the neural components developing slower and later (Sommerfeldt D.W. and Rubin C.T. 2001). The cartilaginous vertebrae are formed during embryo. During the vertebrae development, the cartilage are replaced by bone which is called bone ossification or bone stage development spanning from 7 weeks to 25 years (Sommerfeldt D.W. and Rubin C.T. 2001). There are three primary ossification centers in each cartilaginous vertebra: two for the vertebral arch and one for the body (Maat G.J. et al. 1996)(Figure 1-5). Before puberty, there are five secondary ossification centers generating: two for superior and inferior surfaces of the vertebral body (Figure 1-6), one on the tip of each transverse process, and one on the tip of the spinous process (Figure 1-7). These secondary centers fuse the rest of the bone about the age of twenty-five (Henry Gray F.R.S 1918). In addition, there are two cartilaginous growth plates located between the vertebral centrum and neural arch both on left and right sides (Figure 1-8). Those plates were termed as the neurocentral junction(NCJ), which is bipolar plate and contributes to the development of the vertebral body and the posterior neural arch (Vital J.M. et al. 1989; Yamazaki A. et al. 1998; Rajwani T. et al. 2005). The NCJ presents maximal activities at the age around 5-6 years when it shows the maximal contribution to the morphology of a vertebra. It is closed around 11-16 years during adolescent and could be identified as the boundary of the two ossification centers, the vertebral centrum and the neural arch (Vital J.M., Beguiristain J.L. et al. 1989; Maat G.J., Matricali B. et al. 1996; Yamazaki A., Mason D.E. et al. 1998; Rajwani T. et al. 2002).

There are two kinds of ossification: intramembranous and endochondral ossification (Cohen M.M.Jr. 2006).

- Intramembranous ossification
  This ossification involves the replacement of sheet-like connective tissue membranes with bony tissue, which is termed as intramembranous bones. Intramembranous ossification is

the characteristic way to form the flat bones of the skull and some of the irregular bones (Atchley W.R. and Hall B.K. 1991; Cohen M.M.Jr. 2006)

- Endochondral ossification

The endochondral ossification is the process of the replacement of hyaline cartilage with bone tissue, like for the development of the axial and appendicular skeleton (Cohen M.M.Jr. 2006).
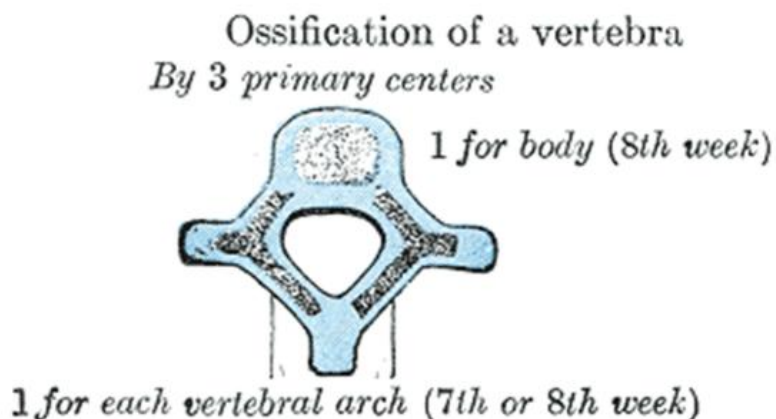
Figure 1-5 primary ossification centers of a vertebra (Henry Gray F.R.S 1918)
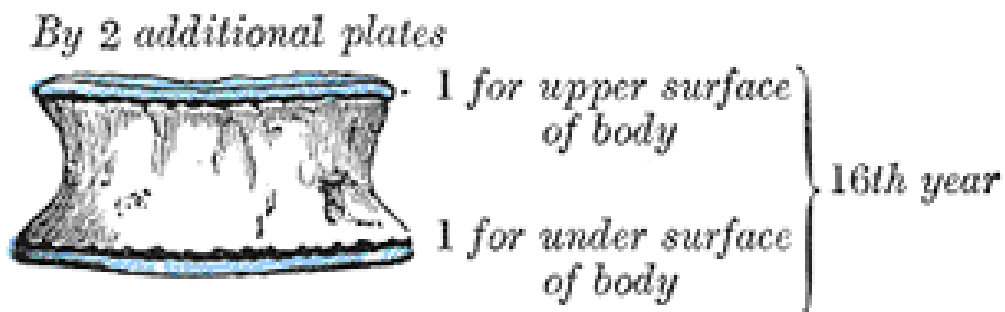
Figure 1-6 Two secondary ossification center on the surfaces of the vertebral body (Henry Gray F.R.S 1918)
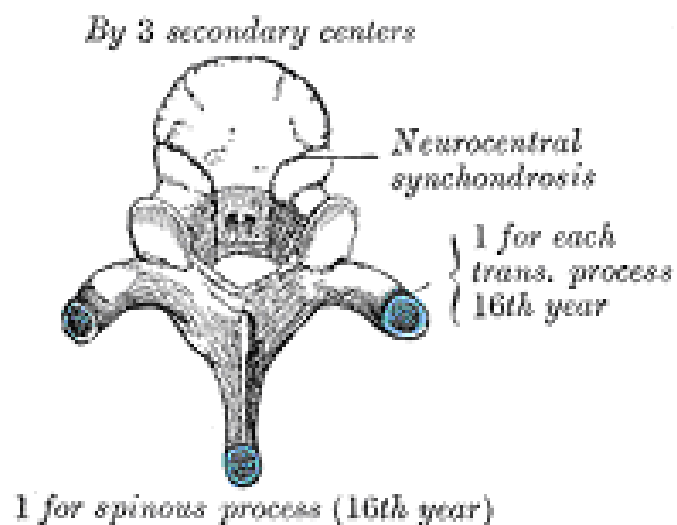
c

Figure 1-7 Three secondary ossification centers on the tips of verterbral processes (Henry Gray F.R.S 1918)
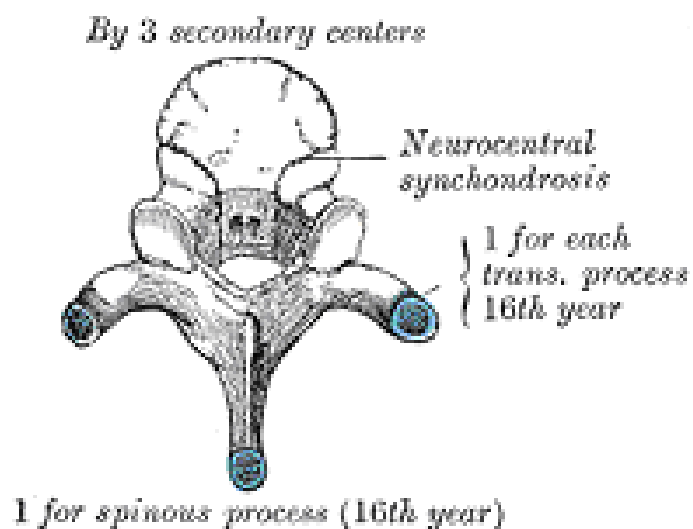
Figure 1-8 The position of the neuro-central junction (Henry Gray F.R.S 1918)

Bone development process includes bone growth, bone modeling and remodelling (Jee W.S.S. and Frost H.M. 1992; Doskocil M. et al. 1993; Cowin S.C 2004; Marotti F. et al. 2004).

Bone growth and modeling are able to control modification of bone length and geometry shape, while bone remodelling governing the bone losses during whole life-span(Jee W.S.S. and Frost H.M. 1992). Those developmental processes work together to determine the final shape and strength of bone and are affected by genetic and epigenetic factors(Carter D.R., Van Der Meulen M.C.H. et al. 1996; Ahmedi S.A.H. et al. 2009).

1.3.1   Vertebral bone growth

The vertebral bone growth takes on the characteristics of the general bone growth, which is the process with increase in number of osteoblasts, increase in amount of collagen molecules in extracellular matrix, and increase of the size of vertebral bone (Mao J.J. and Nah H.D. 2004). Growth in length is triggered by series of biological processes in the growth plate, where the cartilaginous tissues experience following courses: the cooperation of proliferation and hypertrophy of chondrocytes, calcification of the matrix, vascular invasion, and completion of endochodral bone formation. This process can be simplified as the course that cartilage grows and is replaced by bone by the process of proliferation, maturation, calcification and ossification of the cartilage (Wang Y. et al. 2004). Vertebral bone growth in the longitudinal direction is active during from infant to adolescent and takes place at a cartilaginous plate or cartilaginous endplate on each surface of a vertebral body (Doskocil M., Valouch P. et al. 1993; Price J.S., Oyajobi B.O. et al. 1994). This plate is the source for achieving cartilage growth and ossification. The process of bone growth is a similar process to endochondral ossification, which is the growth and replacement of cartilage by bone. The cartilage in this plate area continues to grow by mitosis and transform into chondrocytes. The chondrocytes next to the vertebral bone degenerate and ossify to form bone. This process continues throughout childhood and the adolescent years until the cartilage growth slows and finally stops. Usually, the cartilage growth stops in the early twenties. Normally, the epiphyseal plates on long bones of the skeleton, completely ossifies so that only a thin epiphyseal line remains and the bones no longer grow in length. In contrast, the vertebral cartilaginous endplates are not completely ossified even in adulthood and become a thin plate after growth stoping. (Doskocil M., Valouch P. et al. 1993). Although the genetics plays the most important role on skeletal growth rate, there are several factors affecting the bone growth, such as circulating hormones, nutritional intake, mechanical

load and disease. When a disruption occurs in normal cellular activity of growth plate chodrocytes and/or the cell of bone, this will disturb the bone growth(Leveau B.F. and Bernhardt D.B. 1984; Wang X. and Mao J.J. 2002; Cowin S.C 2004).

1.3.2   Vertebral bone modeling and remodelling

Living bone is continually changing its structure throughout the life due to the biological or the external environments change, while bone growth is stopped in the adulthood. Bone modeling and remodelling are two biological processes to describe those dynamic modifications of bone tissues. Unlike bone growth, which is related to cartilaginous tissues and bony tissues, bone modeling and remodelling only take place on the mature bone. Bone modeling carries out apposition of new bone on the existing bone surface without necessarily being preceded by resorption (Frost H.M. 1990; Frost H.M. 1994; Sommerfeldt D.W. and Rubin C.T. 2001). Bone remodelling is the alternation of bone shape, internal architecture, or mineral content of bone for adaptation of its overall structure to variations of external mechanical environments (Frost H.M. 1990; Cowin S.C. 1993). Bone remodelling includes two processes: deposition and resorption. Four types of bone cells are involved in bone remodeling: osteoblast, osteocytes, osteoclasts and bone lining cells (Buckwalter J.A. and Cooper R.R. 1987; Jacobs C.R. et al. 1997; Cowin S.C 2004; Ahmedi S.A.H., Rouhi G. et al. 2009).

Bone modeling is carried out by active osteoblasts, which deposit new bone on the external bone surface. This process is similar to the process of intramembranous ossification and able to increase the size of bone and make bone bulky. The process for increasing in the thickness or diameter of bone is a kind of bone modeling. This process is similar to the intramembranous ossification. Osteoblasts in the periosteum form compact bone around the external bone surface. At the same time, osteoclastes in the endosteum break down bone on the internal bone surface around the medullary cavity. Bones become bulky and heavy after ossification (Kashii M. et al. 2008). Bone remodelling presents two biological modes: internal remodelling and external remodelling. The internal remodelling is able to change bone histology. During internal remodelling processes, secondary osteons are generated by resorption of the pre-existing bone and formation of new bone tissues. The internal remodeling replaces the primary

bone by carrying out the deposition and resorption throughout the life. The external remodelling is for the modification of bone architecture, such as bone geometry and form.
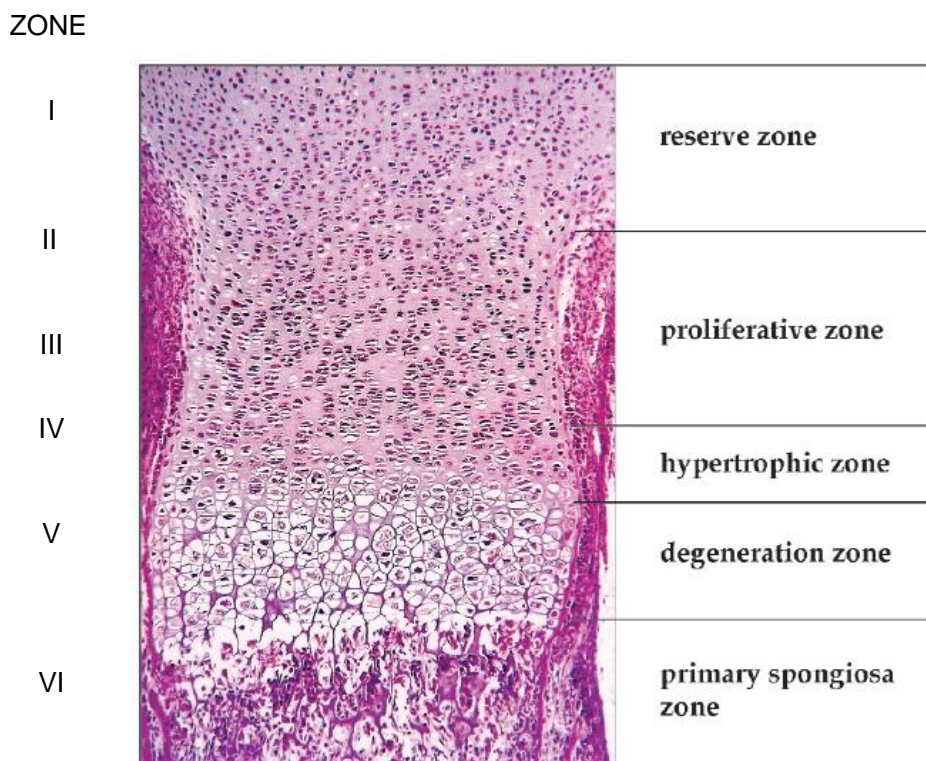
ZONE

Figure 1-9 Different zones of a typical growth plate of a long bone (Burdan F. et al. 2009) (permission was approved)

The bone of a healthy adult keeps balance between bone deposition and resorption, and thus keeps the stable bone mass that is termed homeostasis. The phenomenon of homeostasis implies that adaptive bone remodeling occur in the whole life. Adaptive bone remodeling can be regarded as a process driven by external stimuli, which could come from the mechanical load. When the mechanical load is high enough, the remodeling occurs, while the low load does not affect the bone. Actually, the mechanisms for regulating the remodeling process are unknown. However, it is undoubted that physical factor and the effects of calcium regulation hormones involve the local regulation (Buckwalter J.A. and Cooper R.R. 1987; Sommerfeldt D.W. and

Rubin C.T. 2001; Wang X. and Dumas G A. 2002; Zhu X. et al. 2002; Ruimerman R. 2005). During the process of remodeling, the osteoclasts are attracted by the bone damage caused by the mechanical loads, and the resorption process occurs. After the lacunae are formed, the osteocytes are sensitive to the damage and transmit a chemical signal for recruiting osteoblasts. And the deposition process occurs in the lacunae. As a result, the cavity was filled again, and the bone still keeps homeostasis. Bone development is the repeating processes of modeling and remodeling for maintaining homeostasis of skeleton structure.

1.3.3   Biological structure of the growth plate

Growth in length occurs in the growth plate located on the endplates of a vertebra, where it is the site of the secondary ossification center (Ballock R.T. and O'Keefe R.J. 2003)(Figure 1-6). The endplate, growth plates on vertebral sufaces, on the vertebral body presents the same physiological structure as long bones, where it forms epiphyseal cartilages (Doskocil M., Valouch P. et al. 1993). The vertebra can be considered as a long bone from the point of view of its growth. The epiphyseal growth plate is composed of three kinds of tissues: the cartilage, the bony tissue, and the fibrous tissue that surrounds the growth plate (Price J.S., Oyajobi B.O. et al. 1994). The chondrocyte morphology changes along the longitudinal direction of the growth plate, and thus different sections are formed (**Figure 1-9**)(Price J.S., Oyajobi B.O. et al. 1994). The growth plate can be divided into a series of anatomic zones with different cell morphologies and biochemical stages on the process of the chondrocyte differentiation(Ballock R.T. and O'Keefe R.J. 2003). The cell population in each zone is part of a different stage of maturation in the endochondral sequence. The description of cell population in growth plate was based on the cell size, shape and contents, and according to cells morphology, researchers assumed the function of the cells (Ballock R.T. and O'Keefe R.J. 2003). The growth plate cell biology presents different properties in its different zones(**Figure 1-9**):

- **Zone I** This zone has been described as the reserve or resting zone. Cells in this zone exist singly or in pair separated by an abundant extracellular matrix. They have low rates of proliferation. However, these cells have a high lipid body and vacuole content

- **Zone II** This zone is described as the upper proliferative or columnar region. The function of this zone is matrix production and cell division. This results in the longitudinal growth of bone. The cells in this zone divide actively.

- **Zone III** This zone is similar to zone II. It is under the zone II and it is a more mature region than the proliferating zone.

- **Zone IV** This zone is the upper hypertrophic zone. The size of the cells in this zone increases significantly. But the columnar arrangement is less regular. Hypertrophic chondrocytes are active cells in the metabolism.

- **Zone V** this zone is degeneration zone. The chondrocyte cells die by apoptosis. **Zone VI** This zone is the junction of the growth plate with the bone. It is the area where the transition from cartilage to bone takes place.

Vertebral growth plates present different morphological characteristics at different anatomic sites and material properties at each spinal level. The vertebral endplate, the growth plate on vertebral inferior or superior surfaces, is geometrically described as a central porous region surrounded around the perimeter by an annular rim with dense tissues(Grant et al. 2001). It was reported that the central part of the endplate has weak stiffness and strength compared with the peripheral sites. In addition, the thickness of the endplate also varies at each spinal level and anatomical sites. The published measurement for adult vertebra reported that the thickness of endplate on a lumbar vertebra could be different at superior and inferior sides. Similarly, the thickness of anterior and posterior sides ranged from 0.39mm to 0.90mm(Grant, Oxland et al. 2001).

1.4 Mechanobiology of bone growth

1.4.1 Concept of mechanobiology

It is recognized that skeletal development, including vertebral development, was closely related to mechanical environments(Leveau B.F. and Bernhardt D.B. 1984; Cowin S.C. 1993; Van Der Meulen M.C.H. and Huiskes R. 2002; Cowin S.C 2004; Wang J.H.C. 2006).

Mechanobiology is defined as the biological processes regulated by signals to cells generated by mechanical loading(Van Der Meulen M.C.H. and Huiskes R. 2002). Mechanobiology is specially tied with mechanical factors. Mechanical loading modulates morphological and structural fitness of the skeletal tissue: bone, cartilage, ligament and tendon(Eckstein F. et al. 1997; Silver F.H. and Bradica G. 2002; Wong M. and D.R. 2003). The research of mechanobiology focuses on investigating the biological process of load-bearing tissues modulation for response to biophysical stimuli(ESB 1978; Van Der Meulen M.C.H. and Huiskes R. 2002).

Skeletal mechanobiology has been studied over hundred years by observing the bone structure under mechanical environments (Frost H.M. 1994; Huiskes R. 2000). Trajectorial and mathematical methods were used for explaining the bone histology at the early stage of the mechanobiological study(Huiskes R. 2000). Wolff's law is one of the most significant findings in mechanobiological research. This law indicates that the modification in the form and the function of a bone, or in the function of the bone alone, results in changes of its internal architecture and external form(Wolff J. 1986). Wolff's law is widely quoted by numerous researches and regarded as a basic theory on mechanobiological studies(Frost H.M. 1990; Frost H.M. 1990). Another important finding is the Hueter-Volkmann's law, which classified the relationship between mechanical loads and bone growth(Mahlman C.T. et al. 1997). The Hueter-Volkmann's law indicates that the increased pressure retards growth and decreased pressure stimulates growth(Willy C et al. 2008). Wolff's law and Hueter-Volkmann's law describe the mechanical influence on bone development. Wolff's law concerns bone modeling and remodeling for both children and adult skeletal systems, while Hueter-Volkmann's law focuses on bone growth for unmatured bone(Frost H.M. 1990; Frost H.M. 1990; Mahlman C.T., Araghi A. et al. 1997). Mechanobiology occurs at tendon, cartilage, bone, and other kinds of skeletal tissues, which are involved in skeletal development(Van Der Meulen M.C.H. and Huiskes R. 2002; Wang J.H.C. 2006). The mechanobiological process of vertebral tissues also presents same characteristics as the general skeletal tissues. Lots of external factors, such as the daily exercise, disusing or overusing the tendon or bone, are able to result in the mechanoregulation(Wang J.H.C. 2006). Although mechanical force is considered as general stimuli to trigger the generation and

modification of skeleton tissues, the real mechanobiological process still is not clear, as well as the real nature of the growth modulation stimuli (stress, strain, energy, etc.).

1.4.2   Mechanobiological processes

Bascially, the mechanobiological process includes the mechanosensing, mechanotransduction, and mechanoregulation. Mechanosensing process generate messenger pathways within the cell by conformational changes of cellular components (Silver F.H. and Siperko L.M. 2003).The mechanotransduction is the process by which cells convert mechanical stimuli into biochemical signal (Alenghat F.J. and Ingber D.E. 2002). Mechanoregulation is the cellular response of the skeletal tissues to the mechanical stimuli and present in the modulation on histology and geometry of those tissues (Wu Q.Q. and Chen Q. 2000; Nowlan N.C. and Prendergast P.J. 2005). The mechanobiological process is difficult to be observed because several tissues are included in this process and it is a slow transformation process(Wu Q.Q. and Chen Q. 2000). Currently, the developing technologies in biology allow the experimental study of mechanobiolgy and thus to develop theoretical models contributing to mechanobiological investigation(Katsumi A. et al. 2004).

Davies et al (Davies P.F. and Tripathi S.C. 1993) indicated that force transduction mechanism exist in endothelial cells and mechanical loading alter the structural and functional properties of cells at the cellular, molecular, and genetic levels, which can be considered as mechanotransduction. . Some published literatures figured the osteocytes were the mechanosensory cells of bone in the bone mechanotransduction (Nijweide P.J. et al. 2002; Klein-Nulend J. et al. 2005). There were four reported possible ways for generating cell signal induced by mechanical loading during mechanotransduction: direct contact, diffusible molecules, gap junctions, and imposed tensions and pressures (Figure 1-10). An important finding for identifying the mechanism of mechanobiology was that compressive stress is capable of generating cellular signal by binding the growth factor and receptor of cells(Tschumperlin D. et al. 2004). A published experimental study found the mechanobiological influence induced by distraction, which is able to modify the osteogenesis(Loboa E.G. et al. 2004). The hormones on bone growth were also affected by the mechanical environment and contributed to the modulation

of growth, which was a mechanobiological process(Wertz X. et al. 2006). It was reported that different loading conditions, such as tension and compression, would result in different mechanotransduction, because the different signaling molecules, which were able to further alter the gene expression, were generated by different mechanical environments(Henderson J.H. and Carter D.R. 2002).

Published studies reported that the mechanoregulation resulting from mechanosensing and mechanotransduction was possible to play a negative role in the optimization of skeletal phenotype(Nowlan N.C. and Prendergast P.J. 2005). This finding seemed to be in disagreement with the evolution theory accepted by most biologists. As known, evolution could be a process that form follows the function. However, it was not clear that evolution definitely optimized tissue formation. Whether the causality existed in the relation between mechanoregulation and optimal process should be further studied.

It was reported that several cellular components, such as extracellular matrix(ECM), cytoskeleton, were involved into the mechanotransduction (Wang J.H.C. 2006). Wong's research not only described the function of several cell components to mechanotransduction but also developed a detailed model for explaining the pathway of the mechanotransduction mechanism (Wong M. and D.R. 2003). It was clear that mechanotransduction was not dependent on one kind of cell and organ. To date, the exact mechanism of mechanobiology was not clear. (Van Der Meulen M.C.H. and Huiskes R. 2002; Wong M. and D.R. 2003; Wang J.H.C. 2006).
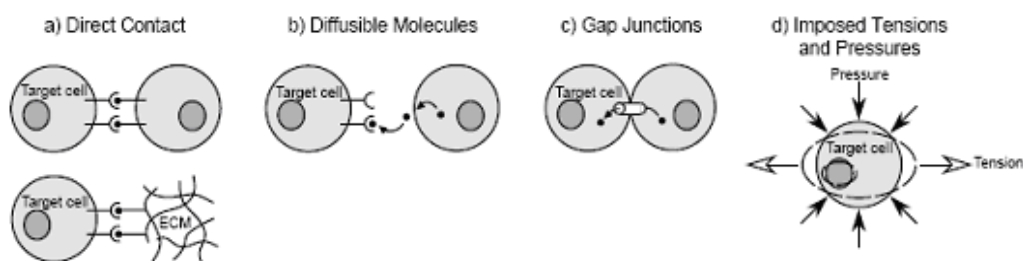
Figure 1-10 Four possible ways for inductive signal transmitting to target cells during mechanotransduction(Henderson J.H. and Carter D.R. 2002) (permission was approved)

The mechanoregulation result mechanobiological growth, mechanobiological modeling, and mechanobiological remodeling(Frost H.M. 1990; Frost H.M. 1990; Lieberman D.E. et al. 2003; Ahmedi S.A.H., Rouhi G. et al. 2009). The mechanobiological growth include the modification of cartilage growth and ossification, which are involved in bone growth(Wang Y., Middleton F. et al. 2004). The mechanobiological modeling and remodeling regulate the activities of bone cells existing in ossified bone and finally modulate the geometry and architecture of bone(Frost H.M. 1990; Frost H.M. 1990).

1.4.3 Mechnobiological growth

1.4.3.1 Mechanism of the mechanobiological growth

Mechanobiological growth is the biological process whereby bone growth is modulated by mechanical loading (Beaupre G.S. et al. 2000; Shefelbine S.J. and Carter D.R. 2004). Several authors refer to this phenomenon as the Hueter-Volkmann law(Bonnel F. et al. 1984; Stokes I.A.F. et al. 1994; Mehlman C.T. et al. 1997; Lerner A.L. et al. 1998), which states that increased pressure on the plates retards bone growth and, conversely, reduced pressure or tension accelerates it. As longitudinal growth, mechanobiological growth in length of vertebrae occurs in the growth plate, located at the superior and inferior vertebra sides. The cartilaginous growth plate presents high biological activities during the childhood and adolescent (Price J.S., Oyajobi B.O. et al. 1994). Mechanobiological growth plays an important role on the development of skeletal systems and is closely related to some skeletal diseases that are caused by abnormal growth, such as scoliosis (Villemure I. 2000; Villemure I., Aubin C. E. et al. 2002; Shefelbine S.J. and Carter D.R. 2004). It is reported that mechanical loads modulate proliferation and hypotrophy of chondrocytes as well as the ossification of cartilage(Castagnola P. et al. 1988; Chen Q. et al. 1995; Wu Q.Q. and Chen Q. 2000). These multiple stages finally change the growth rate and basically include three steps. First, chondrocytes are active in proliferation, which results in the increase of cell number of cartilage. The involvement of mechanical stimuli alters the normal biological running on proliferation(Stokes I.A.F., Clark K.C. et al. 2007). Second, the hypertrophic chondrocytes are able to increase the cartilage volume and thus result in growth of cartilage. The external mechanical load is capable of modulating the size of

hypertrophy and contributes to the growth modulation in terms of experimental observation (Stokes I.A.F., Clark K.C. et al. 2007). At the third stage, both proliferation and hypertrophy of chondrocytes ceased. The chondrocyte undergoes apotosis, the programmed cell death. Mechanical stimuli also present influence at this stage that the ossification rate is altered(Beaupre G.S., Stevens S.S. et al. 2000). The detailed mechanism of these stages have been difficult to study because the mechanobiological growth process present high complexities(Wu Q.Q. and Chen Q. 2000; Villemure I. et al. 2005). Experimental methods are employed for testing the assumption of mechanobiological growth and for finding the quantitative relationship between mechanical stimuli and growth.

Mechanical energy was reported as the stimulus of mechanobiology(Robling A.G. and Turner C.H. 2009). Silver indicated that daily locomotion triggers energy storage and dissipation that change cartilage structure and function by mechanochemical transduction (Silver F.H. and Bradica G. 2002; Freeman J.W. and Silver F.H. 2004). He also described the detail process of energy-based mechanosensing and mechanochemical transduction which would play an important role on vertebrate development (Silver F.H. and Bradica G. 2002; Silver F.H. and Siperko L.M. 2003; Freeman J.W. and Silver F.H. 2004). Carter et al. hypothesized that mechanical energy is the stimulus triggering the modification of endochondral ossification (Carter D.R. and Wong M. 1988). They also proposed that energy can be transferred in biological tissue to regulate the biological remodeling, growth and maintenance of bone (Carter D.R. et al. 1987).

1.4.3.2 Experimental studies of mechanobiological growth

Numerous experimental studies and clinical observations on mechanobiological growth have been published for further identifying the mechanism of this modulation process. The mechanical loads employed in experiments include the axial and non-axial forces. The mechanobiological contribution of axial loading, such as tension and compression, was studied by most experiments. The growing animal is used for testing the mechanobiological influence. Stokes et al observed the modification of proliferation and hypertrophy of chondrocytes in growth plates of immature animals (rat, rabbits, calves) (Stokes I.A.F. et al. 2002; Stokes I.A.F.

et al. 2005; Stokes I.A.F., Aronsson D.D. et al. 2006; Stokes I.A.F., Clark K.C. et al. 2007). Those animal experiments were used to quantitatively model the relationship between mechanical loads and growth. Experimental studies also investigated the impact by static and dynamic tension and compression (Lerner A.L., Kuhn J.L. et al. 1998; Robling A.G. et al. 2001). Those experiments found that both dynamic and static loads were able to modulate growth and the magnitude of applied loads determined the modulation rate of growth. The mechanobiological effect of shear loads, the non-axial loads, also was studied using animal experiements. It was found that shear stresses were capable of modifying endochodral ossification, which is an important step of bone growth, as well as growth plate morphology(Moreland M.S. 1980; Carter D.R. and Wong M. 1988; Carter D.R. and Wong M. 1988; Schwartz L. et al. 2003). Experimental studies investigated mechanobiological impact of hydrostatic pressure, a special pressure applied along the normal directions of the surfaces of tissues. It was observed that hydrostatic pressure suppressed the chondrocyte differentiation and maintained the cartilage in a growth plate. Those observations suggested the retarded role of this pressure on growth (Toshikazu K. et al. 1998; Wong M. et al. 2003). Experimental studies are listed in Appendix A.

By comparison, a few physical experiments investigated mechanobiological impact of non-axial loading. Moreland's experiment used the torsion to test the modification of the growth plate morphology, but the growth modulation was not further observed(Moreland M.S. 1980). It was reported that shear stresses were able to promote cartilage ossification(Carter D.R. and Wong M. 1988). This mechanobiological role can be presented in growth modulation and bone remodeling. Experimental studies of the effect of shear stresses to bone cells reviewed in Table 1-1 presents the experimental studies of shear stresses on bone growth.

The published experiments listed in Table 1-1 concluded about the mechanobiological influence of the shear stress at cellular level. No quantitative model has been developed to describe mechanobiological contribution of shear stresses to bone growth.

Table 1-1 Effects of shear stress on skeletal development

Authors	effects of shear stress
(Li Y.J. et al. 2004; Rubin J. et al. 2006) put the names	Shear stresses are able to change the osteoblast cells number during bone formation
(Norvell S.M. et al. 2004; Batra N.N. et al. 2005)	Shear stresses affect biochemical activities of osteoblast, such as anabolism.
(Kim C.H. et al. 2006)	Shear stresses affect biochemical activites of osteoblasts and osteoclasts and may result in positive remodeling
(Smalt R. et al. 1997; McAllister T.N. and Frangos J.A. 1999; Klein-Nulend J., Bacabac R.G. et al. 2005; Ponik S.M. et al. 2007)	Osteoblastic cells are able to sense the mechanical loading by Shear stresses. The shear stress is able to change the biochemical activities of osteoblasts and osteocytes and thus potentially induced bone remodelling.
(You J. et al. 2001)	Shear stresses are considered as biophysical stimulus in the regulation of bone cell metabolism.

1.4.3.3 Analytical modeling techniques

Quantitative models for mechanobiological growth are investigated for further simulating this biological process, which could be a slow and long-time-span procedure. Analytical models of mechanobiological growth have been developed based on two approaches: experiment-based modeling and theoretical modeling. The representative model of experimental approach is the Stokes's model, and the Carter's model represents the theoretical modeling technique (Carter

D.R. and Wong M. 1988; Stokes I.A.F. and Laible J.P. 1990; Stokes I.A.F., Aronsson D.D. et al. 2006).

Numerous experimental studies investigated the mechanobiological effect of axial loading to the bone growth for fomulizing the Hueter-Volkmann Law and quantifying the relationship between axial loads and mechanobiological growth(Arkin A.M. and Katz J.F. 1956; Stokes I.A.F., Aronsson D.D. et al. 2006). Those experiments mainly measure the morphology change of the growth plate, where the longitudinal growth takes place (Price J.S., Oyajobi B.O. et al. 1994; Stokes I.A.F., Mente P.L. et al. 2002). It is reported that the axial loading was able to modify the height of the hypertrophic zone and the size of the chondrocytes and thus alter the growth rate(Stokes I.A.F., Mente P.L. et al. 2002). According to the reported mechanobiological effect of axial loading, a quantitative expression for the biological process of mechanobiological growth can be written as(Stokes I.A.F., Gwadera J. et al. 2005):

$$\text{Growth= New cells/day} \times \text{Final height}$$

(1-1)

Where the overall growth is determined by the proliferation that generates new cells and the hypertrophy of chondracytes that increase the size of cells. An approximate expression of mechanobiological growth without considering the extracellular matrix between the chondrocyte cells can be written as:

$$\Delta\text{growth}=\Delta\text{new cells/day}+ \Delta\text{Final height}$$

(1-2)

The experimental measurement is used for determining the additional or reduced growth rate under either compression or tension. According to the experimental measurements, Stokes and Laible (Stokes I.A.F. and Laible J.P. 1990)hypothesized a linear relationship between compressive or tensile stresses and mechanobiological growth rate, in which growth plate stresses perpendicular to the growth plates are acting as mechanical stimuli to bone growth. Stokes's model is a simplified mathematical formulation of the Hueter-Volkman principle. It was developed from experimental work on the relationship between mechanical modulation and bone growth rates in response to compressive or tensile stresses(Stokes I.A.F. and Laible J.P. 1990). It is expressed as:

$$\Delta\varepsilon_l = \Delta G_l(1+\beta_l\sigma_{zz}) \tag{1-3}$$

where the z-axis represents the longitudinal direction perpendicular to the growth plate. The resulting growth strain increment $\Delta\varepsilon_l$ (month^{-1}) is expressed as the contribution of the baseline (normal) longitudinal growth increment ΔG_l (month^{-1}) and a mechanically modulated growth increment $\Delta G_l\beta_l\sigma_{zz}$ (month^{-1}). The latter is evaluated based on the sensitivity factor β_l (MPa^{-1}) to the mechanical stimulus, which is hypothesized as on the stress σ_{zz} (Dumas R. et al.) along the longitudinal direction. .

In this model, axial stresses produced by the external mechanical environment on the growth plate, or their variations with respect to a homeostatic condition, are used to determine the resulting modulated growth strain increment $\Delta G_l\beta_l\sigma_{zz}$. The latter is then added to the baseline growth to evaluate the resulting growth strain increment $\Delta\varepsilon_l$. The sensitivity factor β_l is determined from experimental data and is considered independent of the external environment.Stokes's model also considered the non-uniform distribution of the mechanical loads due to inhomogeneous morphology and composition of growth plate, which was observed in experiments (Stokes I.A.F., Aronsson D.D. et al. 2006; Villemure I. et al. 2007).

Villemure et al used Stokes's model to investigate the biomechanical process of growth and deformities of scoliosis(Villemure I., Aubin C. E. et al. 2002; Villemure I., Aubin et al. 2004). This model has been integrated in a beam finite element model of the thoracic and lumbar spine to simulate asymmetrical growth of the rib cage and/or vertebrae (Stokes I.A.F. and Laible J.P. 1990; Villemure I., Aubin C. E. et al. 2002; Carrier J., Aubin C. E. et al. 2004; Villemure I., Aubin et al. 2004). This model has also been integrated in a solid vertebral model to simulate the progression of scoliosis induced by the biomechanical growth modulation(Stokes I.A.F. 2007). Subsequently, the neurocentral junction growth also used this model for studying the role of development of this anatomical part on AIS(Huynh, Aubin C. E. et al. 2007). The deformity of thorax also was studied using this model(Carrier J., Aubin C. E. et al. 2004).

Stokes' model was widely used on investigation of AIS because of the following reasons: (1) this model formulized the Hueter-Volkmann law; (2) numerous animal experiments supported this model and were used to determine the model parameters; (3) using this model on the prediction of the progression of scoliosis obtained helpful conclusions for finding mechanism of adolescent idiopathic scoliosis (AIS) and provided AIS with potential optimization of management. However, it should be noted that the Stokes's model used a finite element model of the spine mainly composed of beam elements. An important characteristic of the Stokes's model was that only axial stresses were taken into account.

Carter et al. proposed a theoretical relationship between bone growth, which incorporated the endochondral growth and ossification, and mechanical loading based on the physiological observations of the ossification of the hand in a 32-month-old child (Carter D.R. and Wong M. 1988; Stevens S.S., Beaupre G.S. et al. 1999; Beaupre G.S., Stevens S.S. et al. 2000). In this approach, mechanobiological growth is associated with cartilage maturation rate, which incorporated cartilage growth and ossification. Bone maturation rate includes the biological maturation rate and mechanobiological modification rate. A simplified maturation model was proposed (Stevens S.S., Beaupre G.S. et al. 1999):

$$\dot{M}(t) = b \times \dot{M}_B(t) + c \times \dot{M}_M(t) \tag{1-4}$$

Where $\dot{M}(t)$ is the overall maturation rate. $\dot{M}_B(t)$ is the biological maturation rate and $\dot{M}_M(t)$ is the mechanobiological contribution to the maturation rate. The biological maturation rate is a natural process depending on age. The mathematical model can be expressed as:

$$\dot{M}_B(t) = \dot{M}_B(M, t) \times F(t) \tag{1-5}$$

The biological maturation rate is proportion to the current maturity M and relative growth rate function $F(t)$. The mechanobiological contribution to maturation rate is a linear combination of maximum octahedral shear stress σ_s and minimum hydrostatic stress σ_h in dynamic load situations:

$$\dot{M}_M(t) = \dot{M}_M(\sigma_s, \sigma_h) = \max(\sigma_s) + 0.35\min(\sigma_h) \tag{1-6}$$

Octahedral shear stress is physically defined as a distortional stress that is able to induce distortion of a tissue shape, while hydrostatic stress terms as dilatational stress that is capable of modification of a tissue volume (Carter D.R. and Wong M. 1988; Carter D.R. and Wong M. 1988). Bone growth model based upon the bone maturation can be expressed as:

$$\dot{\varepsilon} = \frac{d}{dt}(\Delta l/l) = a \times \dot{M} \tag{1-7}$$

Where $\dot{\varepsilon}$ is the overall growth rate, which is the first derivation of the relative length variation rate: $\Delta l/l$. l is the length of bone and Δl is the value of length increase. a is the coefficient. Same as Stokes' model, the overall growth rate is the sum of the biological or baseline growth rate and the mechanobiological contribution rate (Stevens S.S., Beaupre G.S. et al. 1999; Shefelbine S.J. and Carter D.R. 2004; Shefelbine S.J. and Carter D.R. 2004).
It is expressed as:

$$\dot{\varepsilon} = \dot{\varepsilon}_b + \dot{\varepsilon}_m \tag{1-8}$$

where $\dot{\varepsilon}_b$ (month[-1]) is the biological growth rate or baseline normal growth rate, $\dot{\varepsilon}_m$ (month[-1]) is the mechanobiological growth, and $\dot{\varepsilon}$ (month[-1]) is the growth rate resulting from both biological and mechanical contributions. In this model, mechanobiological growth $\dot{\varepsilon}_m$ is further represented by:

$$\dot{\varepsilon}_m = a\sigma_s + b\sigma_h \tag{1-9}$$

where σ_s (Dumas R., Le Bras A. et al.) is the shear stress, σ_h (Dumas R., Le Bras A. et al.) is the hydrostatic stress and parameters a and b ($MPa^{-1}month^{-1}$) are empirical sensitive factors associated to shear and hydrostatic stresses respectively. Under mechanical loading, the

mechanobiological growth rate is hypothesized to be determined by octahedral shear stress and hydrostatic stress. Octahedral shear stress was physically defined as distortional stress able to induced distortion of a tissue shape, while hydrostatic stress , also termed dilatational stress that was capable of modification of a tissue volume(Carter D.R. and Wong M. 1988; Carter D.R. and Wong M. 1988) . In this model, it is hypothesized that the greater the shear stress, the faster the ossification, and the smaller the hydrostatic pressure, the faster the ossification (Carter D.R. and Wong M. 1988; Carter D.R. and Wong M. 1988; Stevens S.S., Beaupre G.S. et al. 1999). This model was used to simulate developmental hip dysplasia with the femur model (Shefelbine S.J., Tardieu C. et al. 2002; Shefelbine S.J. and Carter D.R. 2004).

In this model, it is assumed that bone growth rate is closely related to bone ossification rate. This model does not include a direct relationship between stresses perpendicular to the growth plate and the resulting longitudinal growth rate. Growth modulation rather depends on stresses in all directions, which are represented in terms of octahedral and hydrostatic stresses. This model was integrated in 3D solid finite element models to simulate bone growth and ossification in long bones and pelvis under static loadings (Shefelbine S.J., Tardieu C. et al. 2002; Shefelbine S.J. and Carter D.R. 2004; Shefelbine S.J. and Carter D.R. 2004). In these studies, strain increments were used to determine changes in the bone geometry and ossification patterns within the bone tissue.

As above mentioned, the Carter's model involves octahedral shear stress and hydrostatic stress. This model has been integrated in finite element models of the proximal and distal femur to predict developmental hip dysplasia and femoral bicondylar angle (Shefelbine S.J., Tardieu C. et al. 2002; Shefelbine S.J. and Carter D.R. 2004; Shefelbine S.J. and Carter D.R. 2004) due to the longitudinal growth of the femur. However, it was not used for the spine.

There is no study to investigate differences or similarities of those two modeling techniques on growth. Although it was found that the progression of scoliosis was associated with mechanobiological growth triggered by axial stresses via Stokes`s model, the mechanobiological influence from non-axial stresses on the progression of scoliosis has not been studied.

1.5   Scoliosis

1.5.1   General review

Scoliosis is a three dimensional deformity of the spine and geometrically appreciable lateral deviation in the normally straight vertical line of the spine(Reamy B. and Slakey J.B. 2001; Maried N.E. 2003; Goldberg C.J., Moore D.P. et al. 2008), with abnormal deformation and torsion between and within vertebrae as well as rotation in the transverse plane (Aubin C. E. et al. 1998; Leborgne P. and Aubin C. E. 1998; Petit Y. et al. 2004). Scoliosis is present in 1.5 to 3 percent of population(Lonstein J.E. 1994). In 80% of patients, the cause of scoliosis is unknown(Reamy B. and Slakey J.B. 2001). These cases are called idiopathic and most have a genetic basis and usually develop in middle or late childhood (Lonstein J.E. 1994). Most curves can be treated if they are detected before they become too severe. However, the curvatures in prepubertal children will likely progress. Scoliosis treatment basically includes observation, bracing and surgery. Observation is applied on the patient with low severity of curve. Children or adolescent with the progression of scoliosis are recommended of bracing. Surgery is involved for the patients with severe curvatures.

1.5.2   Scoliosis assessment

The X-rays are basic imaging techniques to perform the assessment. After establishing the image of spine, the physicians measure the curve severity using the Cobb method. The measurement of the Cobb angle is done between the superior endplate of the proximal end vertebra and the lower endplate of the distal end vertebra of a scoliotic segment. (Figure 1-11). It was reported that progression would present for a spine with curvature over 20 degrees(Cobb angle) on post-anterior planes(Dickson R.A. 1996). Another measurement was trunk rotation that defined the angle of thoracic inclination(Bunnell W.P. 1984). Correction was required fro a spine with trunk rotation over 5 degrees because of the progression(Bunnell W.P. 1984).
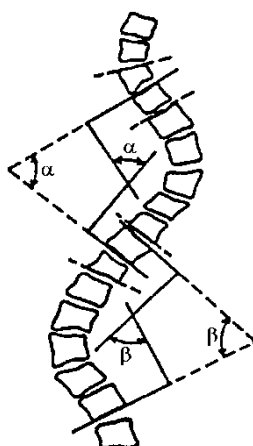
Figure 1-11 Cobb angle measurement

1.5.3   Morphology of scoliotic vertebrae

It is believed that the abnormal vertebral growth, modeling, and remodelling, significant influenced the morphology modification that was able to developed as scoliotic vertebrae (Porter R.W. 2001; Villemure I., Aubin C. E. et al. 2002; Guo X., Chau W.W. et al. 2003; Stokes I.A.F. 2007; Van der Plaats A. et al. 2007; Charles Y P et al. 2008; Day G et al. 2008). The vertebra morphological change involves vertebral wedging, neural arch length, vertebral torsion, etc. No uniform method for the measurement is used in the published studies, and geometric parameters for representing vertebral morphologies also have different definitions (Parent S. et al. 2004; Masharawi Y. et al. 2008).

Vertebral wedging is the angle between the endplates of the vertebral body (Figure 1-12). Wedging angle can be measured from patients' radiography images. However, the wedging presents 3D characteristics with different values under various observing viewpoints(Aubin C. E., Dansereau J. et al. 1998). A scoliotic vertebra displays significant wedging angle observed from the coronal plane due tothe variation of height of vertebra body, where the height of convex side is relatively greater than that of the concave side (Parent S. et al. 2002; Parent S., Labelle et al. 2004). Wedging in the sagittal plane is naturally found from the physiological sagittal curves, but pathological sagittal wedging was not found in the published measurements on scoliotic vertebrae (Parent S., Labelle et al. 2004) . Wedging angles also exist in the intervertebral discs. It is

reported that wedging in disc and vertebral body is increasing with the progression on scoliosis(Modi H.N. et al. 2008). Furthermore, in the thoracic region, the vertebral body has higher wedging angle than disc, while wedging is more in disc than body in the lumbar region (Stokes I.A.F. and Aronsson D.D. 2001; Modi H.N., Suh S.W. et al. 2008).

Assymetry of pedicles is also reported by several published studies. The pedicle width is significantly thinner on the concave side, and the dural sac is shifted toward the concave side of a scoliotic spine(Liljenqvist U.R. et al. 2002; Parent S., Labelle et al. 2002; Catan H. et al. 2007). The length of pedicle is also significantly asymmetric in scoliotic vertebrae; however, the longer pedicle is not invariably on the convexity or the concavity, while normal healthy vertebrae have longer pedicle on the left side (Rajwani T. et al. 2004). It is suggested that the pedicle thinning is secondary to the spinal cord beating on the concavity (Parent S., Labelle et al. 2002). The Roth-Poter hypothesis indicated that the uncouple neuro-vertebral growth is a pathogenesis of idiopathic scoliosis links such morphology to the spinal cord development(Roth M. 1981; Burwell R.G. 2001; Porter R.W. 2001). Clinical measurements confirmed the abnormal ratio between the length spinal cord and spine column on scoliosis, which presented significantly reduced spinal cord to vertebral column ratios in the AIS patients with severe curve (Chu W. C.W. et al. 2006).

Vertebral rotation is an important feature of the scoliotic vertebrae. Several measurement methods have been developed for determining the vertebral axial rotation. Basically, measurements are based on radiography and CT images. The Nash-Moe method is rating the displacement of pedicles with respect to the vertebral width and thus determining the rotation angle (Lam G.C. et al. 2008). The Perdriolle method used a torsion meter as a template to measure vertebral rotation based on the offset of pedicles to the edges of the vertebral body (Weiss H.R. 1995; Lam G.C., Hill D.L. et al. 2008). Rotation defined in Aaro-Dahlborn method is based on the orientation of a vertebral body in relation to the whole human body(Lam G.C., Hill D.L. et al. 2008). The Stokes's method (Figure 1-14) quantifies geometrical orientation of pedicles for calculating the vertebral rotation (Stokes I.A.F. et al. 1986). Hecquet et al developed a method considering the 3D rotation characteristics that involved the sagittal tilt of a

vertebra(Hecquet J. et al. 1998). Haughton et al used the magnetic resonance imaging (MRI) to measure the rotation in vivo by alignment of vertebral images (Haughton V.M. et al. 2002).
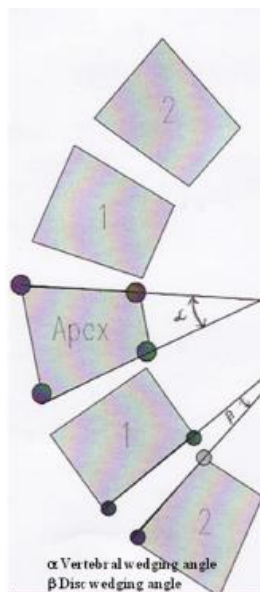
Figure 1-12 Vertebral and discal wedging angle measurement (Modi H.N., Suh S.W. et al. 2008) (permission was approved)
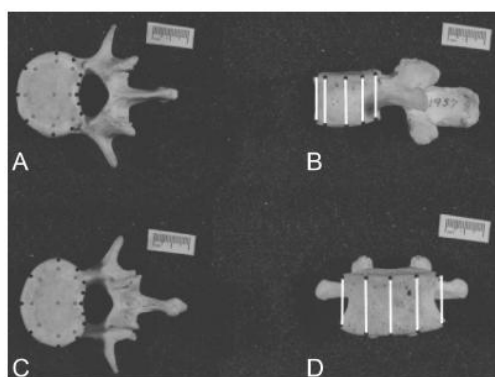
Figure 1-13 Measurement of vertebral heights of a vertebra reported by Parent (Parent S., Labelle et al. 2004) (permission was approved)

$$\tan\theta = \frac{w}{2d} \times \frac{a-b}{a+b}$$
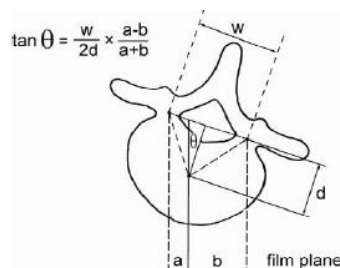
Figure 1-14 The Stokes's axial rotation measurement. Determine a and b from vertebral image, and fix the width W and depth d for rotation calculation (Chi W.M. et al. 2006; Lam G.C., Hill D.L. et al. 2008) (permission was approved)

1.6   Biomechanical studies of the spine

1.6.1   Geometric modeling techniques of the spine

Geometric modeling technique is the basis for the study of vertebral biomechanics and further study of the scoliosis and its progression. 3D reconstruction is able to model the complex spinal structurae with high accuracy. There are two basic reconstruction techniques that have been developed based on the 2D radiographic images and computed tomography (CT) images of transverse slices.

The stereoradiographic 3D reconstruction of the spine is established based on two orthogonal radiographs (posterior-anterior or anterior-posterior (PA or AP) and lateral planes)(Benameur S. et al. 2003; Dumas R., Le Bras A. et al. 2004; Pomero V. et al. 2004). A self-calibration method has been used for 3D reconstruction of a spine based on biplanar radiographic images (Kadoury S. et al. 2009). The reconstruction from CT uses the 3D medical dataset obtained from a large number of millimetric cuts and generates the geometry of vertebrae (Wang Z.L. et al. 2005). A combined technique that merges 3D CT reconstruction of a cadaver spine specimen and reconstruction from 2D radiographs with multi-views of individuals has been developed for generating a personalized spinal model(Delorme S. et al. 2003). This technique is able to reduce patients' exposure in irradiation.

1.6.2 Biomechanical models and application

Geometric model reconstructed from radiographies or CT images is further developed as a biomechanical model, finite element models (FEM).   Finite element model can be used to investigate biomechanics of musculoskeletal structures and its developing processes for orthopaedic purposes (Prendergast P.J. 1997). Currently, there are different types of models for representing the spine: beam models and solid models. Beam modeling technique represents the vertebral body as beams, while the later one models the vertebral body as solid elements. On the FEM of spine, the soft tissues, such as cartilaginous growth plate, ligaments, intervertebral disc, etc., are usually additionally modeled since geometries of these tissues are not included in the reconstruction from images.   Experimental studies on the tissues mechanical properties are contributed to define material properties of a biomechanical vertebral model. Appendix B summarizes the current modeling techniques for spine. The finite element model of cervical, lumbar and whole spine had been developed in order to investigate the biomechanics of a specific segment (Appendix B). As mention above, most studies used the CT scan to generate the geometric shape of spine for further meshing as finite element model. In addition to CT scan technique, parametric technique was also used for creating FEM of the spine (Shirazi-Adl A. 1991; Ezquerro F. et al. 2004). For the parametric modeling technique, vertebral geometries were built based on the anthropometry of vertebrae. The parametric model can be used to study the biomechanical response of vertebrae to daily activities Pediatric and adult finite element models have been developed in published studies. (Rohlmann A. et al. 2007; Schmidt H., Heuer F. et al. 2007; Schmidt H. et al. 2007; Schmidt H. et al. 2007; Natarajan R N et al. 2008; Rohlmann A et al. 2008; Schmidt H. et al. 2008; EI-Rich M. et al. 2009). Growth plate model is an important component in a pediatric model, which can potentially contribute to investigating growth-related spinal development. The growth plate was usually modeled as cartilaginous and cortical plates based on the physiological structure(Sairyo K. et al. 2006; Sairyo K. et al. 2006). Sylvestre et al. developed a growth plate including three layers, reserve, proliferative, and hypertrophic zones, which concerned the detailed structure of the cartilaginous plate (Sylvestre P.L. et al. 2007).

It was recognized that vertebral body model was separated as cortical and cancellous parts. Cortical bone was modeled as cubic or shell shape element, while cancellous bone was

modeled as cubic shape elements (EI-Rich M. et al. 2006). The intervetebral disc was also separated as annulus and nucleus regions with different mechanical properties. The annulus was reinforced by collagenous fibers that were modeled as unidirectional springs. Most published studies modeled intervertebral ligamentous tissues as cable-like element with tension only property. EI-Rich et al. firstly developed belt-like ligamentous tissues with none-linear mechanical properties that were similar to real intervertebral ligaments(EI-Rich M., Arnoux P.J. et al. 2009). Based on the reconstruction from CT scan, they also developed detailed lumbar spine model that separated the vertebral body and posterior area for simulateing the real structure as much as possible.

Due to the limitation of the computation capabilities, most studies created finite element model of a spinal segment, such as a cervical spine or a functional unit(Seifert J. et al. 2000; del Palomar A P et al. 2008). Villemure et al. presented a whole thoracic-lumbar spine model with simplified beam type element (Villemure I., Aubin C. E. et al. 2002). This model was applied on the spinal growth simulation using the Stokes's growth model and simulation of correction of scoliosis(Carrier J., Aubin C. E. et al. 2004; Carrier J. et al. 2005; Clin J. et al. 2007). The whole thoracic-lumbar spine model with solid elements was developed by Ruan et al.(Ruan J. et al. 2003). However, this model was applied on the study of impact response. To date, there is no whole spinal model with solid elements that includes the simulation of growth for studying the pathomechanism of AIS.

CHAPTER 2. OBJECTIVES AND HYPOTHESES

2.1   Summary of project background

Basically, the published theoretical and experimental studies for mechanobiological growth can be summarized as follows:

(1) Tissues in the vertebrae or other bone growth plates are sensitive to the surrounding mechanical environments that are able to trigger mechanobiological regulation of bone development.

(2) Multi-axial stresses from mechanical multi-oriented loads are involved into a mechanobiological process that results in regulation of bone growth for children, modeling, and remodeling.

(3) The mechanobiological contribution of axial loading to bone growth is described by the Hueter-Volkmann phenomenological law, and is supported by many clinical observations and experiments.

(4) The effect of non-axial stresses, which could be generated from shear or torsion, on mechanobiological growth is still poorly understood.

(5) The mechanical stimulus involved in mechanobiological growth is not yet identified.

This doctoral project focuses on the biomechanical study of progression of vertebral deformity induced by unbalanced vertebral growth. It is a sub-project of our group's research program, which emphasizes particularly on both experimental and numerical studies on the mechanobiology of the growth plate and minimal invasive surgery studies for the correction of AIS by modulating the abnormal growth.

2.2   Hypothesis of the proposed project

This study proposes a hypothesis as follows:

Multi-axial loads of a pediatric spine lead to vertebral wedging greater than 2 degrees due to the vertebral unbalance growth caused by those loads.

2.3   Objectives and general approaches

In order to address the hypothesis, the following objectives are proposed in this study:

Objective 1:   comparatively investigate existing modeling techniques.

This objective includes following sub-objectives:

Objective 1.1 Develop a conceptual model of a growth plate and transform it into a FEM. The conceptual model will represent the biological development course of growth and combine the mechanobiological effect. Furthermore, this conceptual model will be transformed into a FEM that agrees with the physiological structure and biological characteristics of the epiphyseal growth plate. This growth plate model will be added into a vertebral FEM. The purpose for development of this concept model is for modeling the vertebral epyphiseal growth plate in order to simulate the geometrical modification due to growth.

Objective 1.2 Evaluate existing models of mechanobiological growth. Two different models representing growth and mechanical growth modulation will be implemented in a finite element model of a vertebra. Resulting growth modulation under different loading conditions will be simulated in order to characterize the limits and strengths of each model.

Objective 2:   Develop a novel physiological mechanobiological growth model of vertebrae:

Objective 2.1 Develop a more physiological mechanobiological growth model than existing models. Mechanical stimulus for developing mechanobiological growth model will be proposed based on enegy. This growth model is an analytical representation of growth, which would be integrated into the growth plate model as described in Objective 1.1 for simulating growth processes. The new growth model is expected to overcome the limits and keep the strengths of existing models (objective 1.2);

Objective 2.2 Simulate longitudinal vertebral growth by integration of this model.

Objective 2.3 Assess the new mechanobiological growth model. Semi-quantitative analyses will include simulations of different physiological loading conditions and experimental studies of vertebral growth modulation, as well as comparative analyses of simulation results.

Objective 3: Identify possible pathomechanism of development of scoliotic vertebrae via growth simulation:

Objective 3.1 Exploit the developed model to analyze the effect of axial and non-axial loading on vertebral morphological development. A FEM of a functional unit will be developed and personalized to an adolescent patient with healthy vertebral morphology in order to agree with the conditions defined in the first hypothesis. The physical conditions, including axial and non-axial loading, refer to published experimental studies. Morphological measurements previously done by our group will be used to evaluate the mechanobiological contribution from different mechanical loading conditions (Parent S., Labelle et al. 2002; Parent S. 2003; Parent S., Labelle et al. 2004);

Objective 3.2 Identify the coupling mechanobiological effects of multi-axial loads on generation of scoliotic vertebrae. The physical conditions representing the second hypothesis will be applied on a normal vertebra for simulating the progressive deformity under 1~2 years. The identification of the coupling pathomechanism will be carried out through two approaches: comparative and theoretical analyses. Carter's theory and simulation results will be used in the comparative analysis for finding how the coupling mechanisms exist in the spinal loading with multi-orientation properties. The proposed methodology for developing the new growth model will be used for further theoretically analyzing the derivation of coupling mechanisms. Finally, it is expected to identify pathomechanisms involved in vertebral morphological progression of AIS.

2.4 Thesis organization

This thesis includes three main works: (1) comparative study of two modeling techniques; (2) development of energy-based model; (3) mechanobiological study of progression of vertebral deformity. Those works are related to the proposed objectives The **Figure 2-1**shows the organization of those works.
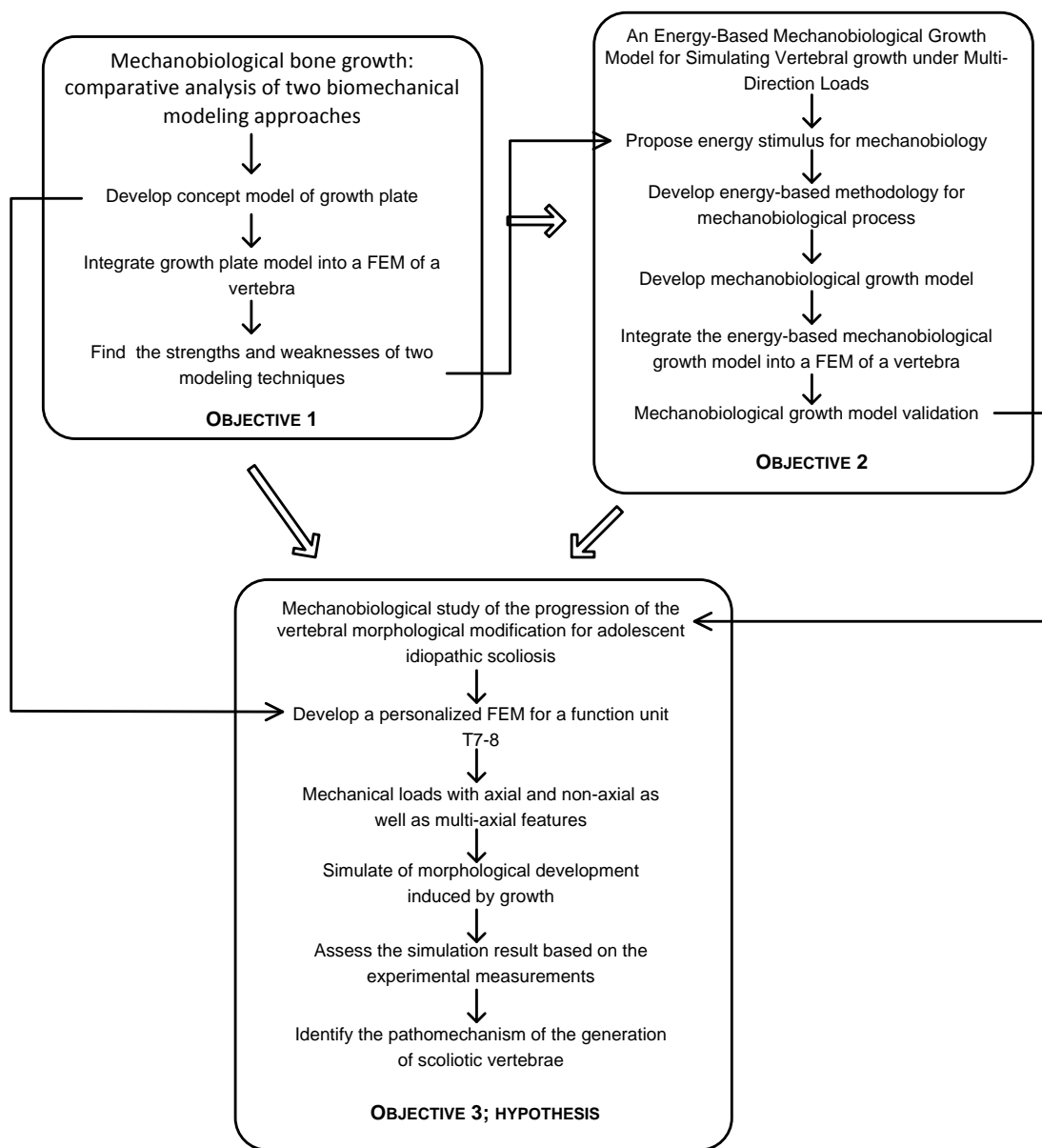
Figure 2-1 The logical relation of the thesis works

CHAPTER 3.   METHODS

The methods for this project are divided into three main groups related to three works described in Chapter 2. This section presents the methods for those works respectively.

3.1   Comparative analysis of two biomechanical modeling approaches

3.1.1   Finite element modeling of a vertebra integrating the growth plate

A finite element model of T7 vertebra was used to compare Carter's and Stokes's models. The initial geometry of the bony vertebra was reconstructed using serial CT-scans of a dry specimen with 1-mm-thick CT-scan slices taken at 1-mm steps. Following segmentation of the bone, generation of the outer surface using the connecting cube algorithm and volume creation (EI-Rich M., Aubin C. E. et al. 2006)), the finite element model was generated by free meshing with 4-nodal orthotropic solid tetrahedron elements using a commercially available FE software package (Ansys 10.0, Ansys Inc., Canonsburg, PA, USA). The meshed vertebra included 4810 nodes and 18762 elements. The geometry was scaled and deformed to a typical geometry of a pediatric T7 vertebra based on bi-planar (posterior-anterior and lateral) radiographies using dual kriging method (Sylvestre P.L., Villemure I. et al. 2007).

The vertebral body was separated into regions of cortical and cancellous bones. Elements attached to the outer lateral surface of the vertebral body were modeled as cortical bone, while interior elements were represented by cancellous bone (**Figure 3-1**a). Cancellous bone was modeled as a linear orthotropic material, while cortical bone was modeled as transverse isotropic material (**Table 3-1**).
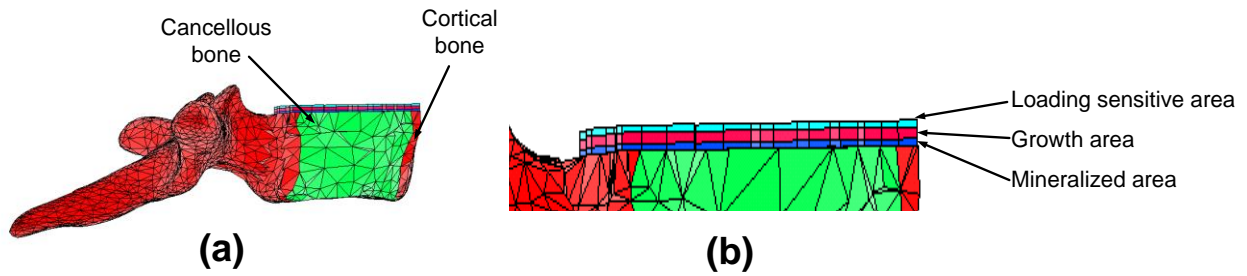
Figure 3-1 Finite element model of the vertebral body and the growth plate: (a) finite element model of the vertebral body (from a 12-year-old patient) including cortical and cancellous bone; (b) three-layer finite element model of the growth plate including loading sensitive, growth, and mineralized areas.
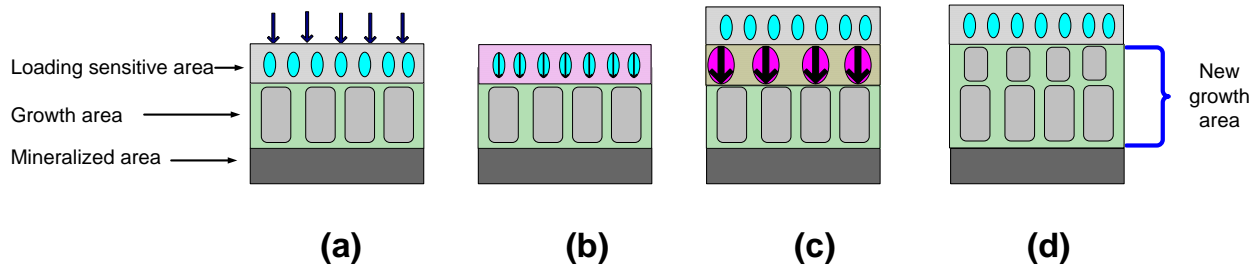
Figure 3-2 Conceptual model of the growth plate and bone growth process: (a) loads were applied on the growth plate; (b) the loading sensitive area recorded mechanical stimuli; (c) biological and mechanobiological changes were triggered in the loading sensitive area; (d) new calcified bone left the loading sensitive area and deposited on the growth area, which combines to previous growth area. The height of new growth area increased, while the new loading sensitive area kept a constant height.

Table 3-1 Mechanical properties of the finite element model of vertebra T7

Tissue	Type of elements	Material properties Elastic Modulus(Dumas R., Le Bras A. et al.)						
		Ex	Ey	Ez	Gxy	Gyz	Gxz	ν
Cortical bone[1]	4-node tetrahedron	8000	8000	14000	3280	3280	3280	0.3
Cancellous bone[1]	4-node tetrahedron	767	401	1157	20.4	24	24	0.12
Growth plate								
- Load sensitive area[2]	8-node hexahedron	23.8	23.8	23.8	10.6	10.6	10.6	0.4
- Growth area[1]	8-node hexahedron	767	401	1157	20.4	24	24	0.12
- Mineralized area[1]	8-node hexahedron	767	401	1157	20.4	24	24	0.12

1: (Sylvestre P.L., Villemure I. et al. 2007)

2: (Schmidt H., Kettler A. et al. 2007)

A conceptual model was created to simulate the bone growth process, as illustrated in **Figure 3-2**(a-d). The load was firstly applied on the growth plate (**Figure 3-2**a), and the mechanical stimuli were recorded by the load sensitive area (**Figure 3-2**b). The mechanical stimuli and inherent biological stimuli in the load sensitive area triggered the mechanobiological and biological growth including chondrocyte proliferation and hypertrophy (**Figure 3-2**c). Grown cartilaginous tissue was then calcified and produced new bone material (**Figure 3-2**d). This new bone had same properties as that of growth area, and thus it was considered that the new bone 'left' the loading sensitive area and deposited in the growth area (**Figure 3-2**d). As the physiological growth process (Price J.S., Oyajobi B.O. et al. 1994; Stevens S.S., Beaupre G.S. et al. 1999; Shefelbine S.J., Tardieu C. et al. 2002; Shefelbine S.J. and Carter D.R. 2004; Shefelbine S.J. and Carter D.R. 2004), this conceptual model represented the growth such as that new calcified bone continually deposited within the growth area thus increasing the height of this area. The loading sensitive area maintained a constant height even though this area experiences temporary change on the height during growth. Only vertebral longitudinal growth perpendicular to the initial growth plate surface was modeled in this study. The material of the loading sensitive area of the growth plate was assumed as isotropic, homogenous and linear elastic. The

Young's modulus of this area was fixed at 23.8 MPa (Schmidt H., Kettler A. et al. 2007). The growth and mineralized areas were considered as the bony endplate and assigned same linear orthotropic material properties as cancellous bone (**Table 3-1**).

The growth plate was created on the upper surface of the vertebral endplate, with an initial flat surface parallel to the bony surface based on preliminary work by Sylvestre et al. (Sylvestre P.L., Villemure I. et al. 2007). Based on the conceptual model proposed above, the growth plate was modeled as a three-layer structure: the loading sensitive area, the growth area and the mineralized area (**Figure 3-1**b). The load sensitive area was assumed 0.3 mm thick and served as the load recording region. This region corresponds to the physiological area including the reserve, the proliferative and part of the hypertrophic zones, since chondrocytes from these areas are sensitive to the mechanical stimuli (Price J.S., Oyajobi B.O. et al. 1994; Stokes I.A.F., Mente P.L. et al. 2002; Wang X. and Mao J.J. 2002; Stokes I.A.F., Gwadera J. et al. 2005). The growth area was modeled as 0.5 mm in thickness and physiologically corresponded to the remaining part of the hypertrophic zone and degenerated cartilage areas where chondrocytes die and surrounding matrix calcifies (Price J.S., Oyajobi B.O. et al. 1994) (**Figure 3-1** a). The growth area is unable to respond to mechanical loading for triggering the mechanobiological growth, but expands in the longitudinal direction due to growth. The mineralized area was located between the growth area and the bony vertebral body. All areas of the growth plate were modeled with one-layer of 8-nodal hexahedron solid elements.

Material properties were taken from published studies for pediatric vertebrae (Schmidt H., Kettler A. et al. 2007; Sylvestre P.L., Villemure I. et al. 2007). The mechanical behavior of the finite element model was insensitive to mechanical properties of bony structure. The cartilaginous material composing the loading sensitive area was much softer than the bony tissues located in other vertebral areas. More precisely, the stiffness in the loading sensitive area was about one-twentieth that of the bony areas at least. Based on this difference in material properties between the loading sensitive area and the bony parts, the mechanical behavior of the whole model was mostly governed by soft tissues. It was then expected that the behavior would remain similar for different bony properties within a realistic range.

3.1.2 Integration of mechanobiological growth in the finite element model

Stokes' (Eq. 1-3) and Carter's (Eq. 1-9) mechanobiological growth models were separately integrated in the above-detailed finite element model of T7 vertebra. In Stokes' model, the sensitive factor β_l was assumed 1.2 MPa^{-1}, based on an experimentally determined range of $0.4 \sim 1.71 \, Mpa^{-1}$ (Carrier J., Aubin C. E. et al. 2004; Stokes I.A.F., Aronsson D.D. et al. 2006). The longitudinal baseline growth for thoracic vertebrae was taken as Gm=0.8mm/year according to the published data on vertebral growth (Dimeglio A. and Bonnel F. 1990). Thus, the baseline growth strain increment ΔG_l was taken as $\dfrac{Gm}{h_g}$, with h_g as the initial height of the growth area. In Carter's model, baseline normal growth rate $\dot{\varepsilon}_b$ was equal to ΔG_l of Stokes's model. The ratio of parameters a and b of this model was defined as $\dfrac{b}{a} \approx 0.5$, and the maximum contribution of mechanobiological growth was assumed to be less than 50% of the biological growth, as suggested by the authors (Shefelbine S.J., Tardieu C. et al. 2002; Shefelbine S.J. and Carter D.R. 2004).

As the models have different formulations and parameters, we first calibrated the two models in order to get equivalent answers for a given loading condition. Because Stokes's model was supported by published experiments (Stokes I.A.F., Mente P.L. et al. 2002; Stokes I.A.F., Gwadera J. et al. 2005; Stokes I.A.F., Aronsson D.D. et al. 2006; Stokes I.A.F., Clark K.C. et al. 2007), Carter's model was calibrated based on Stokes's model under tension. For an overloading condition, the calculated growth modulations based on the two models would be over 50% of the biological growth. Based on the above physiological condition of maximum mechanobiological growth, the growth rates would be set as 50% of the biological growth under those overloading cases. Thus, different overloading conditions would induce same growth modulations based on the physiological condition. In order to test the full impact of mechanical loads, overloading conditions should be avoided. The tension loading for calibration was set at 0.2MPa. One-year growth under this loading condition was simulated using both models. Parameter a (with b ≈ 0.5 a) of Carter's model was adjusted up until the difference of the mean values of the mechanobiological growth between the two models was less than $10 \, \mu m$.

3.1.3 Simulation of the growth process

The growth process was simulated using a stepwise incremental procedure, with each cycle representing one month (**Figure 3-3**). The boundary and external loading conditions were applied at *step 1:* the inferior endplate of T7 vertebra was rigidly fixed along all degrees of freedom. External static loading was applied on the superior endplate of T7 vertebra. Besides the tension loading for calibration, four loading conditions were investigated: compression, shear forces, as well as combined tension/shear and combined compression/shear. Overloading conditions should be avoided in these simulations because the same mechanobiological growth rate (50% of the biological growth) would be produced due to physiological limit (not over 50% of the biological growth). Tension and compression (0.2MPa) were applied perpendicular to the upper surface of the vertebra (**Figure 3-4**a-b). Shear force (82 N) was applied parallel to this surface and equally distributed on each node (**Figure 3-4**c). This loading condition would possibly generate non-uniform shear stresses but significant low axial stresses, which were the expected mechanical environment for this simulation study. Combined tension (0.2MPa)/shear (82 N) and combined compression (0.2MPa)/ shear (82 N) involved axial and non-axial loads in the further comparison (**Figure 3-4**d-e).

1: Application of boundary conditions and external loading

2: Calculation of the modulated growth

3: Removal of external loading

4: Simulation of modulated growth using thermal loading and geometry update
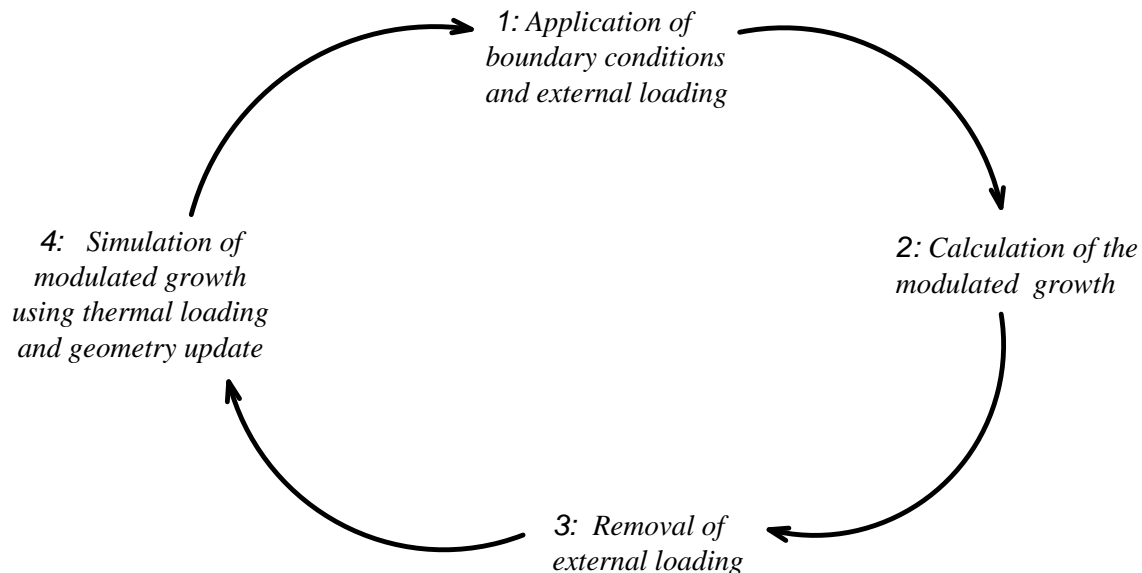
Figure 3-3 Stepwise simulation procedure of the growth of vertebra

At *step 2*, growth modulation rates resulting from loading stimuli were calculated based on stresses distributed in the load sensitive area, which stresses governed the mechanobiological growth (**Figure 3-3**). In Stokes's model, axial stresses σ_{zz} were used to calculate growth modulation, while octahedral and hydrostatic stresses were used in Carter's model.

At *step3*, the external loading applied on the vertebral model were removed in order to simulate the growth by applying thermal loads. To do so, resulting strain rates, which are the sum of the baseline and mechanobiological strain rates, were transformed to equivalent thermal loads (Appendix C).

At *step 4*, thermal loads were applied on each element of the growth area.

Expansion (only in the axial direction) of the solid elements in this area then caused changes in the geometry of the whole model. The vertebral geometry was further updated according to this monthly grown geometry using node redefinition.

After vertebral geometry modification and before cycling again to step 1, thermal loads were removed (**Figure 3-3**). The entire cycle was repeated 12 times to simulate a 12-month growth period.

Mechanobiological growth was evaluated from simulation results as the difference between growth with and without load. For the calibration under tension, growth was calculated as the mean growth value of all nodes on the upper surface of the growth plate (loading sensitive area). The upper surface of the growth plate was divided into edge and middle area for analysis purposes. The outer annulus of the upper surface was defined as the edge area, and the remaining area in this surface was defined as the middle area. Only nodes in the middle area were compared within the calibration step, because of possible abnormal stress distribution in this edge area.
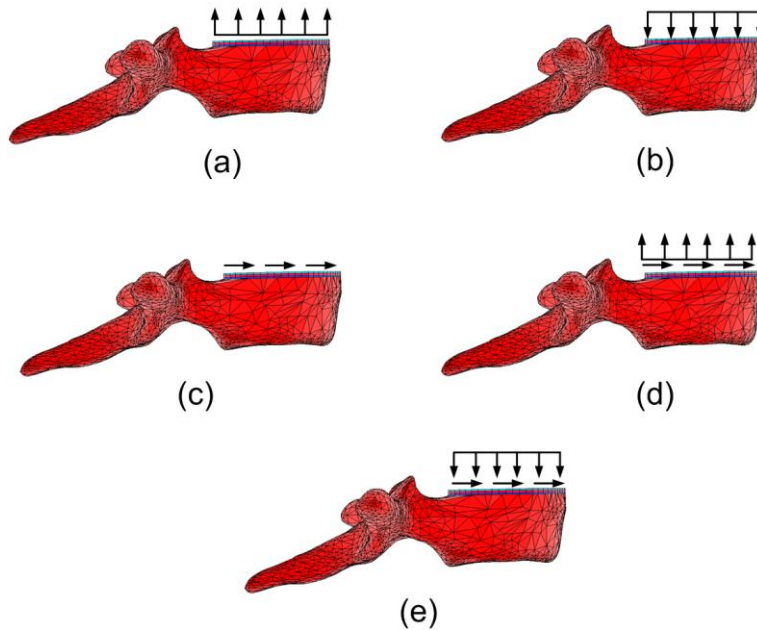
Figure 3-4 Loading conditions: (a) tension of 0.2MPa for calibration purposes; (b) compression of 0.2MPa; (c) shear force of 82 N parallel to the vertebral surface; (d) combined tension of 0.2MPa and shear force of 82 N; (e) combined compression of 0.2MPa and shear force of 82 N

3.2   Energy-based mechanobiological growth model

In this section, firstly, an overall procedure of the development of the growth model is presented. The following sub-sections focus on the each step in the procedure. The final sub-section presents the method to test this new developing growth model.

3.2.1 Conceptual procedure of the energy-triggered mechanobiological bone growth

In order to model the mechanobiological growth model, the first step is to create a conceptual procedure of energy-triggered mechanobological bone growth. The developing process for the growth model will be based on this conceptual procedure.

Based on published studies, the mechanobiological process of bone can be summarized as four basic steps (Huselstein C., Netter P. et al. 2008):

(1)   Mechanosensing, which converted the mechanical force into a detectable stimulus sensed by cells (Huselstein C., Netter P. et al. 2008). This process carried out the conversion of mechanical forces into biochemical responses (Silver F.H. and Siperko L.M. 2003) ;

(2)   mechanotransduction, a conversion of detectable stimulus into electrical, or biochemical reaction;

(3)   Further mechanotransduction, a further conversion of signal at intracellular level (Alenghat F.J. and Ingber D.E. 2002);

(4)   Mechanoregulation, the final regulation of biological action of bone cells.
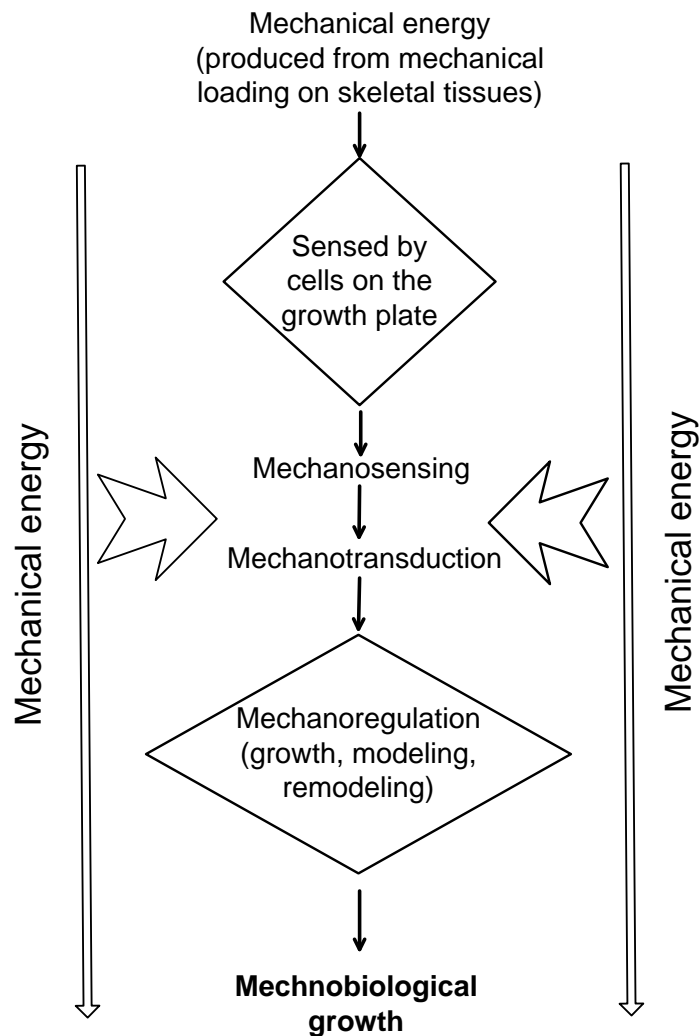
Figure 3-5 the energy-triggered mechanobiological growth process

This study considers the energy as stimulus. The above steps can be further described as a sequence of procedures: mechanical loading induced mechanical energy; mechanical energy could be sensed by tissues cells and induced mechanosensing and thus triggered mechanoregulation (Silver F.H. and Bradica G. 2002; Silver F.H. and Siperko L.M. 2003; Robling A.G. and Turner C.H. 2009). In term of the above summarization of the mechanobiological process, a conceptual procedure for modeling the mechanobiological growth is proposed as represented in **Figure 3-5**. Mechanical loads applied on human body, such as gravity and muscle forces, are able to produce mechanical energy. The mechanical energy in a cartilaginous growth plate physically shows as strains and stresses of tissues. Energy generated from this mechanical process can be sensed by cartilaginous cells and induces mechanosensing. Mechanosensing is capable of converting the mechanical energy into biochemical energy. This procedure carries out the transformation from mechanical stimuli to biochemical stimuli (Silver F.H. and Siperko L.M. 2003). Mechanotransduction is activated by mechanosensing through biochemical action and results in mechanoregulation, which brings about the modification of the tissue structure and function induced by growth, remodeling, etc. (Carter D.R., Fyhrie D.R. et al. 1987; Silver F.H. and Siperko L.M. 2003). The procedure presents developing steps for energy-based growth model. The following sub-sections will focus on corresponding steps in this proposed procedure for finally developing the analytical growth model.

3.2.2 Mechanical energy in tissues

Mechanical forces generated from vertebral surrounding environments are applied on the spine and thus produce mechanical work W. The mechanical work can be written as:

$$W = \int_{\Omega} f \cdot d\delta$$

(3-1)

This mechanical work can be transferred to mechanical energy stored in the tissue of growth plate. The mathematical description of the mechanical energy of the tissue is:

$$U = \int_V U_d dv \tag{3-2}$$

Without considering energy dissipation, the mechanical work should be equal to the mechanical energy if no energy dissipation during the transduction, i.e. $W = U$.

For both a linear-isotropic and linear-anisotropic solid, the strain and stress with respect to axes {x,y,z} can be written as 6-component column vectors based on structural mechanics:

$$[\varepsilon] = [\varepsilon_{xx}, \varepsilon_{yy}, \varepsilon_{zz}, \gamma_{yz}, \gamma_{zx}, \gamma_{xy}]^T, \quad [\sigma] = [\sigma_{xx}, \sigma_{yy}, \sigma_{zz}, \tau_{yz}, \tau_{zx}, \tau_{xy}]^T \tag{3-3}$$

Where $[\varepsilon]$ is the strain, $[\sigma]$ is the stress. The relationship between the stress vector and the strain vector is expressed as:

$$[\varepsilon] = \begin{bmatrix} \varepsilon_{xx} \\ \varepsilon_{yy} \\ \varepsilon_{zz} \\ \gamma_{yz} \\ \gamma_{zx} \\ \gamma_{xy} \end{bmatrix} = \begin{bmatrix} C_{11} & C_{12} & C_{13} & C_{14} & C_{15} & C_{16} \\ & C_{23} & C_{23} & C_{24} & C_{25} & C_{26} \\ & & C_{33} & C_{34} & C_{35} & C_{36} \\ & & & C_{44} & C_{45} & C_{46} \\ & Symm & & & C_{55} & C_{56} \\ & & & & & C_{66} \end{bmatrix} \begin{bmatrix} \sigma_{xx} \\ \sigma_{yy} \\ \sigma_{zz} \\ \sigma_{yz} \\ \sigma_{zx} \\ \sigma_{xy} \end{bmatrix} = [C][\sigma] \tag{3-4}$$

$[C]$ is the coefficient matrix. The general strain energy density can be expressed as (Felippa C.A. and Onate E. 2003):

$$U_d = \frac{1}{2}[\sigma]^T[\varepsilon] = \frac{1}{2}[\sigma]^T[C][\sigma] \tag{3-5}$$

Tissues of a growth plate are assumed as linear and isotropic. Based on the Eq.(3-5), the mechanical energy density can be rewritten as:

$$U_d = \frac{1}{2}(\sigma_x \varepsilon_x + \sigma_y \varepsilon_y + \sigma_z \varepsilon_z + \tau_{xy}\gamma_{xy} + \tau_{xz}\gamma_{xz} + \tau_{yz}\gamma_{yz}) \tag{3-6}$$

The total scalar value of energy density is independent to the coordinate frame. The value of each component in Eq. (3-6) will however be modified with a change in the coordinate frame. Eq. (3-6) can also be written in the following form:

$$U_d = \frac{3(1-2v)}{2E}(\frac{\sigma_x + \sigma_y + \sigma_z}{3})^2 +$$
$$\frac{3}{4G}\left\{ \left(\frac{\sqrt{(\sigma_x - \sigma_y)^2 + (\sigma_x - \sigma_z)^2 + (\sigma_y - \sigma_z)^2}}{3}\right)^2 + 2(\tau_{xy}^2 + \tau_{xz}^2 + \tau_{yz}^2)\right\} \tag{3-7}$$

Eq. (3-7) includes two components, dilatation strain energy density U_{dv} and distortional strain energy density U_{dd}:

$$U_{dv} = \frac{3(1-2v)}{2E}(\frac{\sigma_x + \sigma_y + \sigma_z}{3})^2 \tag{3-8}$$

$$U_{dd} = \frac{3}{4G}\left\{ \left(\frac{\sqrt{(\sigma_x - \sigma_y)^2 + (\sigma_x - \sigma_z)^2 + (\sigma_y - \sigma_z)^2}}{3}\right)^2 + 2(\tau_{xy}^2 + \tau_{xz}^2 + \tau_{yz}^2)\right\} \tag{3-9}$$

Eq. (3-7) can then be rewritten as coordinate-independent expression (Budynas R. 1998):

$$U_d = \frac{3(1-2v)}{2E}\sigma_{oct}^2 + \frac{3}{4G}\tau_{oct}^2 \tag{3-10}$$

where stresses are integrated as octahedral shear and hydrostatic stresses. Octahedral shear stress is also termed distortional stress and refers to a change in the tissue shape. Hydrostatic stress is also termed dilatational stress and refers to a change in the tissue volume (Carter D.R. and Wong M. 1988). According to Eq. (3-7), the overall strain energy stored in a tissue is the combination of dilatation and distortion energies.

3.2.3 Mechanosensing stimulus

Mechanosensing performs conversion of the physical stimuli into a biochemical or electrical responses based on the energy transformation (Silver F.H. and Siperko L.M. 2003). As

the above definition from published studies, mechanosensing was associated with mechanical environments. Mechanosensing stimulus, which is proposed in this study, is produced during this procedure for carrying out mechanoregulation. Mechanosensing stimulus represents cells response to mechanical energy. This stimulus associated mechanical environments with cell response for triggering mechanoregulation. It was reported that the significant correlation between the morphology of cartilaginous tissues and mechanosensing (Silver F.H. and Siperko L.M. 2003; Rubin J., Rubin C. et al. 2006; Vogel V. and Sheetz M. 2006). Thus, the analytical expression of the mechanosensing stimulus should be based upon the tissue morphology.

A basic description of the tissue morphology can be written as the function of strains:

$$\vec{Df} \sim (\varepsilon_x, \varepsilon_y, \varepsilon_z, \gamma_{xy}, \gamma_{xz}, \gamma_{yz})$$
(3-11)

The above expression is difficult to be determined because of the coordinate-dependent property on each strain component. A published method proposed an expression of the cartilaginous tissue morphology based on principal coordinate frame (Wilsn W. et al. 2006). Under the principal coordinate system, the morphology of cartilaginous tissues can be rewritten as:

$$\vec{Df} = \varepsilon_1 \vec{i}_p + \varepsilon_2 \vec{j}_p + \varepsilon_3 \vec{k}_p$$
(3-12)

This expression avoids the coordinate-dependent characteristics of each component. Since energy is the basic stimulus to carry out the whole mechanobiological process (Silver F.H. and Bradica G. 2002; Silver F.H. and Siperko L.M. 2003), the absolute amount of mechanosensing stimulus should be equal to scalar value of energy. In addition, the tissue morphology characteristics should also be involved into the description of mechanosensing stimulus. Thus, mechanosensing stimulus is written as:

$$\vec{Me}_\varepsilon = U \cdot \frac{\vec{Df}}{\left\| \vec{Df} \right\|} = U \frac{\varepsilon_1}{\varepsilon_{Tot}} \vec{i}_p + U \frac{\varepsilon_2}{\varepsilon_{Tot}} \vec{j}_p + U \frac{\varepsilon_3}{\varepsilon_{Tot}} \vec{k}_p$$
(3-13)

where $\varepsilon_{Tot} = \sqrt{\varepsilon_1^2 + \varepsilon_2^2 + \varepsilon_3^2}$ and $\left\| \vec{Me}_\varepsilon \right\| = U$. The equation indicates that mechanosensing stimulus generated from energy can be expressed as a form independent to a coordinate frame. The corresponding stimulus tensor derived from Eq. (3-13) is then:

$$Me_t = \left[U\frac{\varepsilon_1}{\varepsilon_{Tot}} \quad U\frac{\varepsilon_2}{\varepsilon_{Tot}} \quad U\frac{\varepsilon_3}{\varepsilon_{Tot}} \right] \tag{3-14}$$

It is proposed that mechanical energy is sensed by cells through tensor form, which keeps the energy component and adds tissue morphology characteristics. The Eq. (3-13) can also be written as:

$$\vec{Me}_\varepsilon = Me_t \vec{n}_p \tag{3-15}$$

where $\vec{n}_p = (\vec{i}_p, \vec{j}_p, \vec{k}_p)^T$ is the principal vector.

3.2.4 Stimulus contribution index

The mechanosensing stimulus triggers the mechanoregulation including not only the modulation of bone growth but also other modifications, such as modeling and remodeling during bone development. Mechanosensing stimulus, which was developed above based on the tissue morphology, presents orientation characteristics. The longitudinal geometry of tissues was correlated to the proliferation and hypertrophy of chondrocyte and matrix secretion, which governed bone growth (Ascenzi M.G. et al. 2007). The component of mechanosensing stimulus on axial direction, i.e. bone growth direction, is thus proposed as the portion correlated with the mechanoregulation of bone growth. The stimulus contribution index represents the weigh factor for estimating the proportion of the whole mechanosesnting stimulus contributed to bone growth.

For a case where the longitudinal direction of growth is an axis in a coordinate system $\left(\vec{i} \quad \vec{j} \quad \vec{k} \right)^T$, the principal direction is expressed as:

$$\vec{n}_p = \begin{bmatrix} \vec{i}_p \\ \vec{j}_p \\ \vec{k}_p \end{bmatrix} = \begin{bmatrix} n_{p1_x} & n_{p1_y} & n_{p1_z} \\ n_{p2_x} & n_{p2_y} & n_{p2_z} \\ n_{p3_x} & n_{p3_y} & n_{p3_z} \end{bmatrix} \begin{bmatrix} \vec{i} \\ \vec{j} \\ \vec{k} \end{bmatrix} \tag{3-16}$$

Where x, y, and z are the coordinate axes. Eq. (3-15) is then expressed as:

$$\vec{Me}_\varepsilon = \begin{pmatrix} U(\dfrac{\varepsilon_1}{\varepsilon_{Tot}} n_{p1_x} + \dfrac{\varepsilon_2}{\varepsilon_{Tot}} n_{p2_x} + \dfrac{\varepsilon_3}{\varepsilon_{Tot}} n_{p3_x}) \\ U(\dfrac{\varepsilon_1}{\varepsilon_{Tot}} n_{p1_y} + \dfrac{\varepsilon_2}{\varepsilon_{Tot}} n_{p2_y} + \dfrac{\varepsilon_3}{\varepsilon_{Tot}} n_{p3_y}) \\ U(\dfrac{\varepsilon_1}{\varepsilon_{Tot}} n_{p1_z} + \dfrac{\varepsilon_2}{\varepsilon_{Tot}} n_{p2_z} + \dfrac{\varepsilon_3}{\varepsilon_{Tot}} n_{p3_z}) \end{pmatrix} \begin{pmatrix} \vec{i} \\ \vec{j} \\ \vec{k} \end{pmatrix} \tag{3-17}$$

The stimulus contribution index is derived from Eq. (3-17) and expressed as:

$$St_g = \frac{Me_l}{\left\| \vec{Me}_\varepsilon \right\|} \tag{3-18}$$

where Me_l is the mechanosensing contribution to longitudinal growth, which aligns with one of the axis elements detailed in Eq. (3-17). For example, if the longitudinal growth axis is along $\vec{i}$ (x-axis), then $Me_l = U(\dfrac{\varepsilon_1}{\varepsilon_{Tot}} n_{p1_x} + \dfrac{\varepsilon_2}{\varepsilon_{Tot}} n_{p2_x} + \dfrac{\varepsilon_3}{\varepsilon_{Tot}} n_{p3_x})$. The stimulus contribution index St_g is within the following range:

$$-1 \le St_g \le 1 \tag{3-19}$$

A positive St_g index implies that mechanosensing stimulus promotes bone growth, while a negative index refers to growth retardation.

3.2.5 Mechanoregulation index

Mechanoregulation is the overall regulation of bone including bone growth, modeling and remodeling via energy-based mechanosensing (Carter D.R., Fyhrie D.R. et al. 1987). This overall

regulation is evaluated by mechanoregulation index M_I, which represents the combination of ossification index proposed by Carter's studies(Stevens S.S., Beaupre G.S. et al. 1999; Beaupre G.S., Stevens S.S. et al. 2000) with endochondral growth index. The higher the index, the higher stimulus of the development of a growth plate; the lower the index, the milder stimulus for maintaining the normal biological process of the growth plate. Logically, mecahnoregualtion is triggered by mechanosensing stimulus. Thus, mechanoregulation index is the function of the magnitude of the mechanosensing stimulus, i.e. the higher the value of the mechanosensing stimulus, the greater the index value. We should note that the absolute modulus of mechanosensing stimulus is equal to the scalar value of energy, $\left\| \overrightarrow{Me}_\varepsilon \right\| = U$. The mathematical expression of mechanoregulation index is written as:

$$M_I = F_u \left(\left\| \overrightarrow{Me}_\varepsilon \right\| \right) = F_u(U) \tag{3-20}$$

For a micro element, it is assumed that the distribution of the energy density is uniform within this element and the total energy is then simplified as the product of energy density and element volume. The element volume is independent to the mechanobiological process since this process is related to mechanical environments. Therefore, the mechanoregulation index (Eq. (3-20)) is also a function of energy density:

$$M_I = F_u(U_d V) = F_{ud}(U_d) \tag{3-21}$$

Eq. (3-6) indicates that the energy density is the function of stresses and strains, thus, the mechanoregulation index is also a function of stresses and strains:

$$M_I = F_{sS}(\sigma_x, \sigma_y, \sigma_z, \tau_{xy}, \tau_{xz}, \tau_{yz}, \varepsilon_x, \varepsilon_y, \varepsilon_z, \gamma_{xy}, \gamma_{xz}, \gamma_{yz}) \tag{3-22}$$

The Eq.(3-22) should be variable because of the coordinate-dependent properties of components. Furthermore, this equation is difficult to be determined since many variables are involved in this

function. Carter's theory associated the distortion and dilatation energy (Eq.(3-7)-Eq.(3-10)) with the endochodral ossification, which is the biological process of bone growth (Carter D.R. and Wong M. 1988; Beaupre G.S., Stevens S.S. et al. 2000; Cohen M.M.Jr. 2006). The octahedral and hydrostatic stresses were respectively defined as distortion and dilatation stresses in this theory (Carter D.R. and Wong M. 1988). Thus, the mechanoregualtion index can be simplified as the function of these two coordinate-independent stresses:

$$M_I = F_{sI}(\sigma_{oct}, \tau_{oct})$$

(3-23)

The published studies modeled the ossification index by linearly combining these two stresses(Stevens S.S., Beaupre G.S. et al. 1999; Beaupre G.S., Stevens S.S. et al. 2000). This study also linearly combined these two stresses for modeling the mechanoregualtion index according to their contributions to articular cartilage development(Carter D.R. and Wong M. 1988). However, according to the Eq(3-21), mechanoregulation index was initially modeled based on the energy density, which is independent of stresses signs (Eq.(3-10)). Therefore, the mechanoregulation index (Eq. (3-23)) is modeled as:

$$M_I = a_e \tau_{oct} + b_e |\sigma_{oct}|$$

(3-24)

where the ratio of b/a is between 0.3 and 1 (Shefelbine S.J. and Carter D.R. 2004).

3.2.6 Growth model

The mechnobiological growth is one biological modification of mechanoregulation. The high mechanoregulation results in the great mechanobiological growth rate. In addition, stimulus contribution index determines how much proportion of the stimulus is contributed to growth. Thus, the linear property also exists in the relation between stimulus contribution index and mechanobiological growth. Thus, mechanobiological growth ε_{me} is bi-linear to mechanoregulation index M_I and stimulus contribution index St_g :

$$\varepsilon_{me} = M_I St_g$$

(3-25)

Using this concept, the mechanobiological growth model, Eq. (3-25), is the combination of Eq. (3-18) and Eq. (3-24):

$$\varepsilon_{me} = (a_e \tau_{oct} + b_e |\sigma_{oct}|) \frac{Me_l}{\left\| \overrightarrow{Me_\varepsilon} \right\|} \qquad (3\text{-}26)$$

The overall growth ε_{we} is the sum of the baseline biological ε_{be} and mechanobiological growth ε_{me} (Carter D.R. and Wong M. 1988):

$$\varepsilon_{we} = \varepsilon_{be} + \varepsilon_{me} \qquad (3\text{-}27)$$

In this study, both growth and mechanoregulation index are represented as strain increment format and time-dependent quantity ($month^{-1}$). The unit for parameters a_e and b_e are thus defined as ($Mpa^{-1}month^{-1}$)

3.2.7 Testing validity of model by a biomechanical approach

3.2.7.1 Model assessment approach

Based on the published studies on mechanobiological growth, this study tests the rationality of the model on following aspects:

1) to the axial loading, the Hueter-Volkmann law and Stokes's model as well as relevant experiments are used to evaluate the simulation result. The Hueter-Volkmann law has been confirmed by clinicians and researchers. Experiments on axial loading are considered to be physical evidences. The Stokes's model has been recognized on axial loading case since this model derived from numerous animal experiments;

2) to pure shear loading condition, Moreland's experiment using torsion can be physical evidence to judge the growth model;

3) to multi-axial loading including the both axial and shear forces, Carter's theory on positive mechanobiological contribution of shear stresses can be used to decide the rationality of the growth model.

Those evaluations consider both axial and non-axial mechanical loading. The following steps are proposed to biomechanically test its validity:

(1) determination of parameters of energy-triggered mechanobiological growth model (Eq. 3-26);

(2) mechanical loading setting. According to the above validation outline, mechanical loading conditions were set as: : axial loading (compression and tension), pure shear force, combined axial and shear loading

(3) simulating growth under proposed loading conditions.
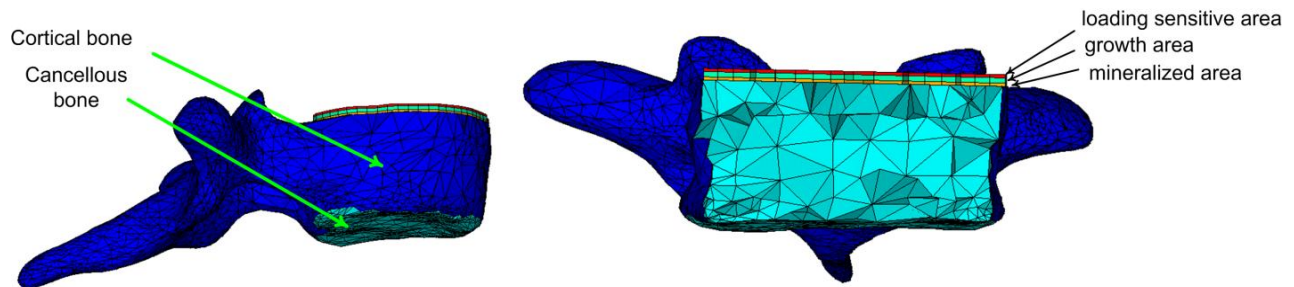
Figure 3-6 Finite element model of vertbra T7 and its growth plate

3.2.7.2 Biomechanical procedures for test

A finite element model (FEM) developed above was used to biomechanically test this new model. Regarding the FEM of a vertebra, the model of cortical bone was modified as 1mm shell covering the outside surface of vertebral body except for superior and inferior endplate (**Figure 3-6**). This improvement considered more accurate structure compared with the real anatomical structure and refered to some published modeling techniques (Thomas Edwards W., Zheng Y. et al. 2001; Schmidt H., Heuer F. et al. 2007). Material properties are presented in **Table 3-1**.

The energy-based mechanobiological growth model was integrated in the above-detailed finite element model of the vertebra. A calibration method was employed to fix the parameters of the energy-based model (Eq. (3-24)). Because Stokes's model was supported by published experiments under axial loading environments (Stokes I.A.F., Mente P.L. et al. 2002; Stokes I.A.F., Aronsson D.D. et al. 2006; Stokes I.A.F., Clark K.C. et al. 2007), the energy-based model was calibrated based on the Stokes's model under tension (Lin H. et al. 2008). The sensitivity factor β_l (MPa^{-1}) was set at $1.5\,MPa^{-1}$ based on published studies (Stokes I.A.F., Aronsson D.D. et al. 2006; Stokes I.A.F., Clark K.C. et al. 2007).
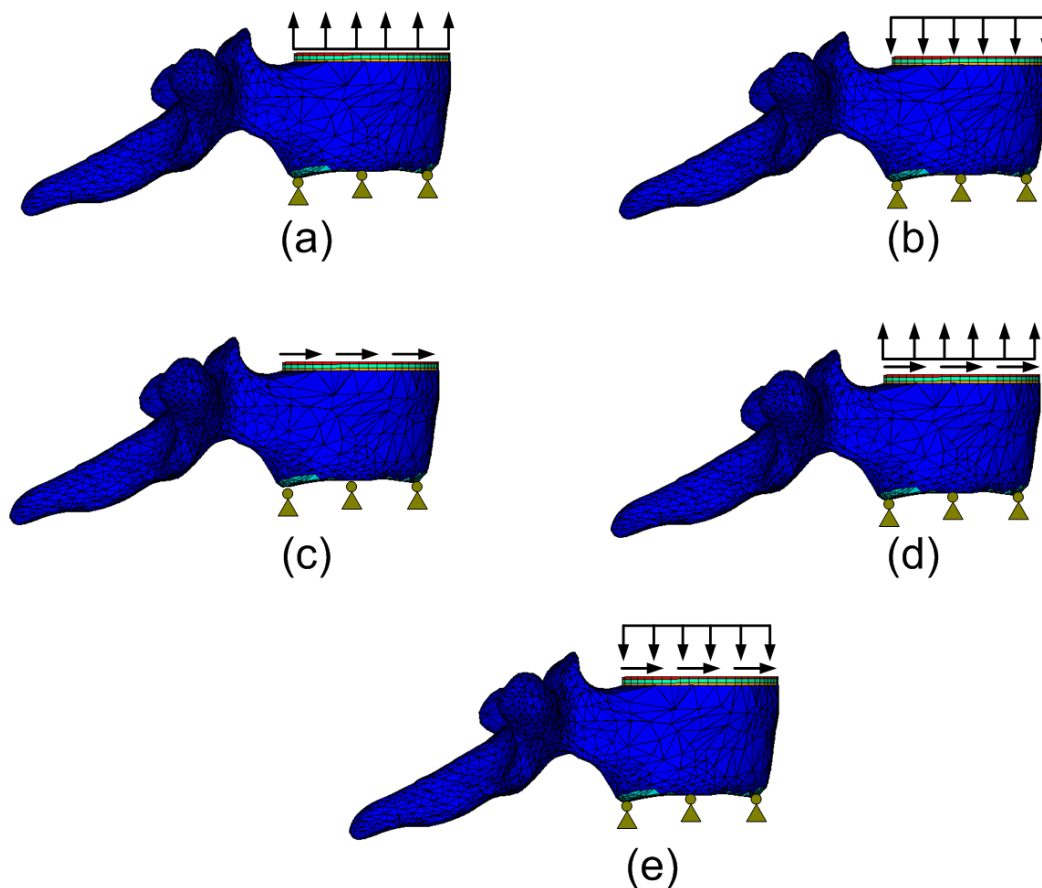
Figure 3-7 Loading conditions: (a) testing tension of 0.1MPa for calibration purposes; (b) compression of 0.1MPa; (c) shear force of 82 N (equivalent to 0.15MPa)) parallel to the vertebral initial surface; (d) combined tension of 0.1MPa and shear force of 82 N; (e) combined compression of 0.1MPa and shear force of 82N.

In the energy-based model (Eq. (3-27)), the baseline normal growth rate ε_{be} is equal to ΔG_l. The ratio of parameters a_e and b_e of this model was set at $\dfrac{b_e}{a_e} \approx 0.35$ (Stevens S.S., Beaupre G.S. et al. 1999), and the maximum contribution of mechanobiological growth was assumed to be less than 50% of the biological growth, as suggested by the published papers of.. (Shefelbine S.J., Tardieu C. et al. 2002; Shefelbine S.J. and Carter D.R. 2004). The tension stress for calibration was set at 0.1MPa (Stokes I.A.F., Aronsson D.D. et al. 2006). One-year growth under this loading condition was simulated using both models. Parameter a_e (with $b_e \approx 0.35\ a_e$) of energy-based model was adjusted up until the difference of the mean values of the mechanobiological growth between the two models was less than $10\,\mu m$ (Lin H., Aubin C. E. et al. 2008).

The growth process was simulated using a stepwise incremental procedure (**Figure 3-3**) (Lin H., Aubin C. E. et al. 2008). The boundary and external loading conditions were applied at the inferior endplate of T7 vertebra that was rigidly fixed along all degrees of freedom. External static loading was applied on the superior endplate of T7 vertebra. Besides tension loading for calibration, four loading conditions including axial and non-axial cases were investigated: compression, shear forces, as well as combined tension/shear and combined compression/shear (**Figure 3-7**). Tension and compression (0.1MPa) were applied perpendicular to the upper surface of the vertebra (**Figure 3-7**a-b). Shear force (82 N, equivalent to 0.15MPa) was applied parallel to this surface and equally distributed on each node (**Figure 3-7**c). Combined tension (0.1MPa)/shear (82 N) and combined compression (0.1MPa)/ shear (82 N) involved axial and non-axial loads in the further evaluation (**Figure 3-7**d-e). The loading values were set in terms of the experimental studies on growth with 0.1-0.2Mpa(Stokes I.A.F., Aronsson D.D. et al. 2006). Mechanobiological growth was evaluated from simulation results as the difference between growth with and without load as our previous study (Lin H., Aubin C. E. et al. 2008).

3.3 Mechanobiological study of the progression of scoliotic vertebral morphology

3.3.1 Finite element model of the functional unit T7-T8

- Vertebral body model

A finite element model (FEM) of a functional unit T7-8 was built for simulating the growth and progression of deformity. The FEM of vertebral bodies for a personalized pediatric vertebral function unit T7- T8, a healthy spine with normal vertebrae from an eleven-year-old male child, was built utilizing a geometric modeling technique developed above (**Figure 3-8** a-d). The vertebral bodies of T7 and T8 were separated into zones of cortical and cancellous bones (**Figure 3-8**c). The cancellous bone zone was meshed as 4-nodal solid tetrahedron elements. The meshed vertebra T7 included 4810 nodes and 18757 elements, and T8 included 5211 nodes and 20599 elements (**Figure 3-8**c).

Cortical bone was modeled as shell covering the outer lateral surface of the vertebral body (Thomas Edwards W., Zheng Y. et al. 2001; Schmidt H., Heuer F. et al. 2007; Schmidt H., Kettler A. et al. 2007; Schmidt H., Kettler A. et al. 2007; Lin H., Aubin C. E. et al. 2008). The shell was meshed as three-node triangular shell elements with 1-mm thickness based on the anatomical measurements on thoracic vertebrae (Thomas Edwards W., Zheng Y. et al. 2001; Schmidt H., Heuer F. et al. 2007; Schmidt H., Kettler A. et al. 2007; Schmidt H., Kettler A. et al. 2007). Cancellous bone was modeled as linear orthotropic material, while cortical bone was modeled as transversely isotropic material (**Table 3-2**).

- Intervertebral tissues

The intervertebral disc of T67 and T78 were created between the inferior and superior growth plate of adjacent vertebrae (**Figure 3-8**c). T6 inferior endplate was simulated by creating a rigid plate modeled as cancellous bone located on the top of T67 disc (**Figure 3-8**a). Discs were meshed as 8-nodal hexahedron solid elements. The nucleus was modeled as elements in the central area and elements in the outring were defined as annulus. The ratio of the volume value between nucleus and whole disc was 50% that agreed with the reported study of (Shirazi-Adl

S.A. et al. 1984). The annulus fibres were modeled as two-layer crisscross fibre layer and were represented as unidirectional spring elements attaching the outer annulus elements. The collagen fibre content was about 16% of the disc volume (Eberlein R. et al. 2001). Tissues of annulus and nucleus were modeled as linear isotropic material based on previous studies on pediatric vertebral model (**Figure 3-8**) (Sylvestre P.L., Villemure I. et al. 2007; Lin H., Aubin C. E. et al. 2008). Vertebral ligaments included anterior (ALL) and posterior (PLL) longitudinal ligaments, ligament flavum (LF), joints capsules (JC), interspinous ligament (Huselstein C., Netter P. et al.), supraspinous ligament (SSL), and intertransverse ligament (ITL) (**Figure 3-8**a). Those ligaments were represented as unidirectional spring elements with linear properties(Sylvestre P.L., Villemure I. et al. 2007). The zygapophyseal (facet) joints were modeled as surface-to-surface contact elements (Clin J., Aubin C. E. et al. 2007). The orientation of the facets agreed with the published observation on the thoracic vertebra anatomy (Panjabi M.M. et al. 1993). Material properties for intervertebral tissues were presented in Table 5.1 and were taken from literature (Clin J., Aubin C. E. et al. 2007; Schmidt H., Kettler A. et al. 2007; Schmidt H., Kettler A. et al. 2007; Sylvestre P.L., Villemure I. et al. 2007; Lin H., Aubin C. E. et al. 2008)

- Growth plate model

Vertebral growth in length occurred in the epiphyseal growth plate physiologically located at the superior and inferior vertebral endplates (Villemure I., Aubin C. E. et al. 2002; Wang Y., Middleton F. et al. 2004; Lin H., Aubin C. E. et al. 2008). The growth plate model was created on the superior and inferior surfaces of vertebra T7 (**Figure 3-8**d). A growth plate was also created on the superior surface of vertebra T8 in order to test the potential modification of position of T7 caused by the growth of T8. Growth plates were modeled as three-layer structures as described above: the loading sensitive area had a thickness of 0.3mm, the thickness growth area was0.5 mm, and the thickness of mineralized area was 0.3mm thickness (Lin H., Aubin C. E. et al. 2008). The definition of the thickness of the growth plate was based on the published measurement on thoracic vertebrae (Roberts S. et al. 1989; Thomas Edwards W., Zheng Y. et al. 2001). The energy-based mechanobiological growth model developed above was used to simulate the growth process (Eq. 3-26; 3-27).
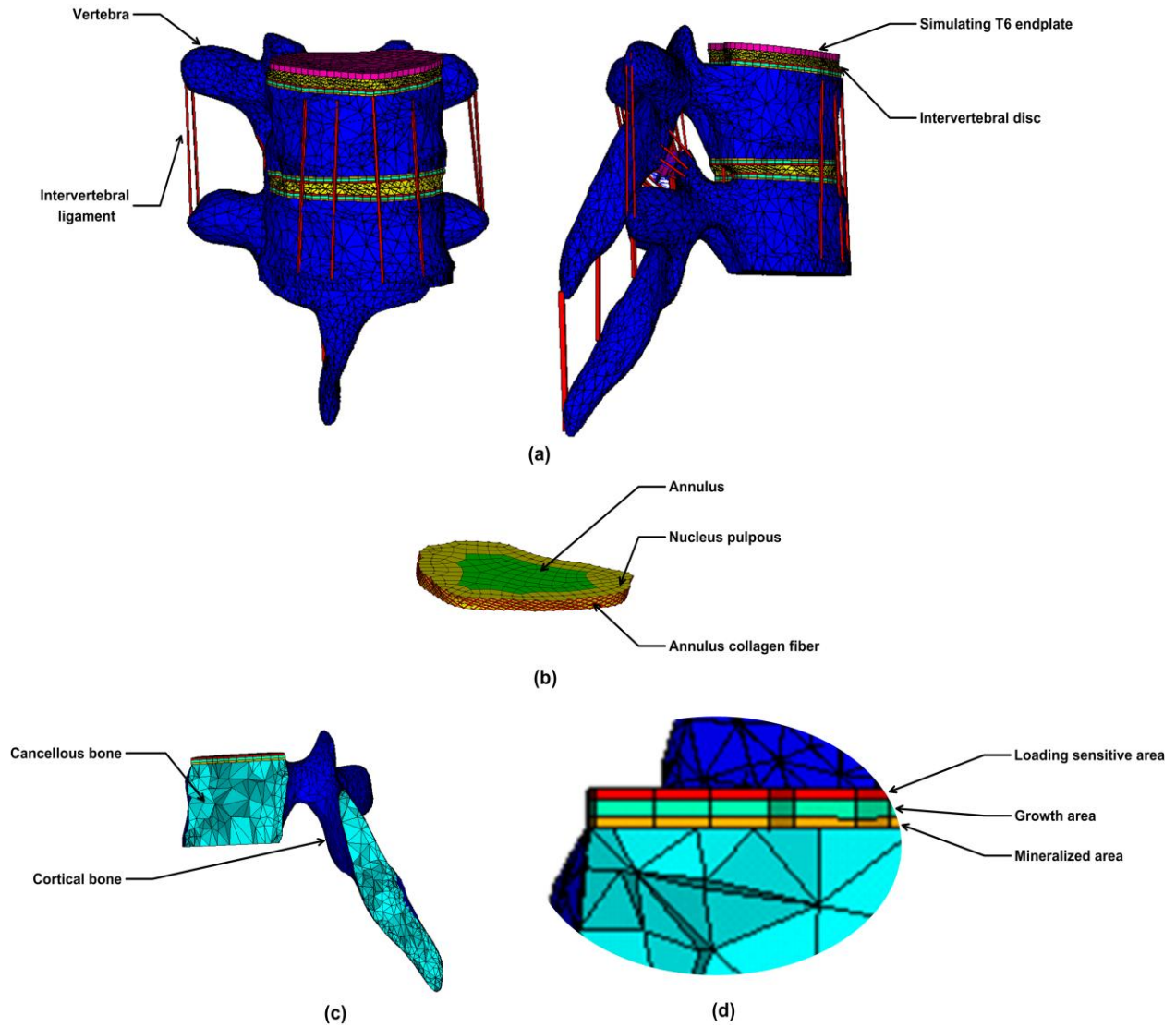
Figure 3-8 The finite element model (FEM) of the functional unit T7-T8: (a) model of vertebrae and intervertebral ligaments; (b) model of disc and collagen fibers in the intervertebral disc; (c) model of cortical and cancellous bone; (d) model of the growth plate including three areas: loading sensitive area, growth area, and mineralized area.

Table 3-2 Material properties of the finite element model

Tissue	Element type	Material properties: elastic modulus (Mpa)						Possion ratio	Area (mm^2)
		Ex	Ey	Ez	Gxy	Gyz	Gxz	v	
Cotical bone[1]	3-node triangular shell (1mm thickness)	8000	8000	14000	3280	3280	3280	0.3	
Cancellous bone[1]	4-node tetrahedron	767	401	1157	20.4	24	24	0.12	
Growth plate									
Loading sensitive area[2,3,4]	8-node hexahedron	23.8	23.8	23.8	10.6	10.6	10.6	0.4	
Growth area[2]	8-node hexahedron	767	401	1157	20.4	24	24	0.12	
Mineralized area[2]	8-node hexahedron	767	401	1157	20.4	24	24	0.12	
Interverbral disc									
Nucleus pulpous[1]	8-node hexahedron	2						0.499	
Annulus[1]	8-node hexahedron	8						0.45	
Annulus collagen fiber[1,5]	2-node link(tension only)	550						0.3	
Intervertebral ligament									
Anterior longitudinal ligament[1]	2-node link(tension only)	20						0.3	38
Posterior longitudinal ligament[1]	2-node link(tension only)	70						0.3	20
Ligament flavum[1]	2-node link(tension only)	50						0.3	60
Interspinous ligament[1]	2-node link(tension only)	28						0.3	35.5
Intertransverse ligament[1]	2-node link(tension only)	50						0.3	10
Supraspinous ligament[1]	2-node link(tension only)	28						0.3	35.5
Facet capsulary ligament[1]	2-node link(tension only)	20						0.3	40

1:(Sylvestre P.L., Villemure I. et al. 2007)

2:(Lin H., Aubin C. E. et al. 2008)

3:(Schmidt H., Kettler A. et al. 2007)

4:(Schmidt H., Heuer F. et al. 2007)

5: (Shirazi-Adl S.A., Shrivastava S.C. et al. 1984)

3.3.2 Measurement methods

The wedging angle was measured between surfaces of superior and inferiror growth plates of T7. The intervertebral rotation was measured between T7 and T8 based on the revised growth plate geometry.
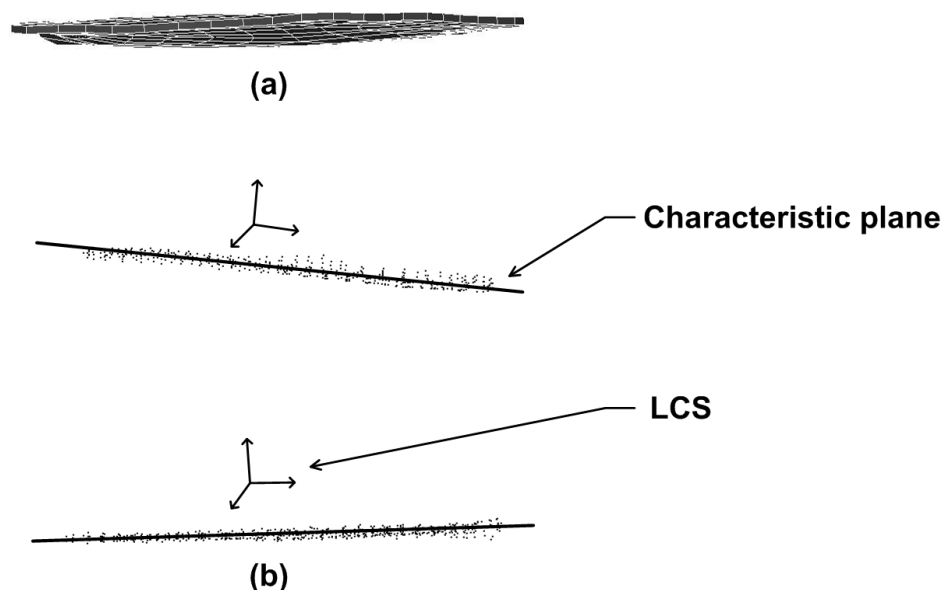
Figure 3-9 determination of the characteristic plane for endplate surface: (a) irregular shape of the growth plate surface after vertebral growth; (b) the characteristic plane for the irregular surface. The local coordinate system (LCS) for each vertebral growth plate was created based on the characteristic plane.

- characteristic plane

We used best fit planes to represent the surfaces of growth plates that exhibited irregular geometries after growth (**Figure 3-9**a). The procedure for the determination of a best fit plane for a growth plate was summerized as following steps:

(1) Creating a coordinate data set of nodes in a surface for a growth plate. Each surface had one corresponding date set, which was written as:

$$X = (x_1, x_2, \cdots x_n)$$
$$Y = (y_1, y_2, \cdots y_n)$$
$$Z = (z_1, z_2, \cdots z_n)$$

(3-28)

Where n is the number of nodes in a growth plate surface (superior or inferiror sides). A data set had three sub-sets, X, Y, Z, which were re coordinate data sets for a coresponding axis under global coordinates.

(2) Calculating covariance between two sub-sets. The covariance can be written as:

$$\underset{va=x,yz;\,vb=x,y,z}{cov(va, vb\ )} = cov(vb, va) = \frac{\sum_{i=1}^{n}(va_i - \overline{VA})(y_i - \overline{VB})}{n-1}$$
$$\scriptstyle VA=X,Y,Z;\,VB=X,Y,Z$$

(3-29)

Where $\overline{VA}$ or $\overline{VB}$ wass the mean value of a sub-sett, and $cov(\ )$ represented the covariance. The above calculations form the following covariance matrix:

$$C = \begin{pmatrix} cov(X,X) & cov(X,Y) & cov(X,Z) \\ cov(Y,X) & cov(Y,Y) & cov(Y,Z) \\ cov(Z,X) & cov(Z,Y) & cov(Z,Z) \end{pmatrix}$$

(3-30)

(3) Determing a best fit plane. The eigenvalues and eigenvectors of the covariance matrix were determined (Eq. 3-30). For a 3×3 matrix, there were three eigenvectors with respect to three eigenvalues obtained from this matrix. The eigenvector with maximum eigenvalue represented a best fit plane, which was best fit for the irregular surface of a growth plate. This plane was term as characteristic plane in this study (**Figure 3-9**b). A local coordinate system (LCS) was created on a characteristic plane. For a characteristic plane, the LCS was defined as Cartesian coordinates with z-axis perpendicular to this

plane (**Figure 3-9**b). Each plane had a corresponding LCS. Those LCSs would be used to orientate mechanical loading and growth simulation as well as measurement of vertebral morphologies.

- Wedging angle and rotation angle

Wedging angle is the most important characteristic for evaluating the vertebral deformity(Parent S., Labelle et al. 2004).Wedging angle of T7,the intervertebral disc T78 was measured in the coronal and sagittal planes utilizing the above defined characteristic plane (Figure 3-10). The measurement of the intervertebral axial rotation was done based on the difference of vertebral rotations of T7 and T8, which was defined by using the Stokes's method (Stokes I.A.F., Bigalow L.C. et al. 1986).
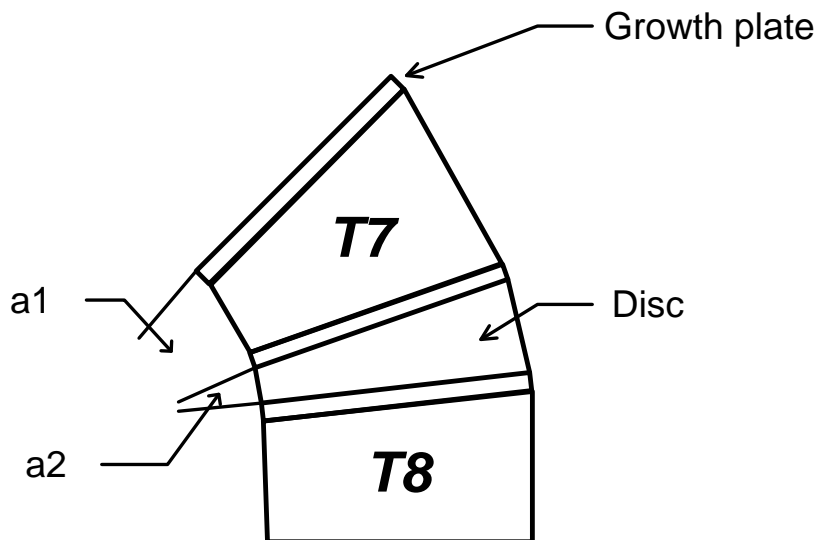
Figure 3-10 Measurement of the vertebral and discal wedging in the coronal plane. a1: T7; a2: intervertebral disc T78.
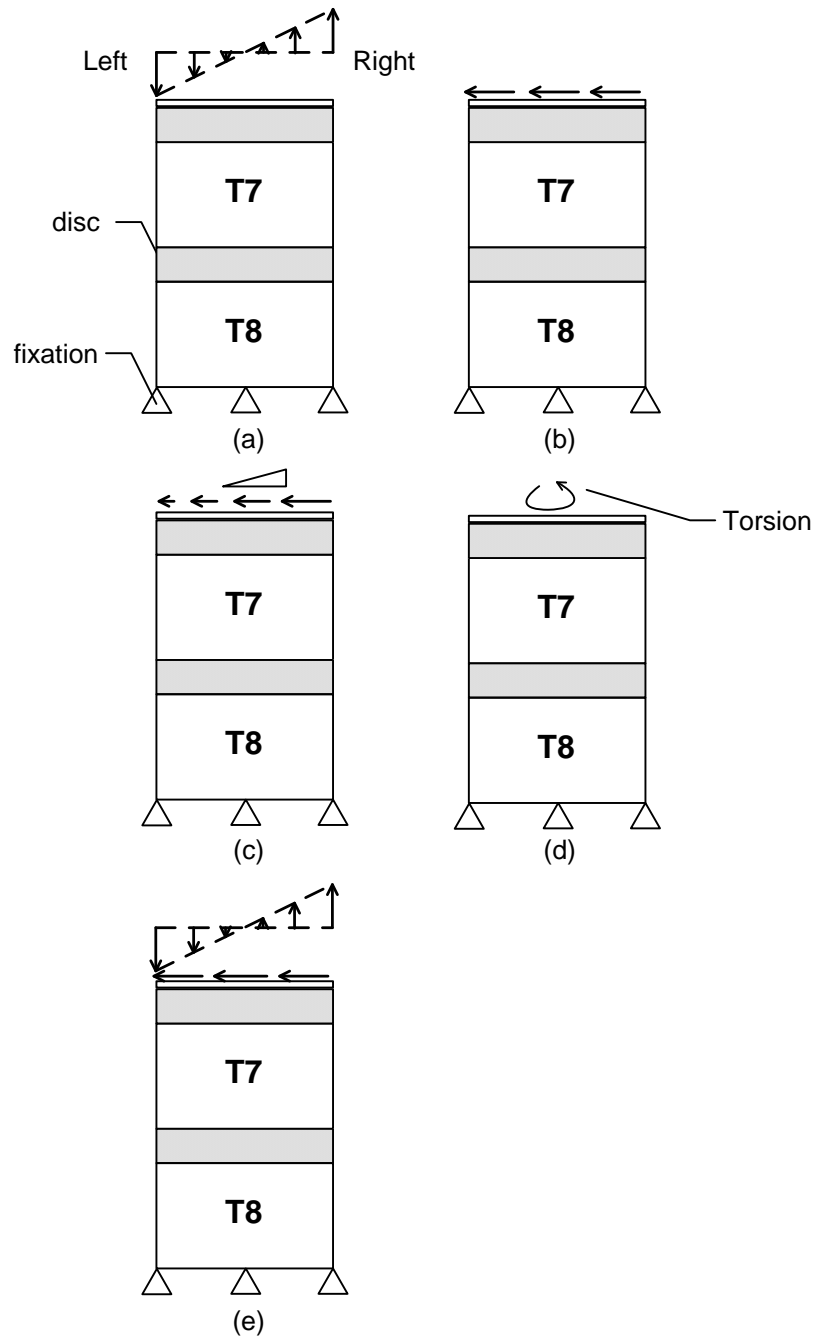
Figure 3-11 Schematic diagram of simulated mechanical environments: (a) Pure axial loading configuration: compression (maximum 0.35Mpa) and tension (maximum 0.35Mpa) with gradient distribution; (b) shear pressure (0.3Mpa); (c) shear pressure with gradient distribution (maximum 0.6Mpa); (d) torsion (0.3Mpa); (e) combined axial loading and shear. Axial loading has gradient distribution with maximal compression 0.35Mpa and maximal tension 0.35Mpa.

3.3.3 Mechanical loading

Particular loading conditions were designed for identifying the mechanobiological influences of those conditions on vertebral morphological modification. A fixed boundary condition was applied on the inferior side of T8, while different mechanical loads were applied on the inferior endplate of T6 (**Figure 3-11**). Usually, a vertebra sustained mechanical loading including compression, tension, shear, torsion, which were generated from the muscle and other soft tissues activated by spinal movement, extension, flexion, bending, and axial rotation (White A.A. and Panjabi M.M. 1990). Four loading conditions were designed in this study in order to analyze the mechanobiological influence from axial and non-axial loading as well as the combined modes: (1) Surface load with gradient distribution of compression and tension(**Figure 3-11**a). (2) Shear, uniform and with a gradient distribution, parallel to the upper surface of the endplate (**Figure 3-11**b-c). (3) Torsion (**Figure 3-11**d). (4) Combined axial and shear loading (**Figure 3-11**e). The component of axial loading was the same as the first loading mode.

It should be noted that the mechanobiological growth was not over 50% of the baseline growth in terms of the physiological condition (Shefelbine S.J. and Carter D.R. 2004). A vertebra may subject to a load with much high magnitude, which was called overloading conditions. Overloading conditions meant that the load was beyond the 'threshold value', which induced maximal mechanobiological growth (50% of biological growth). For example, for a overloading case, the value of mechanobiological growth (ε_{me}) calculated from the Eq. 3-25 would be higher than 50% of baseline growth, ε_{be}. In this case, ε_{me} should be reset as 50%* ε_{be} in terms of physiological restriction of mechanobiological growth. It should be noted that for any overloading case, the mechanobiological growth would be same no matter how high the load was. For instance, if there were two loads, F_1 and F_2, and both loads met the overloading condition, those loads would induce same values of mechanobiological growth. Under overloading conditions, the full mechanobiological contributions of those loads to growth were difficult to identify because growth modulations were always same. Those loading conditions should be avoided for the purpose of testing full impacts of the mechanical loads on morphological modification. The habitual spinal loading was not clear. It was reported that the vertebral growth plates sustained 0.8-0.9 Mpa pressure for nomal mechanical environments and

50% greater magnitude for maximal pressure of those environments (Stokes I.A.F. 2007). The values of loads were set based on experiments and reported studies on mechanical environments of growth plate and non-overloading consideration (Stokes I.A.F., Aronsson D.D. et al. 2006; Stokes I.A.F. 2007).

CHAPTER 4.   RESULTS

This chapter was divided into three sub-sections for presenting simulation results by using corresponding methods described in Chapter 3. The order of those sub-sections was same as what was present in Chapter 3.

4.1 Comparative study of Stokes and Carter's models

The calibrated tension applied on the modeled vertebra induced uniform growth with same magnitudes using both models (**Figure 4-1**). The calibrated parameters a and b of Carter's model were finally fixed at 0.155 and 0.072. Using these parameters, the difference of the mean value of the mechanobiological growth on both models was 7 μm, which was less than the predefined criteria of 10 μm (**Figure 4-1**). After calibration, these parameters were applied on following simulations for their comparisons.
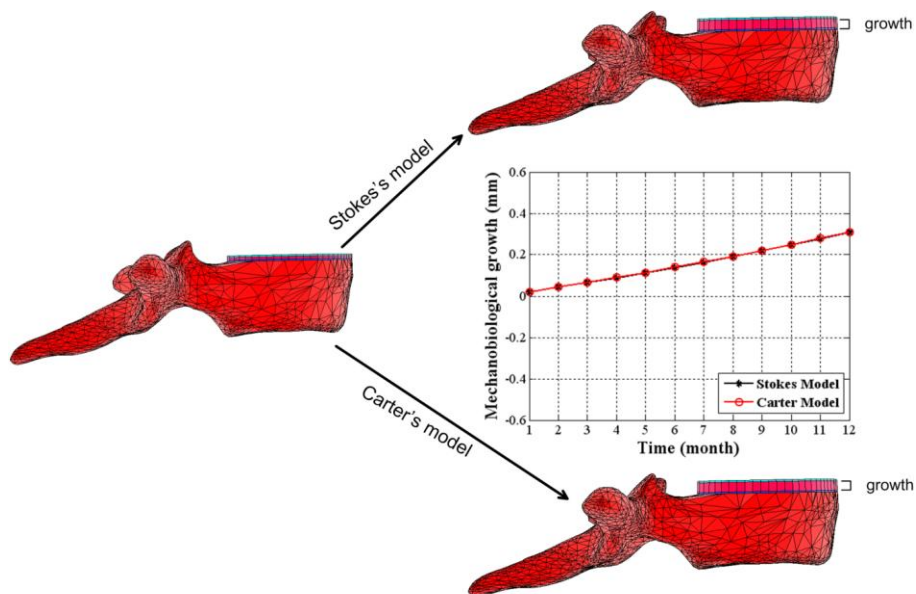
Figure 4-1 Calibration of the two models by applying a tension of 0.2MPa and carrying out one-year of growth. Similar growth is obtained for both models following calibration.

Stokes's model   Carter's model

(a)

(b)

(mm)

(c)

(d)

(e)
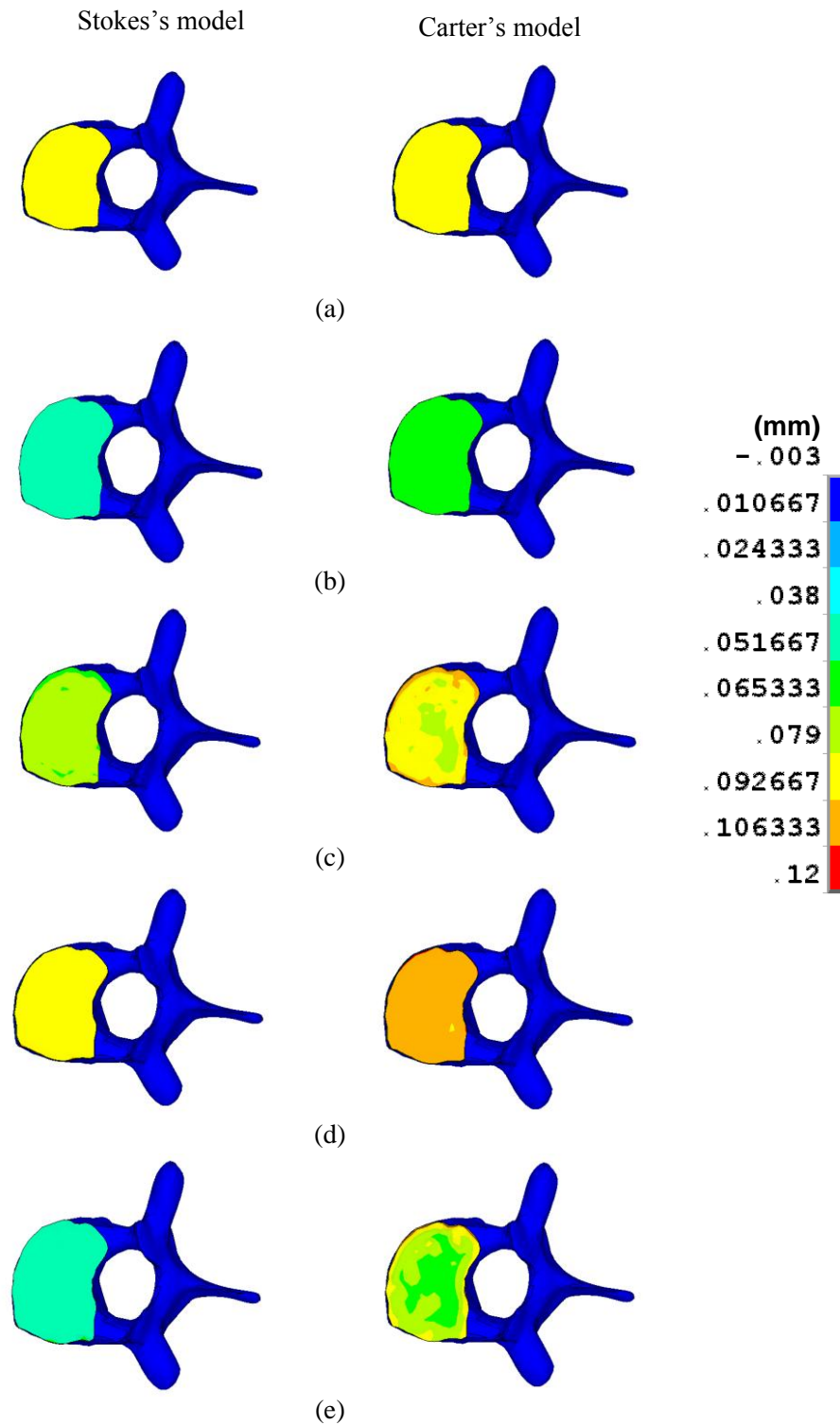
Figure 4-2 Growth distribution on the growth plate using Stokes's and Carter's model under following loading cases; (a) tension; (b) compression; (c) shear force; (d) combined tension/shear; (e) combined compression/shear.

Spatial distribution of growth using Stokes's model presented uniform feature (**Figure 4-2**a-e). Carter's model induced uniform distribution of the growth under calibrated tension (**Figure 4-2**a). Under the compression, the growth presented uniform distribution in the middle area (**Figure 4-2**b).Slightly non-uniform growth distribution with low variation (around 24 μm) was present in the middle area for shear and combined loading cases (**Figure 4-2**c-e).

Different mechanobiological growth patterns resulted from the calibrated models. Negative mechanobiological growth (reduced growth rate) was triggered for the compression loading condition, but Carter's model had 39% less growth modulation than Stokes's model (**Figure 4-3**a and **Table 4-1**). Shear forces generated mainly shear stress with an average of 0.19MPa and very low axial stresses with an average of 0.0005MPa. This loading condition triggered over 10 times more positive growth modulation (growth rate increase) in Carter's model as compared to Stokes's model, which produced negligible growth modulation (**Figure 4-3**b and **Table 4-1**).

Combined loads also induced different growth patterns. Combined tension/shear forces stimulated positive mechanobiological growth in both models. Carter's model induced 51% more growth modulation for this loading case (**Figure 4-3**c and **Table 4-1**). Combined compression/shear forces led to significant low (<<0.1) comparative ratio of mechanobiological growth (Carter's model/Stokes model) (**Figure 4-3**d and **Table 4-1**). Negligible negative growth modulation (8.6 μm) was triggered by the Carter's model. In contrast, negative mechanobiological growth caused by Stokes's model was up to 280.3 μm, which was close to the magnitude under compression, 283.1 μm (**Table 4-1**).

4.2 Energy-based modeling results

The calibrated tension applied on the vertebra induced uniform growth using the energy-based model (**Table 4-2**). The calibrated parameters for vertebral growth a_e and b_e of the energy-based model were finally fixed at 0.2335 and 0.08. Using these parameters, the difference of the mean value of the mechanobiological growth on both models was 0.3 μm, which was less than the predefined criteria of 10 μm (Figure 4-5a, **Table 4-2**) (Lin H., Aubin C. E. et al. 2008). This study also presented the simulation results using the Stokes's model in respect that it was

supported by experiments under axial loading conditions. In addition, Carter's model was not involved in the simulation since this work had been done in the previous study.

Table 4-1 Mechanobiological growth under different loading conditions

Loading conditions	Mechanobiological growth (μm) (average $\pm$ standard deviation)		
	Stokes's model	Carter's model	Ratio (Carter's/Stokes's)
Compression	-283.1 ±5.9	-172.4±6.2	0.61
Shear force	3.1±8.4	218.7±69.3	>>10
Combined tension/shear	310.5±10.1	469.7±46.1	1.51
Combined compression/shear	-280.3±9.8	-8.6±71.4	<<0.1

Basically, the mechanobiological growth presented quasi-linear increase or decrease depending on the loading condtion. Under the compression loading, the energy-based model triggered retardation of growth due to the negative mechanobiological growth (Figure 4-5b, **Table 4-2**). The negative growth modulation rate was slightly higher than that of Stokes's model after 12-month growth with ratio of 1.17. Under the shear case, the mechanobiological growth rate for energy-based model presented a slight fluctuation between -5.5 μm and 5.8 μm at around six months, followed by a quasi-linear increase thereafter. A significant low negative mechanobiological growth rate was triggered after one year's growth with -50.7μm. Stokes's model was insensitive to this loading case, which induced negligible mechanobiological growth (**Table 4-2**;Figure 4-5c).

The combined loading cases, including both axial and non-axial loads, produced significant different growth results from the individual loading. The combined tension/shear triggered higher growth rate (228.8 μm) than tension only case, i.e. the adding of shear force resulted in around 46 μm of the increment of growth, while Stokes's model led to growth modulation of 186.9 μm approximating its tension only condition (183.1 μm) (Figure 4-5d, **Table 4-2**). The energy-based model presented triggered higher growth than Stokes's model under this loading case in terms of ratio of growth modulation rate (1.22) (**Table 4-2**). Combined compression/shear forces resulted

in negative growth modulation using energy-based models. However, this loading case triggered only around 50% of the magnitude of growth modulation in comparison with the compression only case (99 μm vs. 206 μm) (**Table 4-2**), and it was around 100 μm increment of growth modulation due to the involvement of shear forces. In contrast, the growth modulation induced by Stokes's model in this combined loading case (172 μm) was close to the one under compression only condition (175.5 μm) (Figure 4-5e, **Table 4-2**).

Table 4-2 Simulation results under different loading condition using the energy-based model and Stokes's model.

Loading conditions	Mechanobiological growth (μm)		
	Stokes's model	Energy model	Ratio (Energy/Stokes's)
Tension (calibration)	183.1	182.8	1
Compression	-175.5	-206.2	1.17
Shear force	3.7	-50.7	
Combined tension/shear	186.9	228.8	1.22
Combined compression/shear	-172	-99	0.58
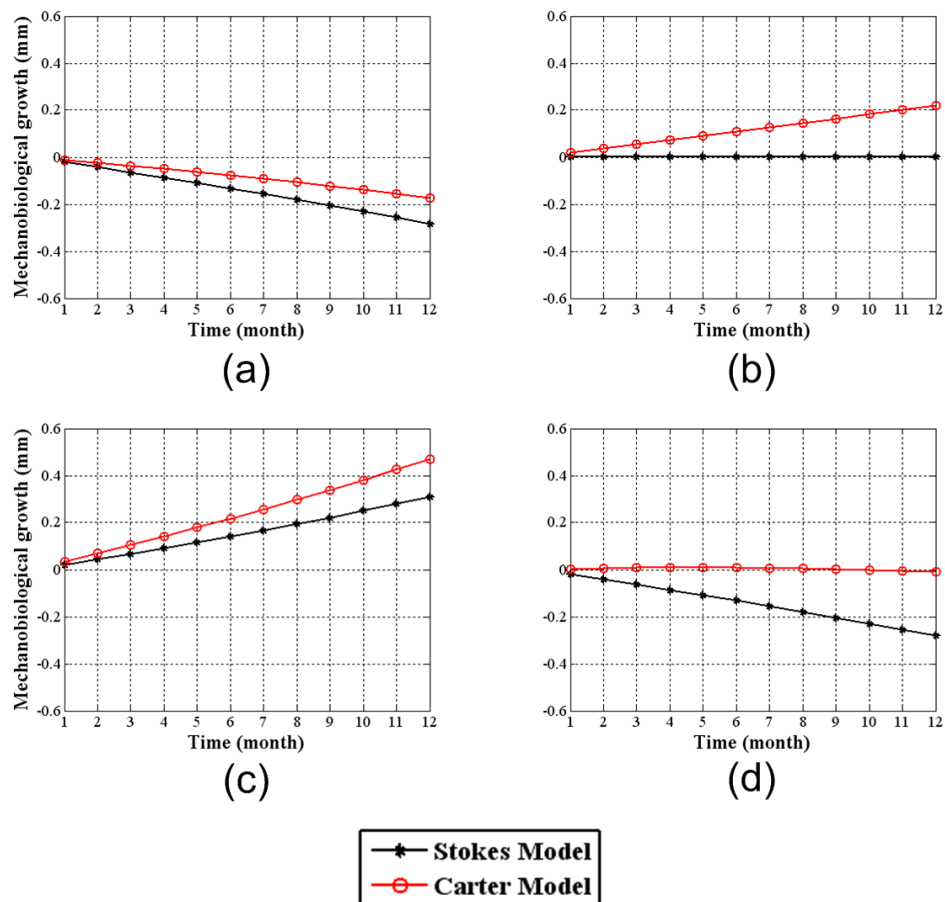
Figure 4-3 Mechanobiological growth rates using Stokes' and Carter's models under the following loading cases: (a) compression; (b) shear force; (c) combined tension/shear; (d) combined compression/shear
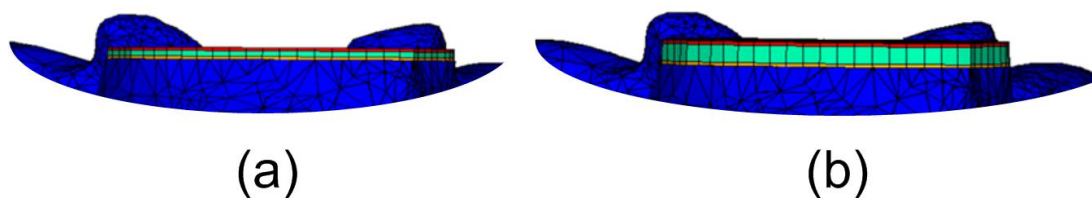
Figure 4-4 The modification of the geometry of the vertebral growth plate after one-year growth: (a) initial model of vertebral growth plate; (b) modified model after one-year growth.
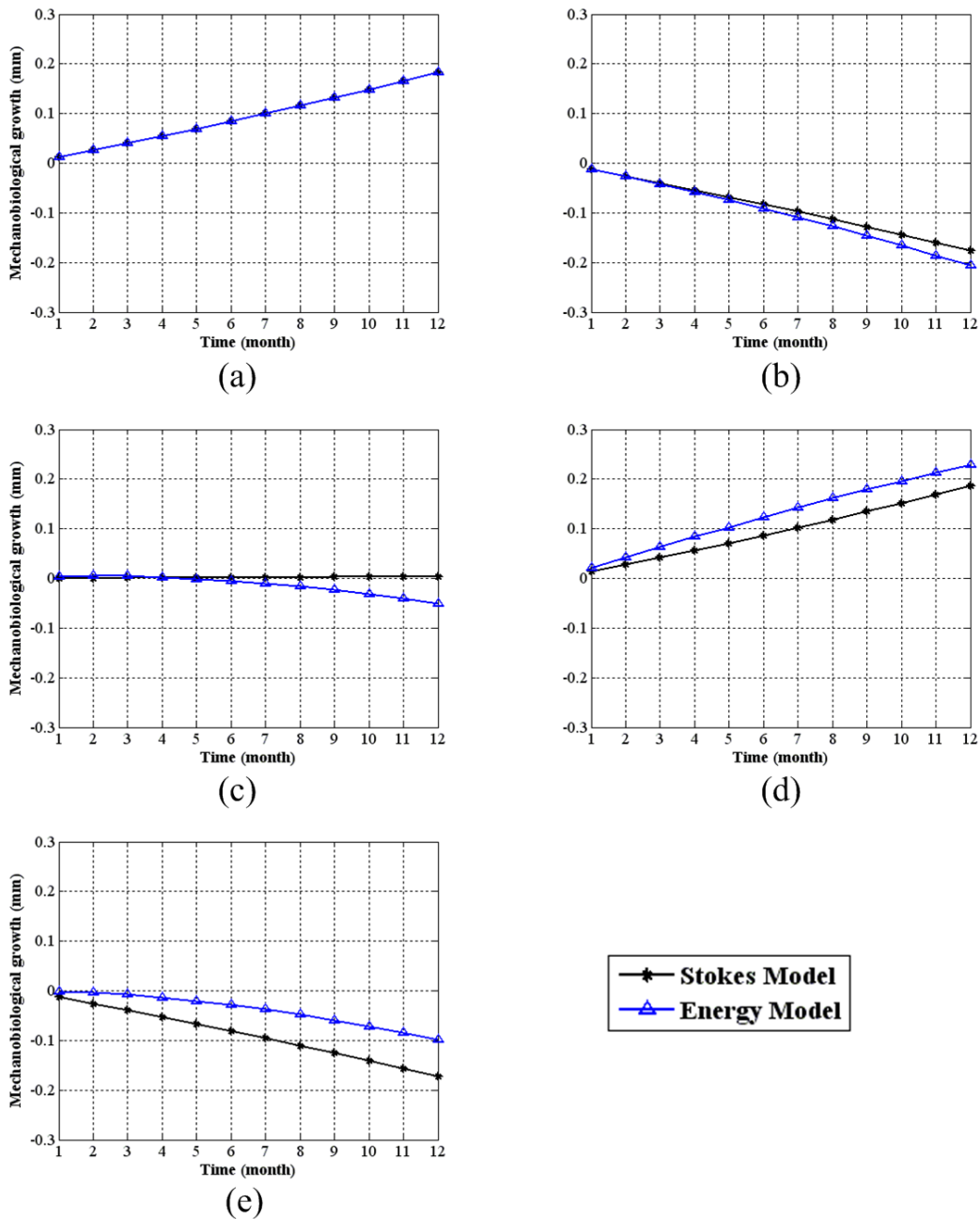
Figure 4-5 Mechanobiological growth rates using Stokes's and energy-based models under the following loading cases: (a) tension; (b) compression; (c) shear force; (d) combined tension/shear; (e) combined compression/shear.

4.3 Results for the simulation study of the progression of vertebral deformities

The initial model presented negligible wedging angle in the coronal plane (0.02 ° and 0.9 ° respectively for T7 and T78 discs). There was also negligible intervertebral rotation (0.3 °) (**Table 4-3**). Under the different loading conditions, the vertebral wedging angle and intervertebral axial rotation presented quasi-linear behavior (**Table 4-3**). The negligible modification of the intervertebral disc wedging (<0.4 °) was obtained in the simulation of deformity of the function unit T7-T8. In addition, there was little modification of the sagittal wedging (<1°) (**Table 4-3**).

Table 4-3 The modification of vertebral wedging in the coronal plane and of intervertebral rotation after two-year growth under different mechanical loads

Loading	description	measurement of T7 wedging		intervertebral axial rotation
		wedging angle: front (initial 0.02^o)	Wedging angle: sagittal (initial 4.7^o)	Rotation angle (initial -0.3^o)
gradient axial loading	compression and tension with maximum 0.35(Mpa)	4.8^o	5.7^o	3.4^o
Lateral shear	Shear pressure with 0.3Mpa	2.5^o	4.6^o	1.7^o
Gradient shear	shear pressure : 0~0.6Mpa	3.0^o	4.2^o	1.9^o
torsion	torison 0.3Mpa	1.4^o	4.1^o	0.4^o
Combined shear and gradient axial loading	compression and tension with maximum 0.35(Mpa); shear pressure 0.3Mpa	2.3^o	4.8^o	1.9^o
Combined shear and gradient axial loading	compression and tension with maximum 0.35(Mpa); shear pressure 0.05Mpa	4.4^o	5.7^o	3.1^o
combined torsion and gradient axial loading	compression and tension with maximum 0.35Mpa; torsion 0.3Mpa	2.4^o	4.3^o	0.9^o
modification range		1.4^o~4.8^o	0.1^o~1.0^o	0.7^o~3.7^o
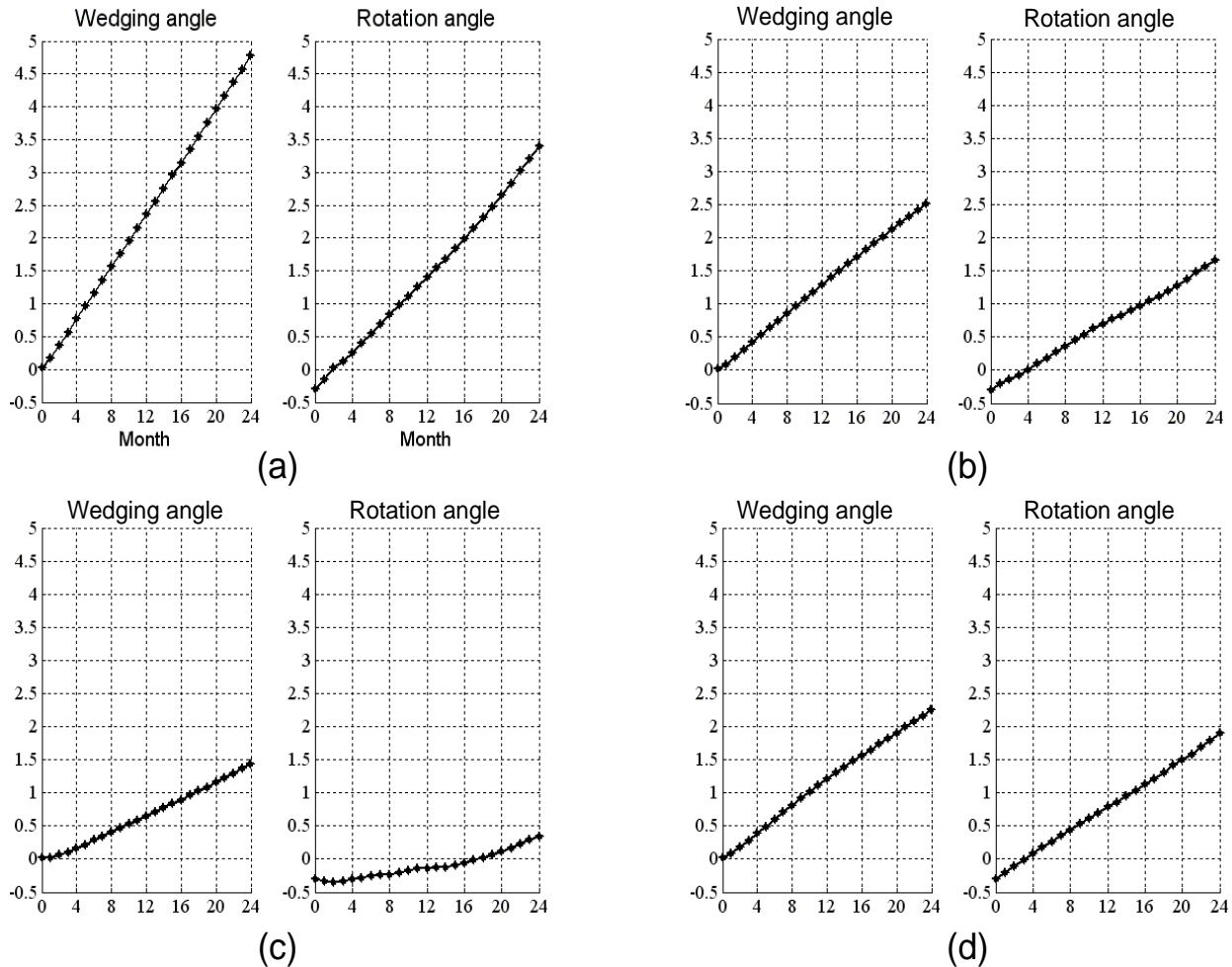
Figure 4-6 simulated wedging angle of T7 (in the coronal plane) and intervertebral axial rotation of T78 during two years growth under the following mechanical loads: (a) compression and tension (maximum 0.35Mpa) with gradient distribution; (b) shear (0.3Mpa); (c) torsion (0.3Mpa); (d) combined axial loading with gradient distribution and shear. The axial loading was a gradient compression and tension with maximal value of 0.35Mpa, and a shear pressure of 0.3Mpa.

For the pure axial loading condition, compression/tension with gradient distribution, the wedging angle of T7 increases by up to $4.8°$ in the coronal plane only, with and intervertebral rotation of $3.4°$ (**Figure 4-6**a;**Table 4-3**). The wedging shape was found in this loading case (**Figure 4-7**). As a loading condition without axial component, the lateral pure shear pressures with uniform and gradient distribution were also able to trigger vertebral wedging and

intervertebral rotation. Those two loading conditions resulted in a wedging angle of 2.5 °and 3.0 ° respectively in the coronal plane (**Table 4-3**; **Figure 4-6**b), and intervertebral axial rotation of 1.7° and 1.1.9° degrees (**Table 4-3**). The torsion load modified less the deformity (1.4 °for the wedging of T7 and 0.4 °of axial rotation) (**Table 4-3**; **Figure 4-6**c).
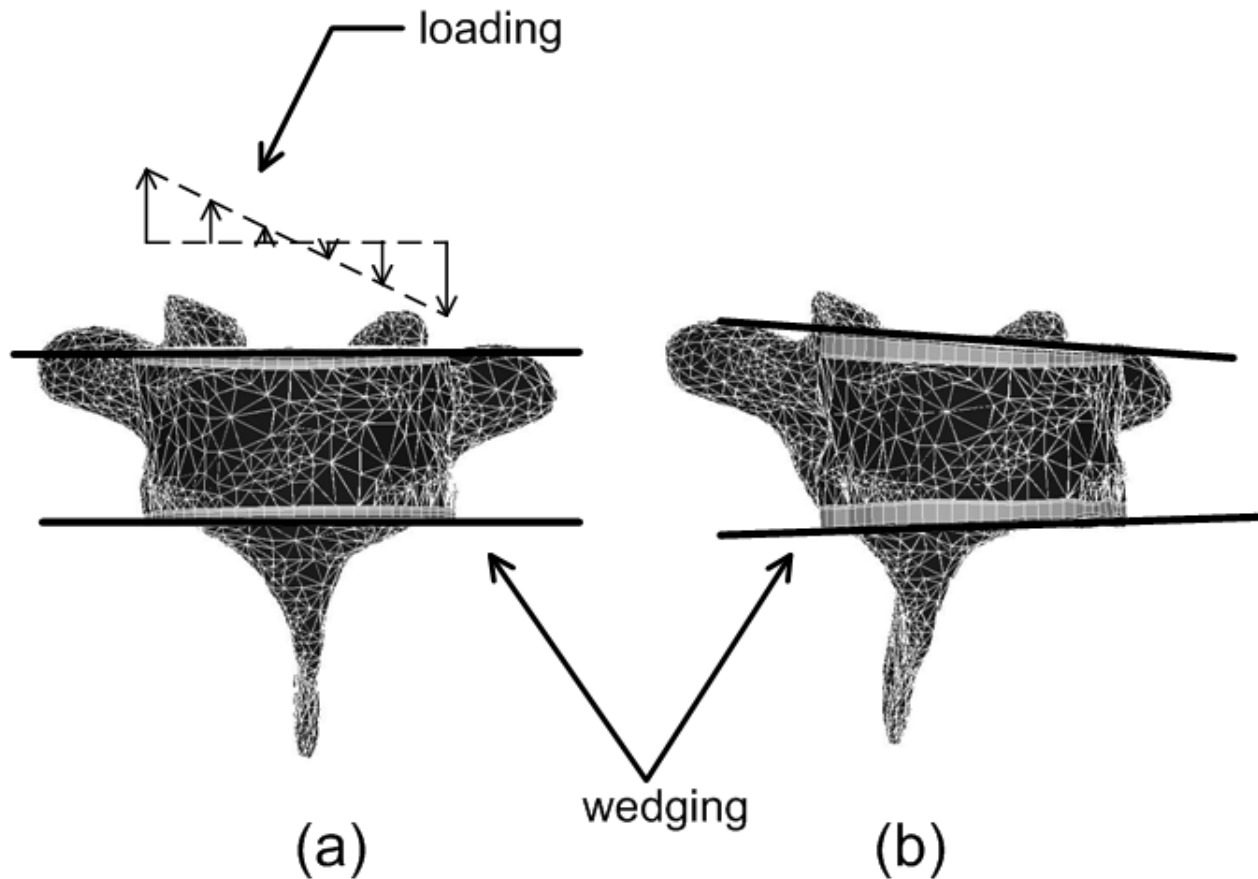
Figure 4-7 Modification of the vertebral body morphology. (a) the initial morphology; (b) wedging after two-year growth.

The combination of gradient compression/tension and shear pressure (**Figure 4-6**e) induced 2.3 °of wedging angle in the coronal plane at T7, and 1.9 °of intervertebral axial rotation (**Table 4-3**, **Figure 4-6**d). Similarly, the combination of gradient axial loading and torsion triggered 2.4 ° of wedging in the coronal plane at T7 and a small intervertebral axial rotation of 0.9 °.

CHAPTER 5.   DISCUSSION

Underlying hypotheses on the nature of stress stimuli explain differences in the increase versus decrease growth modulation resulting from both models for a given loading condition. The model definition basically determined different roles to axial and non-axial stresses. This provided a precondition that induced different results on the tested simulations. As an experimentally based model and formulation of Hueter-Volkmann law, Stokes' model directly associated the mechanobiological growth to the uniaxial longitudinal stress, which was produced and measured by their experimental instruments (Stokes I.A.F., Mente P.L. et al. 2002; Stokes I.A.F., Gwadera J. et al. 2005; Stokes I.A.F., Aronsson D.D. et al. 2006; Stokes I.A.F., Clark K.C. et al. 2007). Carter's model theoretically associated complex mechanical stimuli involving multiaxial stresses to bone formation, which included the addition of new cartilaginous material within the growth plates, followed by the ossification of this cartilaginous tissue at the chondro-osseous junction (Carter D.R. and Wong M. 1988; Carter D.R. and Wong M. 1988; Shefelbine S.J., Tardieu C. et al. 2002; Shefelbine S.J. and Carter D.R. 2004; Shefelbine S.J. and Carter D.R. 2004). As opposed to Stokes' model, this model is not supported any experimental data or studies.

Growth modulation under shear forces highlighted the difference of the two modeling concepts. Stokes' model excluded mechanobiological influences of non-axial stresses, which resulted in the absence of mechanobiological growth upon application of shear forces. Moreland's studies (Moreland M.S. 1980), involving experimental *in vivo* torsional loading of rabbits tibiae, obtained similar results to Stokes' model, where no significant longitudinal growth was observed from torsion forces on growth plates. In contrast, the non-negligible positive mechanobiological growth (increasing the total growth) triggered by Carter's model explicitly exhibited the contribution of non-axial stresses to growth. According to Carter's theory, octahedral shear stress would have a positive role on bone development, and more precisely on the ossification component of that process (Carter D.R. and Wong M. 1988; Carter D.R. and Wong M. 1988; Stevens S.S., Beaupre G.S. et al. 1999; Shefelbine S.J. and Carter D.R. 2004). Indeed, some experiments found positive influences of shear stresses on bone ossification (Schwartz L., H. et al. 2003; Kim C.H., You L. et al. 2006), but no studies were found which

showed that shear forces increased the longitudinal growth rate of a bone. Significant correlations were also found between lesser bone growth rate and high hydrostatic pressure, another mechanical stimulus used in Carter's model (Lerner A.L., Kuhn J.L. et al. 1998). Different mechanobiological responses were also found under uniaxial compression loading. In Carter's model, compression generated a negative hydrostatic stress, while octahedral stresses were always positive. The opposite roles of the two stimuli counteracted their contributions to mechanobiological growth, which resulted in the weak ability of Carter's model to retard growth under compression loading. However, it has been shown that bone growth rate is decreased by non physiological compression, as stated by the Hueter-Volkmann law (Mehlman C.T., Araghi A. et al. 1997) and related experimental studies on *in vivo* animal models (Alberty A., Peltonen J. et al. 1993; Lerner A.L., Kuhn J.L. et al. 1998; Stokes I.A.F., Mente P.L. et al. 2002; Stokes I.A.F., Aronsson D.D. et al. 2006; Stokes I.A.F., Clark K.C. et al. 2007). The weak contribution of compression to retard growth, as simulated using Carter's model (**Figure 4-3**a, **Table 4-1**), has not yet been reported experimentally (Stokes I.A.F., Mente P.L. et al. 2002; Stokes I.A.F., Aronsson D.D. et al. 2006; Stokes I.A.F., Clark K.C. et al. 2007) .

The mechanobiological responses of both models under uniaxial and multi-axial stresses allowed identifying limitations of these two models. Simulation results in this study triggered different contributions of axial and non-axial stresses to the mechanobiological growth, which is involved in progressive skeletal deformity such as scoliosis, hip dysplasia, and other bone diseases (Stokes I.A.F. and Laible J.P. 1990; Shefelbine S.J., Tardieu C. et al. 2002; Villemure I., Aubin C. E. et al. 2002; Carrier J., Aubin C. E. et al. 2004; Shefelbine S.J. and Carter D.R. 2004; Shefelbine S.J. and Carter D.R. 2004; Villemure I., Aubin et al. 2004). The absence of non-axial stresses in Stokes' model could be a limit on applications involving complex loading conditions, which is not rare in the normal mechanical environment of the musculoskeletal system. This model was derived from experiments involving two uniaxial loads, compression or tension (Stokes I.A.F. and Laible J.P. 1990; Stokes I.A.F., Mente P.L. et al. 2002; Stokes I.A.F., Gwadera J. et al. 2005; Stokes I.A.F., Aronsson D.D. et al. 2006; Stokes I.A.F., Clark K.C. et al. 2007). Uses of this model should then be restricted to uniaxial loading conditions. The analytical/experimental divergence observed in Carter's model could be related to the absence of a defined direction for the modified growth. Carter's model predicts a growth increment but does

not specify the direction of the resulting increment. Importantly, this model was initially developed to predict bone formation (Carter D.R. and Wong M. 1988; Carter D.R. and Wong M. 1988). Hence, its application for mechanobiological growth studies, which involve orientation characteristic, should be further evaluated.

A more physiological mechanobiological growth model should take into account multi-axial stresses and integrate growth orientation based on the studies of the two modeling techniques. Experiments on uniaxial loading and Hueter-Volkmann law (Bonnel F., Dimeglio A. et al. 1984; Frost H.M. 1990; Stokes I.A.F. and Laible J.P. 1990; Stokes I.A.F., Aronsson D.D. et al. 1994; Mehlman C.T., Araghi A. et al. 1997; Lerner A.L., Kuhn J.L. et al. 1998; Stokes I.A.F., Mente P.L. et al. 2002; Stokes I.A.F., Gwadera J. et al. 2005; Stokes I.A.F., Aronsson D.D. et al. 2006; Stokes I.A.F., Clark K.C. et al. 2007) offer evidential bases in modeling of this physiological process. In addition, experimental studies (Carter D.R. and Wong M. 1988; Carter D.R. and Wong M. 1988; Stevens S.S., Beaupre G.S. et al. 1999; Beaupre G.S., Stevens S.S. et al. 2000) investigating the effects of shear on longitudinal bone growth would help defining the contribution of this non-axial stress to bone growth.

The energy-based model was developed and tested by this study for overcoming the limits found in previous models. Baed on the energy-based model, the biomechanical simulation results for axial loading condition (tension and compression) using the energy-based model are supported by published experimental studies and a recognized model specific for axial loading (Stokes' model). Simulation results presented the recognized mechanobiological property described by the Hueter-Volkmann law. Furthermore, this growth model quantified the mechanobiological contribution of axial loading to growth, and its quantification accuracy can be evaluated by Stokes' model, which formulized Hueter-Volkmann law based on experimental studies (Stokes I.A.F., Mente P.L. et al. 2002; Stokes I.A.F., Gwadera J. et al. 2005; Stokes I.A.F., Aronsson D.D. et al. 2006; Stokes I.A.F., Clark K.C. et al. 2007). It was suggested that the energy-based model and Stokes' model could be replaced with each other under the axial loading cases.

Actually, for the axial loading conditions, the replaceable property of energy-based and Stokes' model can be theoretically explained based on above modeling techniques. In the case where axial stresses are much greater than non-axial stresses, Mechanoregulation index (M_I) formulized as Eq. (3-22) can be simplified as:

$$M_I \approx \beta_{le}\sigma_l \tag{5-1}$$

By combining Eq. (5-1) and Eq. (3-25) to create a mechanobiological growth model, one obtains:

$$\varepsilon_{ml} \approx \beta_{le}\sigma_l St_g \tag{5-2}$$

where β_{le} is the loading sensitive factor. ε_{ml} is the mechanobiological growth under this special mechanical environment. St_g is the stimulus contribution index. σ_l represents the axial stress. The model described by Eq. 5-2 is similar to Stokes' model (Eq. 1-3), which represents the mechanobiological growth as $\Delta G_l \beta_l \sigma_{zz}$, a formulation of the Hueter-Volkmann law. ΔG_l is the baseline growth strain increment and β_l is the loading sensitivity factor. σ_{zz} is the axial stress that is same as σ_l described in Eq. 5-2. This equivalent characteristic indicates that Stokes' model is a special model for a particular mechanical environment where axial stresses are much greater than non-axial stresses. Basically, mechanobiological growth model has numerous mathematical expressions in terms of Equation (3-21) and (3-22), which presented general mathematical forms. Growth model developed in this study used two specific variables, octahedral and hydrostatic stresses, which were also used by Carter's model. This kind of mathematical expression was based on technical feasibility as described in Chapter 3. Although the new growth model used the same variables as Carter's model, it should be noted that it was not a model that simply improved Carter's model. Firstly, these two models were based on two different theoretical principles. As described in Chapter 3, the energy-based model was derived from a theory of energy-triggered mechanobiology(Silver F.H. and Siperko L.M. 2003), while Carter's model was derived from Carter's conclusions on mechanobiological contribution of two specific stresses, octahedral and hydrostatic stresses. Secondly, as technical development, other

mathematical expressions could be developed according to Equations (3-21) and (3-25). Those expressions would not include these two specific stresses and would be completely different from Carter's model. Thirdly, even though the same stress variables were used in both models, it should be noted that the stimulus contribution index (St_g), which governed the energy contribution rate and growth patterns, stimulating or retarding, was not involved in Carter's model. This resulted in a limitation of Carter's model on representing the mechanobiological growth as above finding.

The energy-based growth model especially contributes to multi-axial loading conditions. As a special loading case, pure shear force presented significant weak contribution to the growth modulation in terms of the simulation results. It should be noted that growth is associated with increments in the longitudinal growth direction for children and adolescents. This result was also supported by an *in vivo* experiment that applied torsion on rabbit tibial growth plates (Moreland M.S. 1980), in which it was found that, although angular bone growth was developed as a consequence to shear loading, the overall longitudinal growth rate was not significantly altered. Pure shear force might contribute to the mechanoregulation of growth plate but induce unobservable modification on longitudinal growth, as reported by (Moreland M.S. 1980). Shear stress was reported as a promoter of ossification that potentially stimulated bone growth (Stevens S.S., Beaupre G.S. et al. 1999; Shefelbine S.J. and Carter D.R. 2004). This characteristic was found in the simulation results under combined loading cases, which supported the positive contribution of shear stress to ossification during growth. Furthermore, the study on Carter's model under similar loading conditions also presented this property.

The energy concept integrates the different mechanobiological influences from multi-axial loading for modeling growth and is potentially able to explain the similar mechanobiological influence induced from different physical stimuli. Physiological mechanical loading is usually present under multi-axial directions. Different orientations of mechanical loads may play different roles on the growth process including endochondral growth and ossification (Carter D.R., Van Der Meulen M.C.H. et al. 1996; Stevens S.S., Beaupre G.S. et al. 1999). The different mechanobiological contributions of stresses generated from a multi-axial loading environment may also present coupling mechanisms that trigger the complex deformities that

could not be predicted if mechanical factors were taken into account independently. In order to carry out the complex growth process, energy physically integrates multi-axial stresses and implements the transformation of mechanical stimuli into the mechanochemical transduction, which regulates the biological growth, maintenance and remodeling (Carter D.R., Fyhrie D.R. et al. 1987; Silver F.H. and Bradica G. 2002; Silver F.H. and Siperko L.M. 2003). In addition, other stimuli, e.g. heat, electric/magnetic field, may also play similar roles on the regulation of bone cell activities (Madreperla S. A. et al. 1985; Ciombor D. M. et al. 2002), but this was not addressed in our study. Unlike the stress especially for mechanical environment, energy is a basic component existing in any kinds of processes including physical and biological process, and furthermore, energy can be considered as an equivalent that is generated from different stimuli but with similar effects. This comprehensive property makes it possible to explain how mechanical stimuli trigger biological modification (Carter D.R., Fyhrie D.R. et al. 1987). In addition, for the mechanical consideration, the energy concept logically integrates the multi-axial loads for comprehensively describing mechanobiological influences and further predicting the vertebra or other bone deformities.

The energy-based model includes advantages such as the integration of multi-axial stresses existing in spinal mechanical environments, which are physically present as, distraction, compression, torsion and shear. Based on the energy-based model, this study simulated the progressive modification of vertebral and discal morphology caused by growth triggered by multi-axial loading. As a human supporting system, the spine sustain both axial and non-axial loading for keeping its flexible movement. It was firstly found that both axial and non-axial loading were capable of independently changing the morphology of vertebrae. However, it was found that axial and non-axial stresses involved in multi-axial loadings have coupling roles on mechanobiological growth and thus modified the vertebral morphology could potentially develop in a scoliotic spine. Basically, the scoliotic morphological characteristics simulated in this study agreed with Parent's measurements on vertebral scoliotic morphology (Parent S., Labelle et al. 2002; Parent S., Labelle et al. 2004):

(1) Significant wedging in the coronal plane of scoliotic vertebrae;
(2) No significant increase in vertebral wedging in the saggital plane;
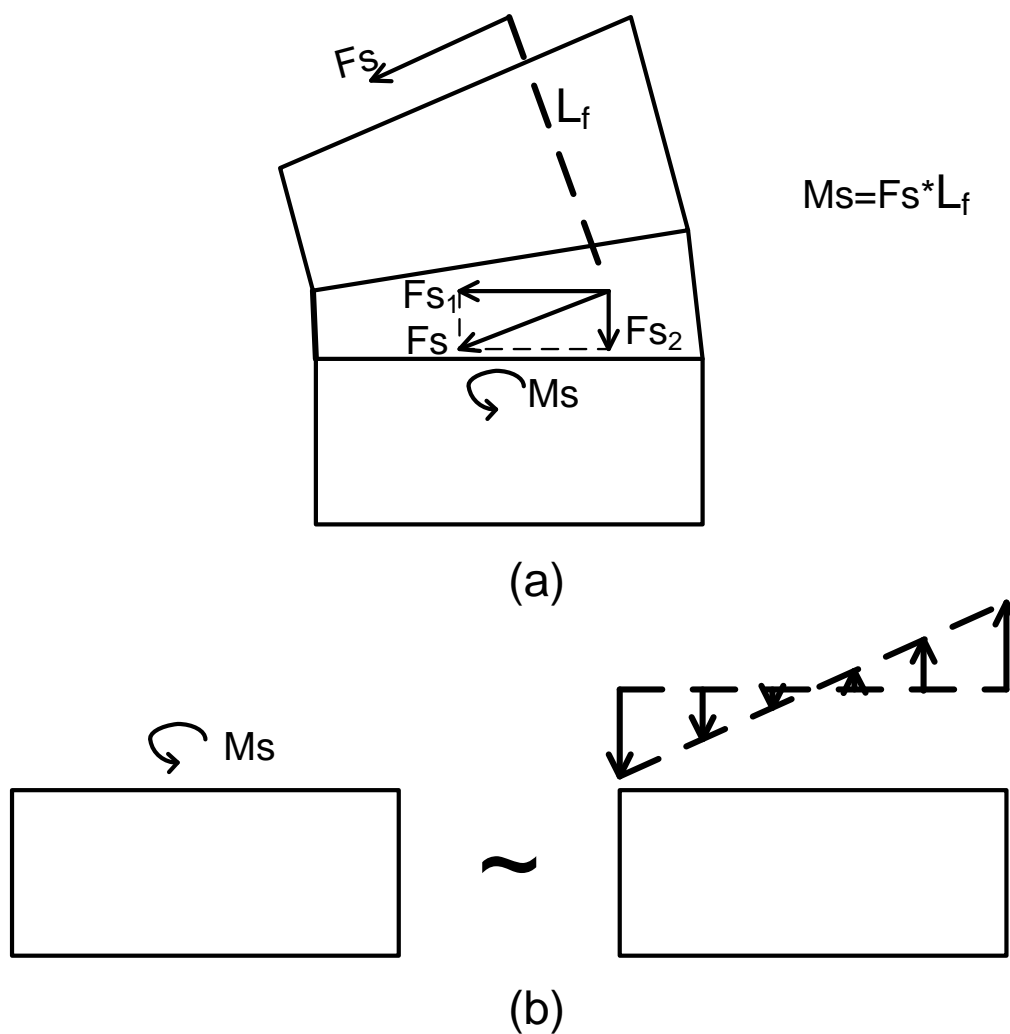
Figure 5-1 Schematic diagram of shear forces decomposition. (a) A shear force Fs is applied to a vertebra. This force can be transferred to a lower vertebra and is divided into two components: the shear force Fs1 and axial loading Fs2. The moment Ms is also generated for the force transferred; (b) the possible equivalent forces pattern generated from the moment.

Axial loading was reported as an important factor to induce or worsen the curvature of scoliotic spine via modifying the normal growth pattern (Villemure I., Aubin C. E. et al. 2002; Stokes I.A.F. 2007). The asymmetric distribution of axial loads induced growth asymmetry and

thus resulted in the increase of vertebral wedging angle, which is one of the most important physiological features of structural scoliosis. With the energy stimulus, it was possible to reproduce the Hueter-Volkmann Law, which only linked the compression and tension to vertebral growth and was demonstrated by experiments (Villemure I., Aubin C. E. et al. 2002; Stokes I.A.F. 2007; Stokes I.A.F., Clark K.C. et al. 2007; Van Der Plaats A. et al. 2007). It should be noted that the vertebral wedging angle (4.8°) triggered by axial loading, compression and tension with gradient distribution, approached the value of Parent's measurements for T7 scoliotic specimens, which included a wedging angle of 5.2° as compared to a 0.4° wedging angle in normal T7 vertebrae (Parent S. 2003). This simulation result suggested that axial loading, if distributed asymmetrically, was able to induce wedging in vertebrae individually. Even though the growth only occurred in the axial direction and remodelling process was not involved in this simulation, the obvious intervertebral rotation was also triggerd by axial loading. This rotation potentially worsened the lateral curvature of a spine that developed as scoliosis. Furthermore, the axial interverterbral rotation feature also agrees with reported observations that the vertebral body (T7) rotates towards the convex side of the spinal curve (Porter R.W. 2001; Castelein R.M. et al. 2005). The above morphological feature indicated that the axial loading was able to trigger the main characteristics of scoliotic vertebrae, which could further develop in structural AIS.

Simulation results (**Table 4-3**) showed that shear loading was capable of modifying the normal growth pattern and inducing the wedging vertebrae. Shear loading was able to modulate vertebral growth as discussed above. In addition, a shear force could generate additional axial loading that resulted in the growth pattern modification. Supposing that an external lateral shear force Fs is applied on a vertebra and transferred to adjacent or other vertebrae (**Figure 5-1**a), it would be an angular force instead of a pure shear force for the adjacent or other vertebrae because of the different orientations of vertebral endplate surfaces. As shown in **Figure 5-1**a, the force Fs was parallel to the surface of the upper vertebra and termed as a shear force. However, Fs was not a pure shear force with respect to the lower vertebra since this force was not parallel with the surface of this vertebra and was termed as angular force. This angular force could be decomposed as two components based on the orientation of a vertebral endplate: the new shear force along the endplate and axial force (compression or tension) perpendicular to the endplate (**Figure 5-1**a). The mechanobiological role of axial loading on morphological modification was

discussed in the above presented sections. Furthermore, moment loads, Ms (**Figure 5-1**b), would be generated during the force transferring. Those moment loads could also transform into either axial loading or non-axial loading on the vertebra for balancing the moment (**Figure 5-1**b). Those additional loadings could also result in morphological changes. However, it should be noted that torsion, a kind of special shear loading, presented poor influence on the morphological modification via the mechanobiological growth, which is in agreement with Moreland's experiments (Moreland M.S. 1980), where obvious rotation features in the epiphyseal plate was observed but significant mechanobiological growth was not to be observed. Moreland's experiment found a rotation of the endplate and concluded that this morphological feature resulted from mechanobiological modeling and remodelling processes. (Moreland M.S. 1980; Huiskes R. et al. 2000; Van Der Meulen M.C.H. and Huiskes R. 2002). This study focuses on mechanobiological growth, which is not able to simulate intravertebral rotation caused by modeling and remodelling. The modeling or remodelling-triggered modification of vertebral morphology should be further studied.

Axial or non-axial loadings were able to modify the vertebral morphology via mechanobiological growth independently. Those loadings with different orientations, when integrated into multi-axial loading conditions, presented coupling mechanobiologicla influences on vertebral morphological development via growth. As shown by the simulation results, the wedging angle triggered by the combined loading was not the linear addition of wedging angles triggered by individual loads. It should be noted that the multi-axial loading induced lower wedging than the axial loading, although multi-axial loading included an axial component in addition to a shear component. In addition, both axial and shear loading triggered similar wedging patterns that relative high growth rate occurred at the right side of the vertebral body compared with the left side. Mechanical energy generated from multi-axial loading might result in the coupling mechanobiological influences induced by loads with different orientations. Mathematically, energy integrated multi-axial stresses with non-linear form, which resulted in the non-linear combination of mechanobiological growths induced by loading from different orientations. As a result, the vertebral morphology was affected by the coupling mechanobiological factors.

The asymmetric mechanical energy distribution pattern on the growth plate might be a potential pathomechanism that induces the structural AIS during the adolescent growth spurt. In chapter 4, using our model it was shown that mechanical energy triggered the mechanoregulation including the mechanobiological growth. This resulted in the vertebral morphological modification. The varied energy density on the growth plate of a vertebra globally affected the wedging feature of this vertebra during growth. This vertebral feature suggested that the growth rate increased or decreased from left to right sides of a vertebral growth plate. The growth on the left side could be stimulated or retarded as opposed to the right side (**Figure 5-2**a). **Figure 5-2**b showed a growth distribution (axial loading **Figure 3-11**a) that presents a gradient increase from left to right sides. Based on this growth characteristic, it was predicted that energy density distribution on a growth plate would be like a parabola with high density in the left and right edges and low density in the middle region (Figure 5-2c). High energy density was able to intensively stimulate or retard growth, while low energy density presented relatively weak mechanobiological impact. This energy density distribution fearture can be seen in **Figure 5-2**d. In order to compare the distribution features of energy density with growth rate, growth plates on vertebrae were divided as six equal width areas numbering as 1 to 6 from the left to right (**Figure 5-3**a), which is similar as **Figure 5-2**b. **Figure 5-3**b-d showed energy distribution features. From Figure 5-3b-d, the contour of a parabola of the energy distribution can be seen. Under the axial loading with gradient distribution, the energy density exhibited high asymmetric distribution. Energy density presented high level on the left and right edges (area 1 and 6) and sharp decline in the middle areas (area 3 and 4). The energy distribution was coincident with the feature of distribution of growth rate as in the above prediction. In other words, the pattern of energy distribution basically determined the general wedging shape, such as the wedging in the frontal plane or sagittal plane. This finding agreed with Robling's conclusion (Robling A.G. and Turner C.H. 2009) that mechanibiological modification was consistent with distribution of mechanical energy for the purpose of adaptive change with the mechanical stimulus.

This study includes a few limitations related to the modeling techniques. Firstly, the model includes a simplified geometry of the growth plate, which presents in reality an irregular shape, as well as variations in height with age and anatomical sites. Secondly, the simplified mechanical properties adopted from published studies were represented as linear properties. The

actual material properties for vertebrae are highly non-linear and inhomogeneous. Thirdly, the application of nodal shear forces, instead of pressures, would result in slightly non-uniform shear stresses. However, this loading case generated mainly shear stresses (average of 0.19 MPa) and significant low magnitude of axial stress (average of 0.0005 MPa), which would have little effects in testing the two models for shear stresses. As another limitation, this study did not take into account the sensitivity of the model parameters (a, b, ….), which would differ from different calibration methods for two models. However, another calibration would not completely eliminate the differences resulting from complementary loading cases. For the comparison of two models, the relative behavior of the models is more important than the absolute results. The proposed relationship between mechanical energy and mechanoregulation has not been directly demonstrated by physical experiments. To date, studies related to energy-triggered mechanobiology still remain at the theoretical level due to this technical limitation. The measurement of electric/magnetic field may be helpful to test energy-related modulation of growing tissues(Ciombor D. M., Lester G. et al. 2002). In addition, the energy exchange in the opening system should be considered during the mechanobiological processes.This study did not create growth plate models of neurocentral juntions because its contribution to vertebral development is not clear (Rajwani T., Bagnall K.M. et al. 2005). This study was not able to simulate the vertebral rotation since growth only occurs in longitudinal direction as its physiological definition, and the vertebral rotation was a bone remodelling process (Moreland M.S. 1980), which was not included in this study. Finally, this study only considered the coupling mechanicsm between mechanobiological influences of axial and non-axial loads. The coupling phenonmemon between mechanobiological and biological impacts was not included in this study.
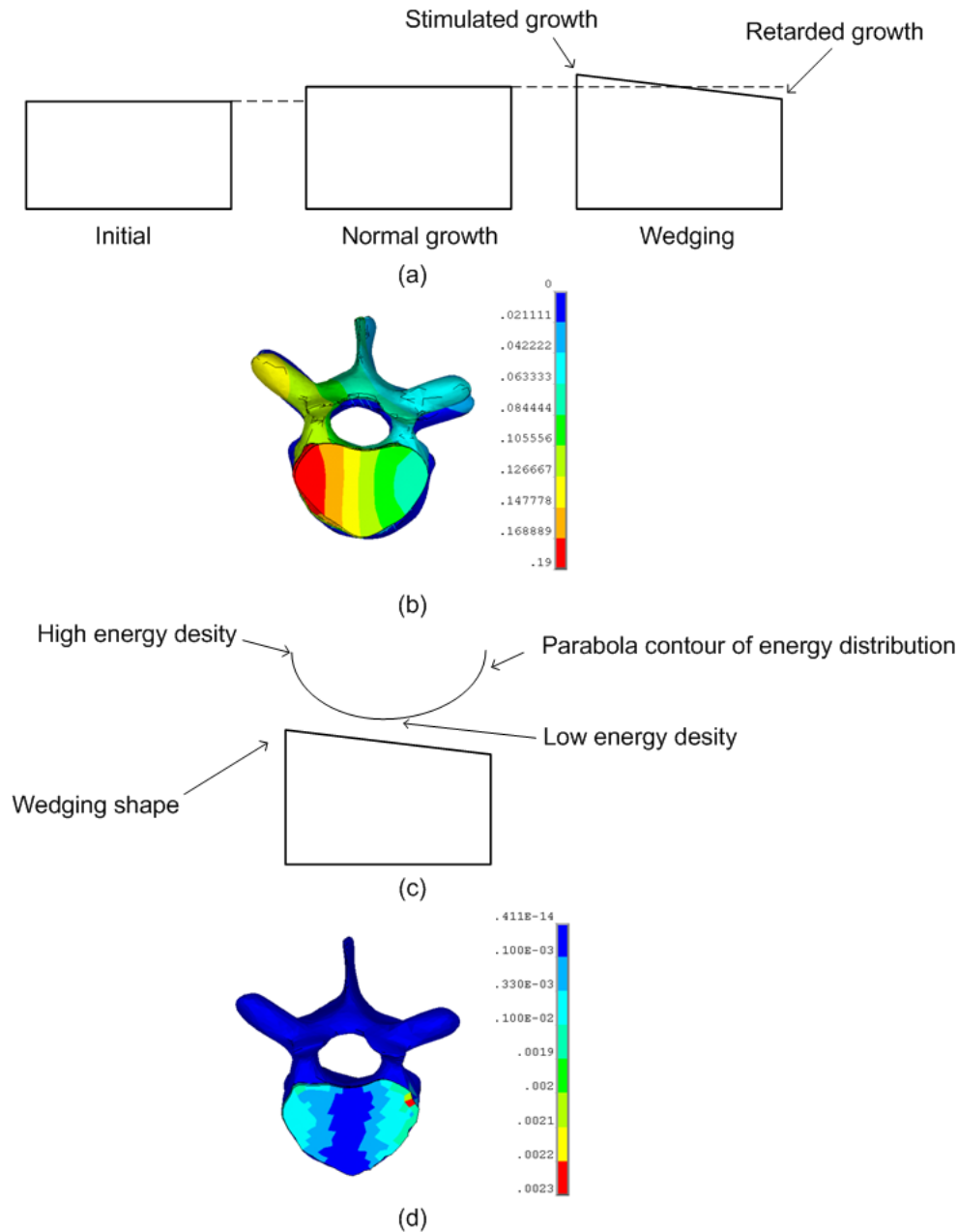
Figure 5-2 Scoliotic vertebra growth characteristic and prediction of energy density distribution (a) The growth feature for a normal and scoliotic vertebra; (b) the growth distribution feature under asymmetric axial loading (Figure 3-11a) (c) the potential energy density distribution on the growth plate. The distribution is like a parabola with high densities on both edges and low density in the middle; (d) the energy distribution feature under asymmetric axial loading (Figure 3-11a)
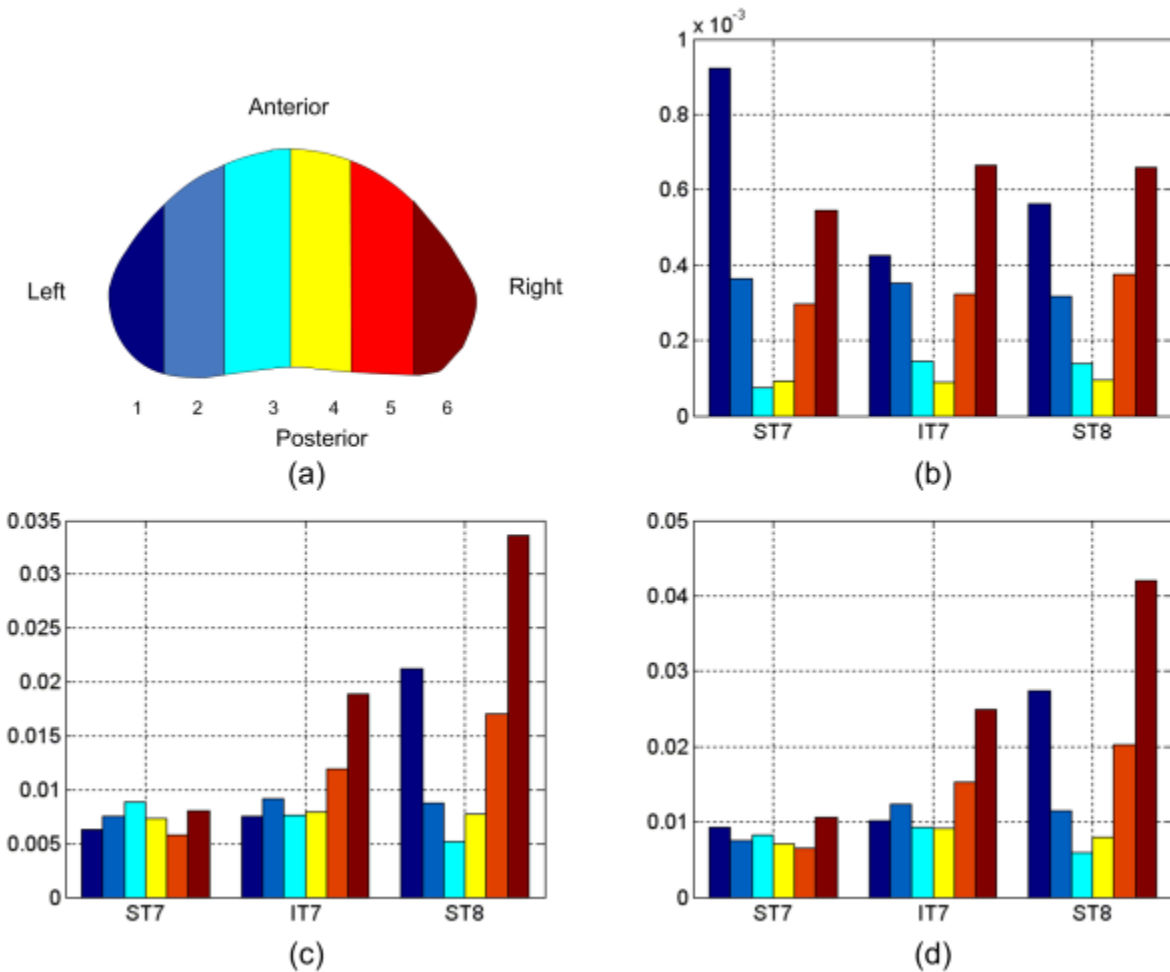
Figure 5-3　Energy density distribution for each growth plate. ST7: T7 superior growth plate; IT7: T7 inferior growth plate; ST8: T8 superior growth plate. (a) The growth plate is divided into six areas with similar width. These areas are numbered as 1 to 6 from left to right sides under postero-anterior view. The mean values of strain energy density for those six areas are calculated. (b) Energy distribution under axial loading with gradient distribution. (c) Energy distribution under shear pressure. (d) Energy distribution under combine axial loading and shear pressure.

CHAPTER 6.   CONCLUSIONS AND RECOMMENDATIONS

This thesis developed an energy-based mechanobiological growth model and studied the scoliotic vertebral development. It combined the FEM of vertebrae and related connective tissues with a growth modeling technique to investigate the potential mechanism of the growth-related AIS. Progression of an analog scoliotic deformity of a thoracic functional unit during adolescent growth spurt was investigated in this study, and some findings on the mechanism of this progression were established. The main conclusions and contributions of this study are summarized below:

- Finding the strength and limits of Stokes and Carter's models. This thesis firstly made a comparative study of these two modeling techniques. Stokes' model has strength on the application on axial only stresses. The limitation of this modeling technique is the exclusion of the non-axial stresses. The strength of Carter's model is that it takes into account the mechanobiological contribution of multi-oriented stresses to growth. Carter's model limitations are: (1) physical evidences for directly supporting this model had not yet reported; (2) the orientation properties of mechanobiological contribution of non-axial stresses are not well-defined.

- Developing a conceptual model of the growth plate. The proposed conceptual growth plate model (**Figure 3-2**) represents the developing stages of new bone generation under mechanical loading. This study firstly represented the vertebral growth plate as a three-layer structure, which shows following advantages compared with published models with non-mechanobiological activities (Schmidt H., Heuer F. et al. 2007; Sylvestre P.L., Villemure I. et al. 2007): (1) separating the mechanobiological-sensitive area from the mechanobiogical-insensitive area for the purpose of carrying out mechanobiological growth; (2) implementing the growth of vertebrae without increasing the geometry of cartilaginous area where it physiologically presented degeneration and thinning as age increased.

- Proposing energy stimulus for mechanobiological growth and developing an energy-based mechanobiological growth model. This study proposed that mechanobiological growth model should be basically represented by energy that was the stimulus for mechanobiology. The mechanobiological process included the mechanosensing, mechanotranduction, and mechanoregulation. Analytically, the energy was used to represent the mechanosensing and mechanoregulation and finally develop growth model

- Testing the energy-based model using the finite element model of a vertebra. The analytical model of mechanobiological growth developed in this study was firstly integrated into the FEM of vertebral growth plate. Based on the simulation study, it was concluded that the energy-based mechanobiological growth model agreed with experimental and theoretical studies mechanobiological growth. The energy-based model allows the simulation of vertebral growth under multi-axial loading conditions.

- Analysing of the mechanobiological role of axial and non-axial loadings on growth. This study investigated the mechanobiological contribution of both axial and non-axial loading to growth. It was concluded that both axial and non-axial loading were capable of altering the growth. Under the mechanical environment with multi-directional loadings, it was found that the overall mechanobiological growth was the non-linear integration of mechanobiological contributions from axial and non-axial loads.

- Investigating the development of scoliotic vertebrae under multi-axial loading during adolescent growth spurt. This study concluded that both axial and non-axial loadings were related to the vertebral wedging development. As a supporting system with flexible motion, spinal development was influenced by its mechanical environment with multi-axial loadings. This combination of axial and non-axial loadings environment was suggested to trigger the abnormality of vertebral morphologies and thus develop scoliosis.

- Finding that the mechanical energy distribution feature on the vertebral growth plate is correlated to the scoliotic vertebra generation. Mechanical energy physically integrates the multi-orientation stresses generated from multi-axial loading. The high energy suggested a severe modulation of the growth, while the low energy suggested a mild

change in growth . Thus, the feature of energy distribution basically reflects the general characteristic of morphological development and could thus predict the generation of scoliotic vertebrae.

- Finding a possible coupling mechanism of mechanobiological modulation of vertebral morphologies generated from axial and non-axial loading existing in multi-axial loading. Both axial and non-axial loadings are capable of modifying vertebral morphology by growth. However, under a multi-axial loading condition, a coupling mechanobiological contribution was found on growth produced from axial and non-axial loads. The coupling mechanism further presents as two aspects: axial loading plays a primary role on uniplanar wedging development and non-axial loading is the secondary factor on modification of vertebral deformity. This coupling mechanism suggests that both correction and prediction of vertebral morphological abnormal development should globally consider the mechanobiological contribution of multi-axial loading.

Generally, this project aimed at identifying the pathomechanisms of progression of adolescent idiopathic scoliosis (AIS) using biomechanical techniques. The finite element technique was introduced to carry out the biomechanical study for attaining the proposed goals indicated in Chapter 2. Based on the review on the biomechanical studies on scoliosis, this study proposed two general hypotheses. The first one aimed to confirm the capability of the finite element technique to simulate vertebral growth under complex mechanical environments with multi-axial loadings condition. The second one was to further identify the meachanobiological contribution of multi-axial loads to scoliosis development.

The biomechanical model of vertebral growth plate was established in order to simulate growing geometry. Based on the anatomical structure and physiological activities of vertebral growth plate, a conceptual model of growth plate was developed with three areas, loading sensitive, growth, and mineralized areas, which carried out different biomechanical functions in the growth process. The loading sensitive area acted as mechanosensing of mechanical loading, and the growth area carried out the growth on geometry, while the mineralized area kept the

geometric connection between growth plate and bony vertebral body. It was important that those functions attached to the three areas had biomechanical connection, which was an innovative point in this conceptual model. The biomechanical connection was that the mechanosensing of the loading sensitive area governed the growth implemented by the growth area.

Based on developed growth plate models, a comparative study, which was the first main objective, was carried out and established the weaknesses of existing models. The comparative study was significant to the following study that addressed on an innovative model development, energy-based model. As the second main objective, this study proposed a basic methodology, energy-based mechanobiological modeling technique, and finally developed energy-based growth model. The rationale of this model was tested based on experimental and theoretical studies (Carter's mechanobiological theory) as well as on a numerical evaluation (Stokes' studies on growth).

The achievement of these two objectives indicated that biomechanical modeling technique can be used to simulate the vertebral growth process with consideration of mechanical influences. Furthermore, as the key technique to simulate growth, the energy-based model integrated the multi-axial stresses generated in the spinal surrounding mechanical environment and thus allowed the simulation of vertebral growth under multi-axial loads.

Energy-based mechanobiology raised the awareness that both axial and non-axial stresses generated from multi-axial loads had impact on growth-related scoliotic vertebrae. As the third main objetve, this study investigated the progression of scoliotic vertebrae by involvement of multi-axial loads. It was found that the asymmetric axial loading stimulated similar wedging characteristics as Parent's measurements on human specimens (Parent S., Labelle et al. 2002; Parent S. 2003; Parent S., Labelle et al. 2004). This finding biomechanically supported the Parent's conclusion that vertebral coronal wedging was an important factor in scoliosis rather than for the formation of lordoscoliosis since the sagittal wedging was not found in his measurements (Parent S., Labelle et al. 2004). In addition, it was found that shear loads also had the capability of stimulating scoliotic vertebrae by imbalanced growth, which was investigated by Castelein et al (Castelein R.M., Van Dieen J.H. et al. 2005). Comparatively, shear and combined loading cases had relative weak influences on stimulating scoliotic vertebrae. It thus confirmed

that axial loading plays a primary mechanobiological role on the progression of regional deformity of scoliotic vertebrae. In addition, the coupling mechanobiological effects generated from axial and non-axial loads was found in the multi-axial loading environment. The energy concept, which non-linearly integrated axial and non-axial stresses, could account for the coupling phenomenon. It further identified the mechanobiological-stimulated scoliotic vertebra as energy-realted pathomechanism. This interpretation was consistent with Roblig's theory that indicated the adaptive response of bone structure to mechanical energy stimulus(Robling A.G. and Turner C.H. 2009). These two findinds, the significant role of multi-axial loads and coupling mechanobiological impacts on scoliotic vertebral development, partially the answered proposed hypothesis.

Some recommendations and future works for further studying the growth-triggered AIS are proposed as follows:

- Development of a FEM of whole thoracic or lumbar spine with solid elements for investigating the progression of AIS. Growth plate models will be added in each vertebra and energy-based model will be integrated into those finite element models. This integrated model would allow reproducing progressive deformities of the spine and identifying the mechanobiological-related mechanism for these deformities.

- Integration of bone remodeling into FEM of vertebrae for simulating both growth and remodelling processes. Bone remodelling was reported as an important factor on vertebral morphological development, which is closely correlated to AIS (Moreland M.S. 1980; Kotwicki T. and Napiontek M. 2008). The mathematical model of bone remodelling was presented in Ahmedi's study (Ahmedi S.A.H., Rouhi G. et al. 2009). This model also considered energy as the mechanical stimulus for bone remodelling. A simulation combining growth and remodelling processes could find how vertebrae adapt to mechanical stimuli and develop as scoliotic vertebrae.

- Mechanobiological growth model considering the detail bone material properties of vertebrae. A FEM including detailed bone material properties, based on CT-scan information, was presented in Sylvestre's study (Sylvestre P.L., Villemure I. et al. 2007).

Those material properties that present non-linear characteristics may affect energy distribution and thus affect the vertebral deformity. The mechanobiological influences of mechanical stimuli on spinal deformity will be more specific by introducing those modeling configuration.

- Integrating a model of the neurocentral junction into the FEM of vertebrae. The neurocentral junction is a bi-planar growth plate located between the neural arch and vertebral centrum (Bunger M.H. et al. 2006). The addition of the neurocentral junction model is recommended in future studies to allow the investigation of the overall growth features of vertebrae. In addition, the mechanism of the development of scoliotic vertebrae will be more specific.

This project developed an innovative approach to analytically study the mechanobiological vertebral growth and address the pathomechanism of progression of AIS caused by mechanobiological growth. This study presented a biomechanical method to find the risk coming from spinal surrounding mechanical environments on worsening the vertebral deformity during growth spurt. It would further contribute to the optimization of AIS prediction and treatment.

REFERENCES

Ahmedi S.A.H., Rouhi G., Katouzian H. and Ahmedi S.A.H. (2009). Simultaneous Presence of Growth and Remodeling in the bone Adaptation Theory. American Journal of Applied Science 6(2): 352-360.

Alberty A., Peltonen J. and Ritsila V. (1993). Effects of Distraction and Compression on Proliferation of Growth Plate Chondrocytes. A Study in Rabbits. Acta. Orthop. Scand. 64: 449-455.

Alenghat F.J. and Ingber D.E. (2002). Mechanotransduction: All Signals Point to Cytoskeleton, Matrix, and Integrins. Science's Stke 119: 1-4.

Andreassen T.T. and Oxlund H. (2001). The effects of growth hormone on cortical and cancellous bone. J Musculoskel Neuron Interact 2(1): 49-58.

Arkin A.M. and Katz J.F. (1956). The Effects of Pressure on Epiphyseal Growth: The Mechanism of Plasticity of Growing Bone. J Bone Joint Surg Am. 38: 1056-1076.

Ascenzi M.G., Lenox M. and Farnum C. (2007). Analysis of the orientation of primary cilia in growth plate cartilage: A mathematical method based on multiphoton microscopical images J Struct Biol. 158(3): 293-306.

Atchley W.R. and Hall B.K. (1991). A model for development and evolution of complex morphological structures. Biol Rev Camb Philos Soc. 66(2): 101-157.

Aubin C. E. (2002). Scoliosis study using finite element models. Stud Health Technol Inform. 91: 309-313.

Aubin C. E., Dansereau J., Petit Y., Parent F., de Guise J.A. and Labelle H. (1998). Three-dimensional measurement of wedged scoliotic vertebrae and intervertebral disks. Eur Spine J. 7(1): 59-65.

Ballock R.T. and O'Keefe R.J. (2003). Physiology and pathophysiology of the growth plate. Birth Defects Res C Embryo Today 69(2): 123-143.

Batra N.N., Li Y.J., Yellowley C.E., You L., Malone A.M., Kim C.H. and Jacobs C.R. (2005). Effects of short-term recovery periods on fluid-induced signaling in osteoblastic cells. J biomechanics 38(9): 1909-1917.

Beaupre G.S., Stevens S.S. and Carter D.R. (2000). Mechanobiology in the Development, Maintenance, and Degeneration of Articular Cartilage. Journal of Rehabilitation Research & Development 37(2): 145-151.

Benameur S., Mignotte M., Parent S., H. Labelle, Skalli W. and de Guise J. (2003). 3D/2D registration and segmentation of scoliotic vertebrae using statistical models. Comput Med Imaging Graph 27(5): 321-337.

Bonnel F., Dimeglio A., Baldet P. and Rabischong P. (1984). Biomechanical activity of the growth plate. Clinical incidences. Anat Clin. 6(1): 53-61.

Buckwalter J.A. and Cooper R.R. (1987). Bone structure and function. Instr Course Lect. 36: 27-48.

Budynas R. (1998). *Advanced Strength and Applied Stress Analysis*, McGraw-Hill Science/Engineering/Math.

Bunger M.H., Foss M., Erlacher K., Hovgaard M.B., Chevallier J., Langdahl B., Bunger C., Birkedal H., Besenbacher F. and Pedersen J.S. (2006). Nanostructure of the neurocentral growth plate: Insight from scanning small angle X-ray scattering, atomic force microscopy and scanning electron microscopy. Bone 39: 530-541.

Bunnell W.P. (1984). An objective criterion for scoliosis screening. J Bone Joint Surg Am. 66: 1381-1387.

Burdan F., Szumilo J., Korobowicz A., Farooquee R., Patel S., Dave A., Szumilo M, Solecki M., Klepacz R. and Dudka J. (2009). Morphology and physiology of the epiphyseal growth plate. Folia Histochem Cytobiol. 47(1): 5-16.

Burwell R.G. (2001). Comment to " The pathogenesis of idiopathic scoliosis: uncouple neuro-osseous growth?" by R.W.Porter. Eur Spine J 10: 482-487.

Carrier J., Aubin C. E., Trochu F. and H. Labelle (2005). Optimization of rib surgery parameters for the correction of scoliotic deformities using approximation models. J Biomech Eng 127(4): 680-691.

Carrier J., Aubin C. E., Villemure I. and H. Labelle (2004). Biomechanical modelling of growth modulation following rib shortening or lengthening in adolescent idiopathic scoliosis. Med Biol Eng Comput 42: 541-548.

Carter D.R., Fyhrie D.R. and Whalen R.T. (1987). Trabecular Bone Density and Loading History: Regulation of Connective Tissure Biology by Mechanical Energy. J. Biomech. 20(8): 785-794.

Carter D.R., Van Der Meulen M.C.H. and Beaupre G.S. (1996). Mechanical Factors in Bone Growth and Development. Bone 18(1): 5s-10s.

Carter D.R. and Wong M. (1988). Mechanical Stresses and Endochondral Ossification in the Chondroepiphysis. Journal of Orthopaedic Research 6: 148-154.

Carter D.R. and Wong M. (1988). The Role of Mechanical Loading Histories in the Development of Diarthrodial Joints. Journal of Orthopaedic Research 6: 804-816.

Castagnola P., Dozin B., Moro G. and Cancedda R. (1988). Changes in the expression of collagen genes show two stages in chondrocyte differentiation in vitro. J Cell Biol. 106(2): 461-467.

Castelein R.M., Van Dieen J.H. and Smit T.H. (2005). The role of dorsal shear forces in the pathogenesis of adolescent idiopathic scoliosis - A hypothesis. Medical Hypothesis 65: 501-508.

Catan H., Buluc L., Amk Y., Ayyildiz E. and Sarlak A.Y. (2007). Pedicle morphology of the thoracic spine in preadolescent idiopathic scoliosis: magnetic resonance supported analysis. Eur Spine J 16: 1203-1208.

Charles Y P, Dimeglio A, Marcoul M, Bourgin J-F B, Marcoul A and Bozonnat M-C (2008). Influence of Idiopathic Scoliosis on Three-Dimensional Thoracic Growth. Spine 33(11): 1209-1218.

Chen Q., Johnson D.M., Haudenschild D.R. and Goetinck P.F. (1995). Progression and recapitulation of the chondrocyte differentiation program: cartilage matrix protein is a marker for cartilage maturation. Developmental Biology 172(1): 293-306.

Chi W.M., Cheng C.W., Yeh W.C., Chuang S.C., Chang T.S. and Chen J.H. (2006). Vertebral axial rotation measurement method. Comput Methods Programs Biomed. 81(1): 8-17.

Chu W. C.W., Lam W.W.M., Chan Y.L., Ng B.K.W., Lam T.P., Lee K.M., Guo X. and Cheng J.C.Y. (2006). Relative Shortening and Functional Tethering of Spinal Cord in Adolescent Idiopathic Scoliosis? Spine 31(1): E19-E25.

Ciombor D. M., Lester G., Aaron R. K., Neame P. and Caterson B. (2002). Low Frequency EMF Regulates Chondrocyte Differentiation and Expression of Matrix Proteins. J. Orthop. Res. 20: 40-50.

Clin J., Aubin C. E. and H. Labelle (2007). Virtual prototyping of a brace design for the correction of scoliotic deformities. Med Biol Eng Comput 45: 467-473.

Cohen M.M.Jr. (2006). The new bone biology: pathologic, molecular, and clinical correlates. Am J Med Genet A. 140(23): 2646-2706.

Cowin S.C (2004). Tissue growth and remodeling. Annu Rev Biomed Eng 6: 77-107.

Cowin S.C. (1993). Bone stress adaptation models. J Biomech Eng 115(4B): 528-533.

Davies P.F. and Tripathi S.C. (1993). Mechanical stress mechanisms and the cell. An endothelial paradigm. Circ. Res. 72: 239-245.

Day G, Frawley K, Phillips G, Mcphee I B, Labrom R, Askin G and Mueller P (2008). The vertebral body growth plate in scoliosis: a primary disturbance of growth? Scoliosis 3:3.

del Palomar A P, Calvo B and Doblare M (2008). An accurate finite element model of the cervical spine under quasi-static loading. Journal of Biomechanics 41: 523-531.

Delorme S., Petit Y., De Guise J.A., H. Labelle, C. E. Aubin and Dansereau J. (2003). Assessment of the 3-D Reconstruction and High-Resolution Geometrical Modeling of the Human Skeletal Trunk From2-D Radiographic Images. IEEE Transactions on Biomedical Engineering 50(8): 989-998.

Dickson R.A. (1996). Spinal defromity: basic principles. Current Orthopaedics 10: 247-255.

Dimeglio A. and Bonnel F. (1990). *Le rachis en croissance scoliosis, taille assise et puberte*. Paris, New York, Spinger Verlag.

Doskocil M., Valouch P. and Pazderka V. (1993). On vertebral body growth. Functional and Developmental Morphology 3(3): 149-155.

Dumas R., Le Bras A., Champain N., Savidan M., Mitton D., Kalifa G., Steib J.P., de Guise J.A. and Skalli W. (2004). Validation of the relative 3D orientation of vertebrae reconstructed by bi-planar radiography. Med Eng Phys 26(5): 415-422.

Eberlein R., Holzapfel G.A. and Schulze-Bauer C.A.J. (2001). An Anisotropic Model for Annulus Tissue and Enhanced Finite Element Analyses of Intact Lumbar Disc Bodies. Computer Methods in Biomechanics and Biomedical Engineering 4: 209-229.

Eckstein F., Jacobs C.R. and Merz B.R. (1997). Mechanobiological Adaptation of Subchondral Bone as a Function of Joint Incongruity and Loading. Med. Eng. Phys. 19(8): 720-728.

EI-Rich M., Arnoux P.J., Wagnac E., Brunet C. and Aubin C. E. (2009). Finite element investigation of the loading rate effect on the spinal load-sharing changes under impact conditions. J Biomech. 42(9): 1252-1262.

EI-Rich M., Aubin C. E., Villemure I. and H. Labelle (2006). A Biomechanical Study of L5-S1 Low-grade Isthmic Spondylolisthesis Using a Personalized Finite Element Model. Stud Health Technol Inform 123: 431-434.

ESB (1978). Inaugural document for the formation of the European Society of Biomechanics, ESB Archives.

Ezquerro F., Simon A., Prado M. and Perez A. (2004). Combination of finite element modeling and optimization for the study of lumbar spine biomechanics considering the 3D thorax-pelvis orientation. Med Eng Phys. 26(1): 11-22.

Felippa C.A. and Onate E. (2003). Stress, strain and energy splittings for anisotropic elastic solids under volumetric constraints. Computers and Structures 81: 1343-1357.

Freeman J.W. and Silver F.H. (2004). Elastic Energy Storage in Unmineralized and Mineralized Extracellular Matrices (ECMs): A Comparison between Molecular Modeling and Experimental Measurements. Journal of Theoretical Biology 229: 371-381.

Frost H.M. (1990). Skeletal Structural Adaptations to M|echanical Usage (SATMU): 3. The Hyaline Cartilage Modeling Problem. Anat. Record 226(4): 423-432.

Frost H.M. (1990). Skeletal structural adaptations to mechanical usage (SATMU): 1. Redefining Wolff's law: the bone modeling problem. Anat Record 226(4): 403-413.

Frost H.M. (1990). Skeletal structural adaptations to mechanical usage (SATMU): 2. Redefining Wolff's law: the remodeling problem. Anat Record 226(4): 414-422.

Frost H.M. (1994). Wolff's Law and bone's structural adaptations to mechanical usage: an overview for clinicians. Angle Orthod. 64(3): 175-188.

Goldberg C.J., Moore D.P., Fogarty E.E. and Dowling F.E. (2008). Scoliosis: a review. Pediatr Surg Int. 24(2): 129-144.

Grant, J. P., Oxland, T.R., and Dvorak, M.F., (2001). Mapping the Structural Properties of the Lumbosacral Vertebral Endplates. Spine 26(8): 889-896.

Guo X., Chau W.W., Chan Y.L. and Cheng J.C.Y. (2003). Relative anterior spinal overgrowth in adolescent idiopathic scoliosis. The Journal of Bone & Joint Surgery 85-B: 1026-1031.

Haughton V.M., Rogers B., Meyerand M.E. and Resnick D.K. (2002). Measuring the Axial Rotation of Lumbar Vertebrae in Vivo with MR Imaging. AJNR Am J Neuroradiol 23: 1110-1116.

Hecquet J., Legaye J. and Duval-Beaupere G. (1998). Access to a three-dimensional measure of vertebral axial rotation. Eur Spine J 7: 206-211.

Henderson J.H. and Carter D.R. (2002). Mechanical Induction in Limb Morphogenesis: The Role of Growth-generated Strains and Pressures. Bone 31(6): 645-653.

Henry Gray F.R.S (1918). *Gray's Anatomy*. New York, Bounty Books.

Huiskes R. (2000). If bone is the answer, then what is the question? J Anat 197(pt2): 145-156.

Huiskes R., Ruimerman R., van Lenthe G.H. and Janssen J.D. (2000). Effects of mechanical forces on maintenance and adaptation of form in trabecular bone. Nature 405: 704-706.

Huselstein C., Netter P., de Isla N., Wang Y., D. V. Gillet P., Muller S., Bensoussan D. and Stoltz J.F. (2008). Mechanobiology, chondrocyte and cartilage. Biomed Mater Eng. 18(4-5): 213-220.

Huynh, A. M., Aubin, C. E.,, Mathieu, P. A., and Labelle, H., (2007). Simulation of progressive spinal deformities in Duchenne muscular dystrophy using a biomechanical model integrating muscles and vertebral growth modulation. Clinical Biomechanics 22: 392-399.

Huynh, A. M., Aubin C. E., Rajwani T., Baqnall K.M. and Villemure I. (2007). Pedicle growth asymmetry as a cause of adolescent idiopathic scoliosis: a biomechanical study. Eur Spine J. 16(4): 523-529.

Jacobs C.R., Simo J.C., Beaupre G.S. and Carter D.R. (1997). Adaptive bone remodeling incorporating simultaneous density and anisotropy considerations. Journal of Biomechanics 30(6): 603-613.

Jee W.S.S. and Frost H.M. (1992). Skeletal adaptations during growth. Triangle 31(2/3): 77-88.

Kadoury S., Cheriet F. and Labelle H. (2009). Self-Calibration of Biplanar Radiographic Images through Geometric Spine Shape Descriptors. IEEE Trans Biomed Eng.

Kashii M., Hashimoto J., Nakano T., Umakoshi Y. and Yoshikawa H. (2008). Alendronate treatment promotes bone formation with a less anisotropic microstructure during intramembranous ossification in rats. J Bone Miner Metab 26(1): 24-33.

Katsumi A., Orr A.W., ATzima E. and Schwartz M.A. (2004). Integrins in mechanotransduction. J Biol Chem. 279(13): 12001-12004.

Kim C.H., You L., Yellowley C.E. and Jacobs C.R. (2006). Oscillatory fluid flow-induced shear stress decreases osteoclastogenesis through RANKL and OPG signaling. Bone 39(5): 1043-1047.

Klein-Nulend J., Bacabac R.G. and Mullender M.G. (2005). Mechanobiology of bone tissue. Pathologie Biologie 53: 576-580.

Kotwicki T. and Napiontek M. (2008). Intravertebral deformation in idiopathic scoliosis: a transverse plane computer tomographic study. J Pediatr Orthop. 28(2): 225-229.

Lam G.C., Hill D.L., Le L.H., Raso J.V. and Lou E.H. (2008). Vertebral rotation measurement: a summary and comparison of common radiographic and CT methods. Scoliosis 3(16).

Leborgne P. and Aubin C. E. (1998). *Global finite element model of the spine dedicated to biomechanical scoliosis analysis*. 11th Conference of the ESB, France.

Lerner A.L., Kuhn J.L. and Holllister S.J. (1998). Are regional variations in bone growth related to mechanical stress and strain parameters? Journal of Biomechanics 31: 327-335.

Leveau B.F. and Bernhardt D.B. (1984). Developmental Biomechanics. Effect of Forces on the Growth, Development, and Maintenance of the Human Body. Phys. Ther. 64: 1874-1882.

Li Y.J., Batra N.N., You L., Meier S.C., Coe I.A., Yellowley C.E. and Jacobs C.R. (2004). Oscillatory fluid flow affects human marrow stromal cell proliferation and differentiation. J Orthop Res., 22(6): 1283-1289.

Lieberman D.E., Pearson O.B., Polk J.D., Demes B. and Crompton A.W. (2003). Optimization of bone growth and remodeling in response to loading in tapered mammalian limbs. The Journal of Experimental Biology 206: 3125-3138.

Liljenqvist U.R., Allkemper T., Hackenberg L., Link T.M., Steinbeck J. and Halm H.F.H. (2002). Analysis of Vertebral Morphology in Idiopathic Scoliosis with Use of Magnetic Resonance Imaging and Multiplanar Reconstruction. J. Bone Joint Surg. Am. 84: 359-368.

Lin H., Aubin C. E., Parent S. and Villemure I. (2008). Mechanobiological Bone Growth: Comparative Analysis of Two Biomechanical Modeling Approaches. Med. Biol. Eng. Comput. 47(4): 357-366.

Loboa E.G., Fang T.D., Warren S.M., Lindsey D.P., Fong K.D., Longaker M.T. and Carter D.R. (2004). Mechanobiology of mandibular distraction osteogenesis: experimental analyses with a rat model. Bone 34: 336-343.

Lonstein J.E. (1994). Adolescent idiopathic scoliosis. Lancet 344(8934): 1407-1412.

Lonstein J.E. (1994). Adolescent idiopathic scoliosis. The Lancet 344(8934): 1407-1412.

Maat G.J., Matricali B. and Van Meerten E.L. (1996). Postnatal development and structure of the neurocentral junction. Spine 21(6): 661-666.

Madreperla S. A., Louwerenburg B., Mann R. W., Towle C. A., Mankin H. J. and Treadwell B. V. (1985). Induction of Heat-shock Protein Synthesis in Chondrocytes at Physiological Temperatrures. J. Orthop. Res. 3: 30-35.

Mahlman C.T., Araghi A. and Roy D.R. (1997). Hyphenated History: the Hueter-Volkmann Law. Am. J. Orthop. 26(11): 798-800.

Mao J.J. and Nah H.D. (2004). Growth and Development: Hereditary and Mechanical Modulations. American Journal of Orthodontics and Dentofacial Orthopedics 125(6): 676-689.

Maried N.E. (2003). *Essential of human anatomy and physiology*, Pearson Education Inc.

Marotti F., Bertolani M.F. and Palumbo C. (2004). Bone growth, modeling and remodeling in a supernumerary metatarsal bone associated with segmental gigantism in cutis marmorata telangiectatica congenita. Histol Histopathol 19: 413-420.

Masharawi Y., Salame K., Mirovsky Y., Peleg S., Dar G., Steinberg N. and Hershkovitz I. (2008). Vertebral Body Shape Variation in the Thoracic and Lumbar Spine: Characterization of Its Asymmetry and Wedging. Clinical Anatomy 21: 46-54.

McAllister T.N. and Frangos J.A. (1999). Steady and transient fluid shear stress stimulate NO release in osteoblasts through distinct biochemical pathways. J Bone Miner Res. 14(6): 930-936.

Mehlman C.T., Araghi A. and Roy D.R. (1997). Hyphenated history: the Hueter - Volkmann Law. Am J Orthop 26(11): 798-800.

Modi H.N., Suh S.W., Song H. R., Yang J.H., Kim H.J. and Modi C.H. (2008). Differential wedging of vertebral body and intervertebral disc in thoracic and lumbar spine in adolescent idiopathic scoliosis -A cross sectional study in 150 patients. Scoliosis 3(11): 1-9.

Moreland M.S. (1980). Morphological Effects of Torsion Applied to Growing Bone. The Journal of Bone & Joint Surgery 62-B(2): 230-237.

Natarajan R N, Williams J R, Lavender S A, An H S and Andersson G B (2008). Relationship between disc injury and manual lifting: a poroelastic finite element model study. Proc. IMechE Part H: J. Engineering in Medicine 222: 195-207.

Netter F.H. (1987). *Musculoskeletal system: anatomy, physiology, and metabolic disorders*. New Jersey, Ciba-Geigy Corporation

Nijweide P.J., Burger E.H. and Klein Nulend J. (2002). The Osteocyte. *Principles of Bone Bioloy*. Bilezikian J.P., Raisz L.G. and Rodan G.A. San Diego, CA, USA, Academic Press. **1:** 93-108.

Norvell S.M., Alvarez M., Bidwell J.P. and Pavalko F.M. (2004). Fluid shear stress induces beta-catenin signaling in osteoblasts. Calcif Tissue Int. 75(5): 396-404.

Nowlan N.C. and Prendergast P.J. (2005). Evolution of Mechanoregulation of Bone Growth will Lead to Non-optimal Bone Phenotypes. Journal of Theoretical Biology 235: 408-418.

Panjabi M.M., Oxland T., Takata K., Goel V., Duranceau J. and Krag M. (1993). Articular facets of the human spine. Quantitative three-dimensional anatomy. Spine 18(10): 1298-1310.

Parent S. (2003). Analysis of the specimens of scoliotic vertebra, University of Montreal. **PhD**.

Parent S., H. Labelle, Skalli W. and de Guise J. (2004). Vertebral Wedging Characteristic Changes in Scoliotic Spines. Spine 29(20): E455-462.

Parent S., H. Labelle, Skalli W., Latimer B. and De Guise J. (2002). Morphometric Analysis of Anatomic Scoliotic Specimens. Spine 27: 2305-2311.

Pauwels F. (1980). *Biomechanics of the Locomotor Apparatus*. Berlin, Springer-Verlag.

Petit Y., Aubin C. E. and H. labelle (2004). Spinal shape changes resulting from scoliotic spine surgical instrumentation expressed as intervertebral rotations and centers of rotation. Journal of Biomechanics 37: 173-180.

Pomero V., Mitton D., Laporte S., de Guise J.A. and Skalli W. (2004). Fast accurate stereoradiographic 3D-reconstruction of the spine using a combined geometric and statistic model. Clin Biomech (Bristol, Avon) 19(3): 240-247.

Ponik S.M., Triplett J.W. and Pavalko F.M. (2007). Osteoblasts and osteocytes respond differently to oscillatory and unidirectional fluid flow profiles. J Cell BIochem. 100(3): 794-807.

Porter R.W. (2001). Can a short spinal cord produce scoliosis? Eur Spine J 10: 2-9.

Porter R.W. (2001). The pathogenesis of idiopathic scoliosis: uncoupled neuro-osseous growth? Eur Spine J 10: 4730481.

Prendergast P.J. (1997). Finite element models in tissue mechanics and orthopaedic implant design. Clin Biomech (Bristol, Avon) 12(6): 343-366.

Price J.S., Oyajobi B.O. and Russell R.G.G. (1994). The Cell Biology of Bone Growth. Eur. J. Clin. Nutr. 48: S131-S149.

Rajwani T., Bagnall K.M., Lambert R., Huang E.M., Secretan C., Moreau M., Mahood J., Raso V.J. and Bhargava R. (2005). Evaluating MRI as a technique for visualizing the neurocentral junction. Spine 30(7): 807-812.

Rajwani T., Bagnall K.M., Lambert R., Videman T., Kautz J., Mpreau M., Mahood J., Raso V.J. and Bhargava R. (2004). Using magnetic resonance imaging to characterize pedicle asymmetry in both normal patients and patients with adolescent idiopathic scoliosis. Spine 29(7): E145-152.

Rajwani T., Bhargava R., Moreau M., Mahood J., Raso V.J., Jiang H. and Bagnall K.M. (2002). MRI characteristics of the neurocentral synchondrosis. Pediatr Radiol 32(11): 811-816.

Reamy B. and Slakey J.B. (2001). Adolescent Idiopathic Scoliosis: Review and Current Concepts. Am Fam Physician 64(1): 111-116.

Roberts S., Menage J. and Urban J. P. (1989). Biochemical and structural properties of the cartilage end-plate and its relation to the intervertebral disc. Spine 14(2): 166-174.

Robling A.G., Duijvelaar K.M., Geevers J.V., Ohashi N. and Turner C.H. (2001). Modulation of Appositional and Longitudinal Bone Growth in the Rat Ulna by Applied Static and Dynamic Force. Bone 29(2): 105-113.

Robling A.G. and Turner C.H. (2009). Mechanical signaling for bone modeling and remodeling. Crit Rev Eukaryot Gene Expr. 19(4): 319-338.

Rohlmann A, Zander T, Bock B and Bergmann G (2008). Effect of position and height of a mobile core type artificial disc on the biomechanical behaviour of the lumbar spine. Proc. IMechE Part H: J. Engineering in Medicine 222: 229-239.

Rohlmann A., Burra N.K., Zander T. and Bergmann G. (2007). Comparison of the effects of bilateral posterior dynamic and rigid fixation devices on the loads in the lumbar spine: a finite element analysis. Eur Spine J 16: 1223-1231.

Roth M. (1981). Idiopathic Scoliosis from the Point of View of the Neuroradiologist. Neuroradiology 21: 133-138.

Ruan J., EI-Jawahri R., Chai L., Barbat S. and Prasad P. (2003). Prediction and analysis of human thoracic impact responses and injuries in cadaver impacts using a full human body finite element model. Stapp car Crash J. 47: 299-321.

Rubin J., Rubin C. and Jacobs C.R. (2006). Molecular Pathways Mediating Mechanical Signaling in Bone. Gene 367: 1-16.

Ruimerman R. (2005). Modeling and Remodeling in Bone Tissue, Eindhoven : Technische Universiteit Eindhoven,. **PhD**.

Sairyo K., Goel V.K., Masuda A., Vishnubhotla S., Faizan A., Biyani A., Ebraheim N., Yonekura D., Murakami R. I. and Terai T. (2006). Three-dimensional finite element analysis of the pediatric lumbar spine. Part I: pathomechanism of apophyseal bony ring fracture. Eur Spine J 15: 923-929.

Sairyo K., Goel V.K., Masuda A., Vishnubhotla S., Faizan A., Biyani A., Ebraheim N., Yonekura D., Murakami R. I. and Terai T. (2006). Three dimensional finite element analysis of the pediatric lumbar spine. Part II: biomechanical change as the initiating factor for pediatric isthmic spondylolisthesis at the growth plate. Eur Spine J 15: 930-935.

Schmidt H., Heuer F., Claes L. and Wilke H.J. (2008). The relation between the instantaneous center of rotation and facet joint forces - A finite element analysis. Clin Biomech (Bristol, Avon) 23(3): 270-278.

Schmidt H., Heuer F., Drumm J., Klezl Z., Claes L. and Wilke H.J. (2007). Application of a Calibration Method Provides More Realistic Results for a Finite Element Model of a Lumbar Spinal Segment. Clinical Biomechanics 22: 377-384.

Schmidt H., Kettler A., Heuter F., Claes L. and Wilke H.J. (2007). Intradiscal Pressure, Shear Strain, and Fiber Strain in the Intervertebral Disc under Combined Loading. Spine 32(7): 748-755.

Schmidt H., Kettler A., Rohlmann A., Claes L. and Wilke H.J. (2007). The Risk of Disc Prolapses with Complex Loading in Different Degrees of Disc Degeneration-A Finite Element Analysis. Clinical Biomechanics 22: 988-998.

Schwartz L., M. H., Stolz C., Steayert J.M., Ho Ba Tho M.C. and Halphen B. (2003). Growth and cellular differentiation: a physico-biochemical conundrum? The example of the hand. Medical Hypothesis 61(1): 45-51.

Seifert J., Totoribe K., Goel V., Traynelis C. and Clark C. (2000). *Spinal Cord Deformation in Flexion and Extension - A Finite Element Study*. Engineering in Medicine and Biology Society, Proceedings of the 22nd Annual International Conference of the IEEE Chicago IL.

Shefelbine S.J. and Carter D.R. (2004). Mechanobiological Predictions of Femoral Anteversion in Cerebral Palsy. Annal of Biomedical Engineering 32(2): 297-305.

Shefelbine S.J. and Carter D.R. (2004). Mechanobiological Predictions of Growth Front Morphology in Developmental Hip Dysplasia. Journal of Orthopaedic Research 22: 346-352.

Shefelbine S.J., Tardieu C. and Carter D.R. (2002). Development of the Femoral Bicondylar Angle in Hominid Bipedalism. Bone 30(5): 765-770.

Shirazi-Adl A. (1991). Finite-Element Evaluation of Contact Loads on Facets of an L2-L3 Lumbar Segment in Complex Loads. Spine 16(5): 533-541.

Shirazi-Adl S.A., Shrivastava S.C. and Ahmed A.M. (1984). Stress analysis of the lumbar disc-body unit in compression. A three-dimensional nonlinear finite element study. Spine 9(2): 120-134.

Silver F.H. and Bradica G. (2002). Mechanobiology of Cartilage: How Do Internal and External Stresses Affect Mechanochemical Transduction and Elastic Energy Storage? Biomechan. Model Mechanobiol. 1: 219-238.

Silver F.H. and Siperko L.M. (2003). Mechanosensing and Mechnochemical Transduction: How Is Mechanical Energy Sensed and Converted into Chemical Energy in an Extracellular Matrix? Critical Reviews in Biomedical Engineering 31(4): 255-331.

Smalt R., Mitchell F.T., Howard R.L. and Chambers T.J. (1997). Induction of NO and prostaglandin E2 in osteoblasts by wall-shear stress but not mechanical strain Am J Physiol Endocrinol Matab 273(4): E751-E758.

Sommerfeldt D.W. and Rubin C.T. (2001). Biology of bone and how it orchestrates the form and function of the skeleton. Eur Spine J 10: s86-s95.

Stevens S.S., Beaupre G.S. and Carter D.R. (1999). Computer Model of Endochondral Growth and Ossification in Long Bones: Biological and Mechanobiological Influences. J. Orthop. Res. 17(5): 646-653.

Stokes I.A.F. and Aronsson D.D. (2001). Disc and vertebral wedging in patients with progressive scoliosis. J Spinal Disord. 14(4): 317-322.

Stokes I.A.F., Aronsson D.D. and Urban J. P. (1994). Biomechanical factors influencing progression of angular skeletal deformities during growth. Eur j Musculoskel Res. 3: 51-60.

Stokes I.A.F., Bigalow L.C. and Moreland M.S. (1986). Measurement of axial rotation of vertebrae in scoliosis. spine 11: 213-218.

Stokes I.A.F. (2002). Mechanical Effects on Skeletal Growth. J. Musculoskel. Neuron. Interact. 2(3): 277-280.

Stokes I.A.F. (2007). Analysis and Simulation of Progressive Adolescent Scoliosis by Biomechanical Growth Modulation. Eur. Spine. J. 16: 1621-1628.

Stokes I.A.F., Aronsson D.D., Dimock A.N., Cortright V. and Beck S. (2006). Endochondral Growth in Growth Plates of Three Species at Two Anatomical Locations Modulated by Mechanical Compression and Tension. Journal of Orthopaedic Research 24(6): 1327-1334.

Stokes I.A.F., Clark K.C., Farnum C.E. and Aronsson D.D. (2007). Alterations in the Growth Plate Associated with Growth Modulation by Sustained Compression or Distraction. Bone 41: 197-205.

Stokes I.A.F., Gwadera J., Dimock A., C. E. Farnum and Aronsson D.D. (2005). Modulation of Vertebral and Tibial Growth by Compression Loading: Diurnal versus Full-time loading. Journal of Orthopaedic Research 23: 188-195.

Stokes I.A.F. and Laible J.P. (1990). Three-dimention Osseo-ligamentous Model of the Throax Representing Initiation of Scoliosis by Asymmetric Growth. J. BIomech. 23(6): 589-595.

Stokes I.A.F., Mente P.L., Latridis J.C., C. E. Farnum and Aronsson D.D. (2002). Enlargement of Growth Plate Chondrocytes Modulated by Sustained Mechanical Loading. J. Bone Joint. Surg. Am. 84: 1842-1848.

Sylvestre P.L., Villemure I. and Aubin C. E. (2007). Finite Element Modeling of the Growth Plate in a Detailed Spine Model. Med. Biol. Eng. Comput. 45(10): 977-988.

Thomas Edwards W., Zheng Y., Ferrara L. A. and Yuan H. (2001). Structural Features and Thickness of the Vertebral Cortex in the Thoracolumbar Spine. Spine 26(2): 218-225.

Toshikazu K., Isao K., Kenji T., Yuji A., Toshihiro I., Takumi I., Suzuyo O., Jiro I. and Yasusuke H. (1998). Interleukin 8 is produced by hydrostatic pressure in human osteoblast cell line, MG-63. Pathophysiology 5(3): 199-204.

Tschumperlin D., Dai G., Maly I.V., Kikuchi T., Laiho L.H., McVittie A.K., Haley K.J., Lilly C.M., So P.T.C., Lauffenburger D.A., Kamm R.D. and Drazen J.M. (2004). Mechanotransduction through growth-factor shedding into the extracellular space. Nature 429: 83-86.

Van Der Meulen M.C.H. and Huiskes R. (2002). Why Mechanobiology? A Aurvey Article. Journal of Biomechanics 35: 401-414.

Van Der Plaats A., Veldhuizen A.G. and V. G.J. (2007). Numerical Simulation of Asymmetrically Altered Growth as Initiation Mechanism of Scoliosis. Annal of Biomedical Engineering 35(7): 1206-1215.

Van der Plaats A., Veldhuizen A.G. and G. J. Verkerke (2007). Numerical Simulation of Asymmetrically Altered Growth as Initiation Mechanism of Scoliosis. Annal of Biomedical Engineering 35(7): 1206-1215.

Villemure I. (2000). Study biomechanical process of growth and deformation of scoliosis. Montreal, University of Montreal. **PhD**.

Villemure I., Aubin C. E., Dansereau J. and H. Labelle (2002). Simulation of Progressive Deformities in Adolescent Idiopathic Scoliosis Using a Biomechanical Model Integrating Vertebral Growth Modulation. ASME J. Biomech. Eng. 124(6): 784-790.

Villemure I., C. E. Aubin, Dansereau J. and H. Labelle (2004). Biomechanical simulations of the spine deformation process in adolescent idiopathic scoliosis from different pathogenesis hypotheses. Eur Spine J 13(1): 83-90.

Villemure I., Chung M.A., Seck C.S., Kimm M.H., Matyas J.R. and Duncan N.A. (2005). Static Compressive Loading Reduces the mRNA Expression of Type II and X Collagen in Rat Growth-Plate Chondrocytes During Postnatal Growth. Connective Tissue Research 46: 211-219.

Villemure I., Cloutier L., Matyas J.R. and Duncan N.A. (2007). Non-uniform strain distribution within rat cartilaginous growth plate under uniaxial compression. Journal of Biomechanics 40(1): 149-156.

Villemure I. and Stokes I.A.F. (2009). Growth plate mechanics and mechanobiology. A survey of present understanding. Journal of Biomechanics doi:10.1016/j.jbiomech.2009.05.021.

Vital J.M., Beguiristain J.L., Algara C., Villas C., Lavignolle B., Grenier N. and Senegas J. (1989). The Neurocentral Vertebral Cartilage: Anatomy, Physiology and Physiopathology. Surg Radiol Anat 11(323-328).

Vogel V. and Sheetz M. (2006). Local Force and Geometry Sensing Regulate Cell Function. Nature reviews. Molecular cell biology 7(4): 265-275.

Wang J.H.C. (2006). Mechanobiology of Tendon. Journal of Biomechanics 39: 1563-1582.

Wang X. and Dumas G A. (2002). Simulation of bone adaptive remodeling using a stochastic process as loadinghistory. Journal of Biomechanics 35: 375-380.

Wang X. and Mao J.J. (2002). Chondrocyte Proliferation of the Cranial Base Cartilage upon in Vivo Mechanical Stresses. J. Dent. Res. 81(10): 701-705.

Wang Y., Middleton F., Horton J.A., Reichel L., C. E. Farnum and Damron T.A. (2004). Microarray analysis of proliferative and hypertrophic growth plate zones identifies differentiation markers and signal pathways. Bone 35: 1273-1293.

Wang Z.L., Teo J.C., Chui C.K., Ong S.H., Yan C.H., Wang S.C., Wong H.K. and Teoh S.H. (2005). Computational biomechanical modelling of the lumbar spine using marching-cubes surface smoothened finite element voxel meshing. Comput Methods Programs Biomed 80(1): 25-35.

Weiss H.R. (1995). Measurement of vertebral Rotation: Perdriolle versus Raimondi. Eur Spine J 4: 34-38.

Wertz X., Schoevaert D., Maitournam H., Chassignet P. and Schwartz L. (2006). The Effect of Hormones on Bone Growth is Mediated through Mechanical Stress. C. R. Biologies 329: 79-85.

White A.A. and Panjabi M.M. (1990). *Clinical Biomechanics of the Spine*, J.B. Lippincott Company.

Willy C, Schneider P, Engelhardt M, Hargens A R and Mubarak S J (2008). Richard von Volkmann. Clin Orthop Relat Res 466: 500-506.

Wilsn W., Driessen N.J.b., Van Donkelaar C.C. and I. K. (2006). Prediction of collagen orientation in articular cartilage by a collagen remodeling algorithm. Osteoarthritis and Cartilage 14(11): 1196-1202.

Wolff J. (1986). *The Law of Bone Remodeling*. New York, Springer.

Wong M. and C. D.R. (2003). Articular cartilage functional histomorphology and mechanobiology: a research perspective. Bone 33: 1-13.

Wong M., Siegrist M. and Goodwin K. (2003). Cyclic tensile strain and cyclic hydrostatic pressure differentially regulate expression of hypertrophic markers in primary chondrocytes. Bone 33: 685-693.

Wu Q.Q. and Chen Q. (2000). Mechanoregulation of chondrocyte proliferation, maturation, and hypertrophy: ion-channel dependent transduction of matrix deformation signals. Exp Cell Res. 256(2): 383-391.

Yamazaki A., Mason D.E. and Caro P.A. (1998). Age of closure of the neurocentral cartilage in the thoracic spine. J Pediatr Orthop 18(2): 168-172.

You J., Reilly G.C., Zhen X., Yellowley C.E., Chen Q., Donahue H.J. and Jacobs C.R. (2001). Osteopontin Gene Regulation by Oscillatory Fluid Flow via Intracellular Calcium Mobilization and Activation of Mitogen-activated Protein Kinase in MC3T3-E1 Osteoblasts. J Biol Chem. 276(16): 13365-13371.

Zhu X., Gong H., Zhu D. and Gao B. (2002). A study of the effect of non-linearities in the equation of bone remodeling. Journal of Biomechanics 35: 951-960.

Zvi B.S. (2007). The Osteoclast: A Multinucleated, Hematopoietic-Origin,Bone-Resorbing Osteoimmune Cell. Journal of Cellular Biochemistry 102(5): 1130-1139.
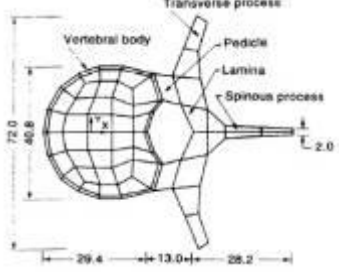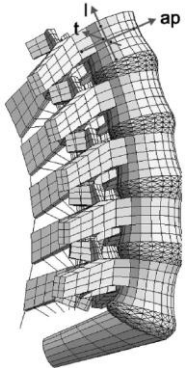
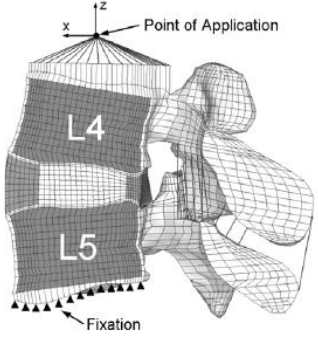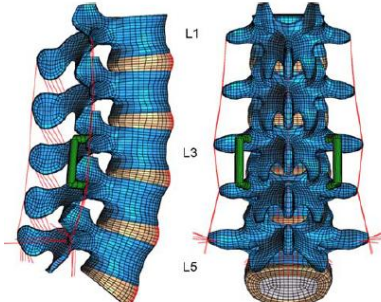# APPENDIX A. EXPERIMENTAL STUDIES FOR MECHANOBIOLOGICAL GROWTH

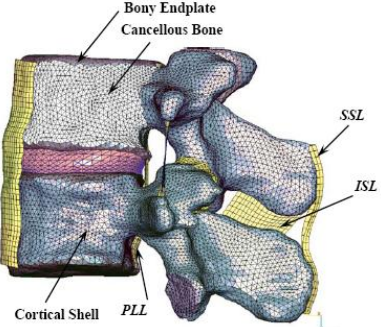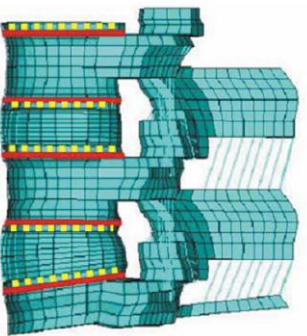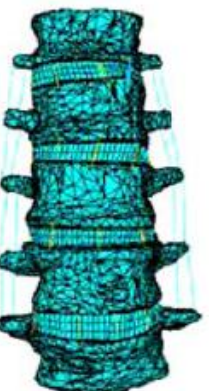| Literature	Conclusion of experiments	Experiment description	Contribution of experimental studies	limits
(Stokes I.A.F., Gwadera J. et al. 2005)	compression was able to reduce the amount of hypertrophic chondrocytic enlargement and the chondrocyte proliferation. Thus, it was concluded that compression loading was capable of suppressing growth	Compression was applied on tibial and tail vertebral growth plate of growing Sprague – Dawley rat. Four kinds of loads were applied: full-time load; day-loading; night-loading; and sham instrumented.	Demonstrated that compression was able to suppress the bone growth	The loading condition limited in the static compression, which mechanobiological role was indicated in Hueter-Volkmann Law
(Lerner A.L., Kuhn J.L. et al. 1998)	High compressive stresses were correlated with reduced bone growth rate.	Rabbits with different ages were chose for representing the different development stages of femur bone. Finite element (FE) models generated from micro-CT images of these rabbits. Applied mechanical loading on the FE model for testing the correlation between growth and mechanical stresses	Linked the experimental observation of animal model and mechanical model of bone for finding the mechanobiological influence of compressive stresses on growth.	The growth in vivo under designated mechanical environment was not observed.
(Stokes I.A.F., Mente P.L. et al. 2002; Stokes I.A.F., Aronsson D.D. et al. 2006; Stokes I.A.F., Clark K.C. et al. 2007)	Compression and distraction modulate the growth rate by corresponding changes in the number of the proliferative chondrocytes and in the final height of the hypertrophic chondrocytes. Reduced growth rate and increased growth rate were presented in compression and distraction respectively.	Sustained compression and tension were applied in the growth plate of immature animals(rats, rabbits, calves). Observe the growth modulation under those mechanical loads.	Indicated that both compression and tension were able to modulate growth by changing of proliferation and hypertrophy of chondrocytes.	The experiment for non-axial loading was not included

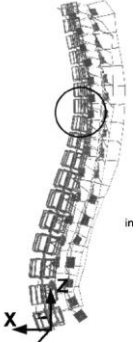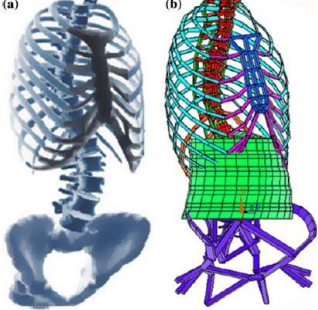|			
(Robling A.G., Duijvelaar K.M. et al. 2001)	Static compressive loads suppressed bone growth but affected little on endocortical bone formation. Dynamic loads were able to modulate the bone growth in term of its magnitude. Dynamic loads could also trigger bone remodeling.	Growing male rats were divided into three groups, and these groups of rats received 10 minutes bouts of static loading at 17N, static loading at 8.5N, and dynamic loading at 17 N respectively.	It was found both static and dynamic loading had mechanobiological contribution to bone growth. Mechanobiological growth rate was depended on the magnitude of applied loads instead of the average value.	No quantified correlation between mechanical loads and growth modulation was developed. The sensitivity of mechanobiological growth to the frequency of loading was not tested.
(Carter D.R. and Wong M. 1988; Schwartz L., H. et al. 2003)	As an important process of bone growth, endochodral ossification can be promoted by shear stresses. In addition,hydrostatic compression inhibits cartilage ossification.	Observed the ossification of hand through X-ray picture. Simulated bone ossification using finite element model, and validated simulation results in term of the published experiments from Gebhardt and Pauwels(Pauwels F. 1980; Carter D.R. and Wong M. 1988)	Found the mechanobiological contribution of shear stresses to bone growth. Indicated the mechanobiological role of the non-axial loading.	It was not a hard evidence to demonstrate the affection of shear stress because it depended on the X-ray picture. No real force was applied on the real bone tissues.
(Toshikazu K., Isao K. et al. 1998)	Hydrostatic pressure can alter the biochemical activities of bone cells. This result the modification of bone formation.	Experimental testing the biochemical influence of hydrostatic pressure on osteoblast cell.	This experiment demonstrated the mechnobiological contribution of hydrostatic pressure to bone formation, which partially affected bone growth	Only osteoblast cell was included into this experiment, but bone growth was related to several kinds of tissues.
(Moreland M.S. 1980)	Torsion forces result in the angular growth of bone and change the morphology of epiphysial plate. Significant longitudinal growth is not observed in this experiment	Torsion was applied on the tibiae of immature New Zealand White rabbits. Radiographic and histological analysis were used for evaluating experiment results	The torsion forces were able to modify the morphology of bone. However, significant contribution of torsion to longitudinal growth was not	The longitudinal growth was not observed in detail. The torsion was not a pure torsion since the irregularity of

			observed.	the shape of the growth plate.
(Wong M., Siegrist M. et al. 2003)	Cyclic tension stimulated the activities of hypertrophic chondrocytes, and cyclic hydrostatic pressure suppressed the chondrocyte differentiation and preserved the cartilage phenotype.	Chondrocytes were taken from calf bovine humeral head cartilage. Those cells were exposed to cyclic tension or cyclic hydrostatic pressure.	The mechanobiological role of cyclic loading was investigated in this experiment. A special loading mode, cyclic hydrostatic pressure was firstly employed to study its modulation abilities on growth. This loading mode was rare in the published studies.	The direct measurement of the modulation rate for cyclic loading to growth was not carried out in this experiment. The sensitivity of the chondrocyte activities to the frequency of cyclic load was not investigated.

APPENDIX B.   FINITE ELEMENT MODELS OF THE SPINE

Authors	Special characteristics of the modeling technique	Model description	Application of models	Model picture (permissions were approved)
Lumbar spine model				
Shirazi-Adl et al., 1991	Vertebrae geometries were based on the anthropometry on vertebrae	FEM of Lumbar L2-L3 segment was developed. Vertebral body was created using the geometric drawing based on the measurement of vertebrae. Vertebral body was meshed as brick elements. Shell elements represented the cortical bone covering the vertebral body. Intervertebral disc was divided into annulus and nucleus. Annulus was modelled as composite including the ground substance and collagenous fibres. Nucleus was modelled as incompressible inviscid fluid.	Analyze the loading distribution in the articular joints of lumbar spine.	
Ezquerro et al., 2004	A vertebra is parametric and defined by a set of geometric parameters	Each vertebra is modelled as eight-node solid element. The annulus of intervertebral disc was modeled as solid element and defined as composite material. The nucleus was simulated as incompressible fluid using solid element. Ligaments were defined as cable element.	Study the biomechanical response of lumbar spine to normal activities	
Natarajan et	Lumbar spine L4-L5	Vertebral bodies and the	Study the potential risk	

A Parametric model

al., 2008		represented by solid elements. The geometric shape of a lumbar motion segment was reconstructed from CT scan.	intervertebral disc were modeled as eight-node three dimensional elements. ligaments were simulated as cable elements.	of disc damage under a loading condition. Simulate the biomechanical responses of the lumbar disc on normal lifting activities: sagittal lifting, lifting and twisting, lifting and bending	
Schmidt et al, 2007;2008		Detail lumbar spine model represented by solid elements. Endplate was created in this model. Model geometry was taken from CT scans	A Lumbar spinal segment was modeled as non-linear and 3D FE model. FE model included the vertebral body with cortical and cancellous components, intervertebral disc and ligaments. Further more, endplates including the bony and cartilaginous parts, were also modelled.	Investigate the loading situation affected by the degenerated disc.	
Rohlmann et al., 2007;2008		Solid elements for whole lumbar spine L1-L5. The geometry was reconstructed from CT scans	A whole lumbar FE model was generated based on the geometry taken from CT scans. Vertebral bodies were meshed by eight-node elements. Intervertebral discs and ligaments were created based on the anatomic structure.	Investigated the spinal loading modification by bilateral posterior dynamic implant. Study the spinal loading feature affected by the disc implant.	

EI-Rich et al., 2009		Solid element model of a function unit L2-L3. The vertebral geometry was reconstructed from 0.6-mm-thick CT scan.	Cortical and cancellous bones were modeled as 3-node shell and 4-node solid element. Intervertebral disc was separated as annulus and nucleus. The intervertebral ligament was modeled as 1-mm-thick shell.	Investigated the biomechanical response of the L2-L3 to the flexion and extension. Studied the potential risk of rupture at a area with abnormal loading distribution under the motion segment L2-L3.	
Sairyo et al., 2006		A pediatric lumbar spine L3-L5geometry was derived from available adult geometric model of lumbar spine. Solid element model for representing the lumbar segment.	Vertebral bodies with cancellous bone were modeled as solid elements. Cortical bone was modeled as shell covering the vertebral bodies. Intervertebral discs were divided into nucleus and annulus representing by solid elements. Growth plates and apophyseal bony ring were added into pediatric spine model, while these parts were not included in adult spine model.	Investigate the biomechanical cause of apophyseal bony ring fracture. Study the biomechanical response of pediatric spondylolishthesis	
Sylvestre et al., 2007	pediatric model	A personalized geometry was generated based on the combination of radiographs of a pediatric patient, and CT scans of vertebral specimens. A pediatric lumbar spinal model was created using solid elements.	The vertebral body was meshed using tetrahedron element. Cortical and cancellous bone elements were assigned different stiffness based on the CT number. The whole model presented non-linearity. A detail model of growth plate with three zones, reserve zone, proliferative zone, and hypertrophic zone, was created in this model.	Investigate the biomechanical responses f growth plates to different loading cases, i.e. flexion, extension, axial torsion, and lateral bending.	

		Intervertebral discs and ligaments models were also created based on the anatomic structure.		
		Whole spine model		
Villumure et al., 2002	A beam model represented the whole spinal column. The personalized model geometry reconstructed from X-ray radiographs.	Each vertebral body was represented by 10-beam model. the posterior element and intervertebral disc were modeled as beam elements. Intervertebral ligaments were model as tension-only cable. Growth and growth modulation were integrated into the FE model for simulation the progression of sciliosis.	Study the progressive deformity of AIS during growth spurt.	
Carrier et al., 2004; Clin et al., 2007	The whole FE model termed as thoraco-lumbo-sacral model contained the spine, rib cage, pelvis using 3D beam elements. A personalized geometry was reconstructed from X-ray radiographs of adolescent patients.	The osseo-ligamentous model of the spine, rib, sternum, pelvis and abdominal tissues, was represented by 3D elements. Intervertebral discs and ligaments were also modeled as beam models in the corresponding position based on the anatomical structure.	Investigate the influence of rib length to the long term correction of scoliotic spine of AIS. Predict the potential correction result for AIS using brace.	

APPENDIX C.   GROWTH SIMULATION USING THERMAL LOADING METHOD

In this project, the thermal load is employed for calculating the growth and updating the coordinate. The growth increments will be modeled with a proportional thermal deformation by applying temperature in the direction of growth. The relationship between strain increment and thermal loading can be written as:

$$\varepsilon = \alpha\Delta T = \alpha(T - T_0) \tag{C-1}$$

Where ε is the strain; α is the thermal dilatation coefficient; T and T_0 are the applied temperature and initial temperature. The Eq. a-1 can be transformed as:

$$T = T_0 + \frac{\varepsilon}{\alpha} \tag{C-2}$$

The Eq a-2 determines the thermal load of an element. With respect to the dilatation coefficient, different values of α are defined corresponding to the different axes. The material is defined as anisotropic for thermal properties. This study only considers the longitudinal growth, and no growth occurs in the cross section. Thus, the configuration of dilatation coefficients is able to allow the longitudinal growth and suppress the transverse growth when thermal load is applied. There is no special requirement for setting the dilatation coefficient α. This study set $\alpha = 0.1$. The dilatation coefficient for other transverse direction should be far smaller than the longitudinal direction for suppressing the growth in these directions. In this study, dilatation coefficients for other directions are set as 0.0001. The stain can be obtained from the simulation when applying loading.

According to the growth plate structure, elements in both loading sensitive area and growth area have mapping relation and should be identified. The stress and strain in the loading sensitive area can be obtained firstly. Based on the stress and stain distribution in the elements of this area, the growth rate can be calculated according to the growth models. The expanding rate in the growth area will be calculated based on the growth rate. The expand rate will be

transformed to thermal load and applied on corresponding elements using mapping relation defined in this model. The geometry of the growth area will be modified at each growth iteration.

The simulation process is composed of the following steps:
1) Apply loading and boundary condition on the model and calculating
2) Obtain the stress on the longitudinal direction of every element of the loading sensitive area
3) Obtain all stresses of the all elements of the loading sensitive area
4) Calculate the octahedral shear stress and hydrostatic stress of loading sensitive area
5) Calculate the thermal load. For the Stokes's model, the axial stresses are used to calculation thermal load. For the Carter's model, stressed obtained from step 4 are used for calculating
6) Remove the loading on the model
7) Apply the thermal load on the growth area.
8) Update the coordinate after calculation.
9) Repeat from step 1 to step 8

In the step 5, the calculation of thermal load is based upon the strain calculated by using Stokes's and Carter's model. The strain should be adjusted since the height of the growth area is changed during the growth. According to the stain analysis, the strain can be expressed as $\varepsilon = \dfrac{\Delta h}{h}$. Because the height h is modified in each iteration, the adjustment should be required and is described as:

$$\left. \begin{aligned} \varepsilon_{calculation} &= \frac{\Delta h_i}{h_0} \\ h_i &= h_0(1+\varepsilon_1)(1+\varepsilon_2)\cdots(1+\varepsilon_i) \\ \varepsilon_{i+1} &= \frac{\Delta h_i}{h_i} \end{aligned} \right\} \Rightarrow \varepsilon_{i+1} = \frac{1}{(1+\varepsilon_1)(1+\varepsilon_2)\cdots(1+\varepsilon_i)}\varepsilon_{calculation} \qquad \text{(C-3)}$$

where h_i is the height of last iteration, $\varepsilon_{calculation}$ is the value of strain calculated in new iteration. This stain should be adjusted. The final value of strain is ε_{i+1}, and ε_{i+1} is used in calculating the thermal load.